„Dunărea de Jos" University of Galați

Doctoral School of Mechanical and Industrial Engineering

PhD THESIS

EXTENDED ABSTRACT

A TRIBOLOGICAL STUDY OF LUBRICANTS BASED ON RAPESEED OIL AND NANO ADDITIVES FOR REDUCING FRICTION AND WEAR

PhD Student,

eng. Traian Florian IONESCU

Scientific coordinator

prof. eng. Lorena DELEANU, PhD

Series I6: Mechanical Engineering No. 58

Galați 2021

„Dunărea de Jos" University of Galați

Doctoral School of Mechanical and Industrial Engineering

PhD THESIS

EXTENDED ABSTRACT

A TRIBOLOGICAL STUDY OF LUBRICANTS BASED ON RAPESEED OIL AND NANO ADDITIVES FOR REDUCING FRICTION AND WEAR

PhD Student
eng. Traian Florian IONESCU

President	**prof. eng. Eugen Victor Cristian RUSU, PhD** „Dunărea de Jos" University of Galați
Scientific coordinator	**prof. eng. Lorena DELEANU, PhD** „Dunărea de Jos" University of Galați
Scientific referent	**prof. eng. Dan Mihai CONSTANTINESCU, PhD** Politehnica University of Bucharest
Committe	**prof. eng. Alexandru Valentin RĂDULESCU, PhD** Politehnica University of Bucharest
	prof. eng. Iulian Gabriel BÎRSAN, PhD „Dunărea de Jos" University of Galați

Series I6: Mechanical Engineering No. 58

GALAȚI 2021

Seriile tezelor de doctorat susținute public în UDJG începând cu 1 octombrie 2013 sunt:

Domeniul **ȘTIINȚE INGINEREȘTI**

- Seria I 1**: Biotehnologii**
- Seria I 2**: Calculatoare și tehnologia informației**
- Seria I 3**. Inginerie electricã**
- Seria I 4**: Inginerie industrialã**
- Seria I 5: **Ingineria materialelor**
- Seria I 6**: Inginerie mecanicã**
- Seria I 7**: Ingineria produselor alimentare**
- Seria I 8**: Ingineria sistemelor**

Domeniul **ȘTIINȚE ECONOMICE**

- Seria E 1**: Economie**
- Seria E 2**: Management**

Domeniul **ȘTIINȚE UMANISTE**

- Seria U 1**: Filologie- Englezã**
- Seria U 2**: Filologie- Românã**
- Seria U 3: **Istorie**

UNIUNEA EUROPEANĂ

Instrumente Structurale 2014-2020

Programul Operațional Capital Uman
Axa prioritară 6 - Educație și competențe
Proiect: Burse pentru educația antreprenorială în rândul doctoranzilor și cercetătorilor postdoctorat (BeAntreprenor!)
Cod MySMIS: 124539

PhD Thesis

Extended Abstract

A TRIBOLOGICAL STUDY OF LUBRICANTS BASED ON RAPESEED OIL AND NANO ADDITIVES FOR REDUCING FRICTION AND WEAR

Author: eng. Traian Florian IONESCU

Coordinator: prof. eng. Lorena DELEANU, PhD

Study realized within the frame of the project

„Scholarships for entrepreneurial education among doctoral students and postdoctoral researchers (Be Entrepreneur!)

Contract no. 51680/09.07.2019 POCU/380/6/13 – SMIS code: 124539

Acknowledgement

First of all, I want to return thanks to professor Lorena Deleanu, who, as a scientific coordinator, has given me permanent guidance, encouragement and support during the doctoral study and elaboration period of the thesis.

I would like to express my sincere thanks to the commission for the guidance and evaluation of this paper, composed of professor Adrian Cîrciumaru, lecturer Dumitru Dima and associate professor Constantin Georgescu, especially for the offered help, but also for the competent guidance and recommendations with a high degree of professionalism.

This PhD thesis would not have been complete without the help of lecturer Cornel Camil Suciu from „Ștefan cel Mare" University of Suceava, for helping me in recording the texture of worn surfaces.

I want to thank to associate professor Petrică Alexandru for the support given in using optical microscope.

I want to thank to lecturer Alina Ceoromila for support in using the SEM microscope.

I would like to thank to the National Institute of Aerospace Research "Elie Carafoli" in Bucharest, for access to the dedicated software and to scientifical researcher Cătălin Pîrvu, for the support given to the design to the FEM model of the 4-ball tribotester.

I would like to thank the company Expur Bucharest, for providing the basic material of this thesis, the rapeseed oil.

I also want to thank to the company Digital Surf Headquarters, which gave me access for the Mountains SPIP 8 software, with which the textures of worn surfaces were investigated.

With great gratitude and love, I render thanks to my wife, Olimpia and to my daughter, Patricia, who encouraged me, surrounded me with their affection and patience and who supported me from all points of view during this period.

Traian Florian Ionescu

Table of content

Introduction

From the studied literature, the author concluded that there is a research trend concerning the additivation of vegetal oils, for their use as lubricants, especially for specific applications such as forestry, naval industry, textile industry, etc.

Rapeseed oil is produced in Romania and is an environmentally friendly resource, both in terms of production and applications.

The formulation of the package of additives in a lubricant based on vegetal oils must take into account the requirements of the application, but also its compatibility with the components of vegetal oils. For this study, the author selected two nanoadditives as friction and wear modifyiers, TiO_2 and ZnO, which could improve the tribological behavior of the rape seed oil.

Attention should be focused on the dispersion of the nanoadditive and the selection of the dispersant and the testing should be performed on the basis of a test campaign with appropriate variables, close to future applications.

The aim of this thesis is to improve the tribological behavior of nanoadditivated rapeseed oil, based on tests on the 4-ball machine, through which the performance of the lubricants newly formulated by the author can be compared with other mineral or synthetic oils. The selected variables were the nanoadditive concentration and parameters of the test regime (in normal regime, the force and speed of sliding, in severe regime, the force applied on the tribotester).

The author evaluated the tribological behavior by analyzing several parameters (coefficient of friction, diameter of the wear scar and wear rate of the diameter of the wear scar, roughness parameters). The reported results are satisfactory, but should be extended to operating regimes closer to the applicable ones.

The obtained results showed that the nanoadditivation of rapeseed oil with TiO_2 and ZnO reduced the wear rate of the average diameter of the wear scar especially at high loads and speeds, the influence in normal regime being reduced, but in severe regime the influence of the additive proved beneficial, increasing the length with a small slope of the curve wear-load. The reporting of the results favors the comparison of these data with those of the specialized literature and the formulation of pertinent recommendations for the lubricants formulated by the author. Following this study, it can be concluded that the additivation of rapeseed oil with TiO_2 and ZnO would be effective for systems operating with variable loads and possible large regime variations (towards severe regime).

The thesis presents a simplified, original model of the 4-ball tribotester, using experimental results and knowledge gained from studying contact modeling works. The model introduces friction as a shear stress between moving surfaces, according to Coulomb's law ($\tau_f = \mu F_n$) and considered as a criterion of similarity between the model and the real system, the value of the approach in the z direction of the two balls as the same as that from the real system. The proposed model is useful for evaluating the distribution of equivalent stresses and strains, so that it can estimate a working range for the test parameters and detect the transition from normal working mode (acceptable load and strain throughout operation) to a severe regime (by identification of maximum equivalent stresses and high elasto-plastic deformations). Relatively small differences were obtained between the case with the value of the coefficient of friction of 0.08 and the one in which the coefficient of friction has a value

of 0.1, but the cases were analyzed because that they are specific to the mixed or limit lubrication regime, characteristic of vegetal oils.

Based on the documentation did by the author on the additivation of vegetal oils with friction and wear modifiers, the author chose crude rapeseed oil as the base oil and as friction and wear modifiers, TiO_2 and ZnO. The author took over the technology of mixing/dispersing the nanoparticles from a previous research, carried out within the Research Center "Mechanics and Tribology of Surface Layers". Unlike many other scientific reports on lubricant testing, which focused on a single test regime, this thesis aimed to test newly formulated lubricants in both normal and severe regimes. This new approach has made possible to highlight the role of nanoadditives in the severe regime, in which, although they did not form a continuous film, they still led to the protection of contact surfaces and the reduction of the WSD characteristic obtained from tests on the 4-ball machine.

Four tribological parameters were analyzed, the coefficient of friction, the wear scar diameter (WSD), the wear rate of the wear scar diameter and the temperature in the oil bath, in order to have a clearer picture of the behavior of the tested lubricants. Analyzing the values of these parameters, the conclusions are formulated separately for the normal regime and the severe regime. The correlation of wear parameters with surface quality can be qualitative, through images and appearance of the Abbott-Firestone curve, but also quantitative, through the values obtained and the function of dependence between them.

Tribologists are interested in functions of the form f (v, F, t, WSD, texture parameter) = 0, from which it is possible to evaluate an optimization or a delimitation of the working regime on the criteria of wear and surface quality. In the case of WSD correlation with texture parameters, a group of parameters was observed to "reflect" the wear, but also other parameters are almost insensitive to tribological parameters related to wear. In order to evaluate the quality of a surface as close to reality as possible with the help of 3D parameters, the step of the profilometer must be as fine as possible, and the investigation area as large as possible. The profilometry study concludes with some pertinent observations on the Abbott-Firestone curve for normal and severe wear surfaces.

This study resulted from the fact that the additivaton of vegetal oils is still in its infancy, as the reported results are not as effective as compared to the additivation of the classic lubricant alternative - mineral oils and synthetic oils. But research needs to continue as these vegetal oils have become a renewable resource for formulating environmentally-friendly lubricants.

Chapter 1
An analysis of recent research in the field of additivated vegetal lubricants

1.1. SWOT analysis of lubricants based on vegetal oils

Vegetal oils can act as anti-wear and friction modifying additives, due to the strong interactions with the surfaces they come in contact with, especially with metallic surfaces [88]. The molecular chains of fatty acids and the presence of polar groups in the structure of vegetal oils give them the opportunity to adhere and stay on contact surfaces, even at relatively severe regimes [2].

SWOT analysis for introducing vegetal oils as lubricants indicates that a number of properties must be considered when deciding on this lubrication solution [51], [24].

Strengths are**:**

- biodegradable character [54],
- environmental protection and/or acceptability (non-polluting or environmentally friendly) [60], [91], [64],
- extraction from renewable resources or possibility of recycling or reuse of lubricant [12],
- high viscosity index [24],
- good flammability characteristics, self-ignition points and high ignition temperatures on hot surfaces [29], [77].

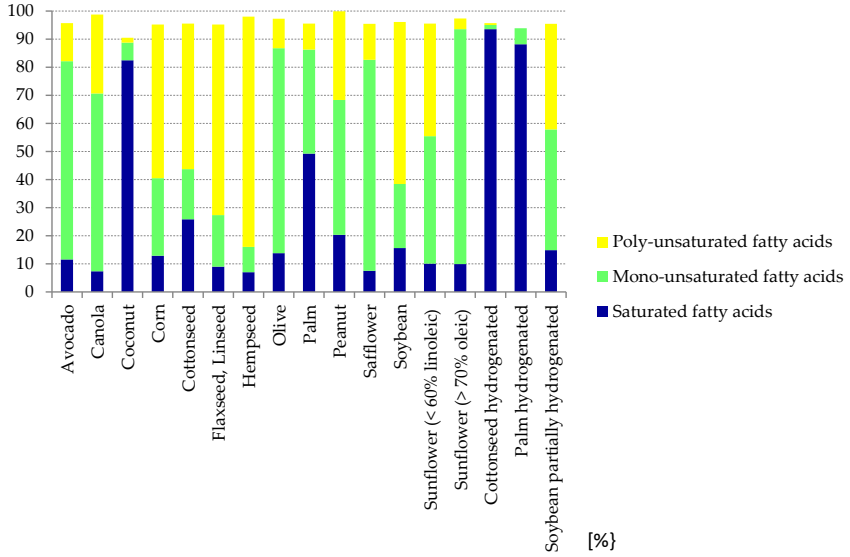

Fig. 1.1. Fatty acid composition for vegetal oils [79], [26]

Weaknesses are often related to the chemical composition of these oils that consists of mixtures of unsaturated fatty acids (Fig. 1.1.), having a great influence in reducing the reliability of oils used as lubricants:

- low viscosity as compared to mineral and synthetic oils [61], [9], [53], [63],
- oxidation and low chemical stability [25], [82]; there is a correlation between the degree of unsaturation of vegetal oils and their oxidative stability [58];
- sensitivity to humidity,
- lower temperature range than mineral and synthetic oils [45],
- many of the properties of vegetal oils are more time-dependent than those of mineral and synthetic oils,
- poor properties at lower temperatures for vegetal oils than other lubricants [83],
- low limits in severe regimes when testing on 4-ball machine [30], [16].

Opportunities are:

- complying with stricter environmental requirements reduces the risks of pollution and disease,
- the high risk of depletion of oil resources and the need to replace them is an issue that needs to be addressed for the global economy.

Threats include:

- the need to redesign equipment that use biofluids, a solution that will certainly increase their price,
- the accepted decrease of certain parameters of system operation (especially load and maintenance, not limited to them),
- the still high price,
- the diversity of environmental protection and safety specifications and a global policy that it did not clearly address environmental issues.

1.2. Nanoadditives for lubricants

The formulated lubricants based on vegetal oils used high-performance additives, similar to those for petroleum-based oils, which are largely non-polar, while triglycerides are extremely polar. Thus, conventional additives used for petroleum-based oils have problems when added to vegetal oils. Frequently, a dispersing agent must be used.

Vegetal oil lubricants require special care to increase their service life. It should also point out that water in any existing lubrication system is not a positive factor at all, for several reasons, including the fact that many additives will deteriorate, increasing acid formation, damaging seals, creating rust and accelerating wear. Most fluids based on vegetal oils are more susceptible to hydrolytic degradation, the result of which may be acid formation, more susceptible to additive precipitation and, as mentioned above, are prone to oxidative instability.

However, stocks of oilseeds (rapeseed, soybean etc.) have increased over the last decade, new chemical additives have improved, and in lubricant formulation knowledge have allowed for developing biodegradable research products with similar or better performance than conventional oil fluids.

Nanoadditivation could increase the size of the load in the lubricant, such as hexagonal Bohr nitride (70 nm) in SAE 15W-40 diesel engine oil [1]. A concentration of 0.3% volume of surfactant (oleic acid) was added to prevent sedimentation of the nanoparticles. The load's increased from 196 N to 1570 N, were applied, each test lasting 10 seconds.

Based on the recent literature [67], [66], lubricant additives can be grouped as in Table 1.1. Multifunctional additives in vegetal oils are of particular interest, as they can provide an improvement in several characteristics, in particular viscosity and oxidation stability.

Table 1.1. A classification of additives for lubricant, after [58], [66] [78], [69], [90], [56], [18]

Modifiers of chemical properties	**Modifiers of physical properties**	**Anti-wear and friction modifiers**		**Extreme pressure additives**
		Inorganic	**Organic**	
•deposit control additives •anti-oxidation additives •detergents •anti-toxicity agents •biodegradabi-lity promoters	viscosity control additives poor point depressants anti-foaming additives dispersants	metal [41], [43], [46] salts oxides (metallic or not) carbonic materials	amides imides amines organic polymers (methacrylates) carboxylic acids and derivatives stearic acid and esters, phosphoric acid	ZDDP sulfurized isobutene fatty oils and olefins sulfurized synthetic esters sulfurized fatty oil+olefin

1.3. Issues related to vegetal oil additivation

The number of additives compatible with vegetal oils, synthetic esters or polyalkyl glycols is small as compared to the number of additives compatible with basic mineral oils [91]. A package of additives for vegetal oils may contain: detergents, dispersants, anti-corrosion and anti-oxidants, anti-foaming agents, viscosity modifiers and anti-wear additives, depressurizers for the poor point. It is difficult to determine the synergic influence of such a package of additives, but the additives must be ash-free (containing Ca, Na, K, Mg and not other metals) and also not be toxic [37], [33].

Problems related to the nanoadditivation of vegetal oils are generally related to:

- concentration, shape and size of nanoparticles,

- compatibility with oil composition,
- chemical and physical stability in time and at parameters of the operating regime,
- agglomeration, sedimentation and dispersion of nanoparticles,
- poor additivation caused by water that could be present in any lubrication system; water also increases acid formation, sealing damage, rust generation and accelerated wear. Most bio-fluids are sensitive to hydrolytic breakdown, and the result can lead to acid formation and additive precipitation.

Reviews on lubricant additives appear in the literature [69], [78], [4], [76], but only some of them deal with the influence of nanoadditives in vegetal oils, the results being insufficient satisfactory as compared to the additivation of mineral and synthetic oils. The additivation of nanoparticles to a base oil (mineral, synthetic, vegetal) is a promising approach for improve characteristics, such as abrasion and wear resistance, thermal and chemical resistance, but the literature has not given any clear recommendations on the formulation and the use of new additive lubricants, without laboratory tests, especially those that could provide data that can be compared to conventional additives.

Small particles with the size of nanometers, such as graphite and graphene [16], boron nitride [1], [44] natural and synthetic minerals, MoS_2 [13], WS_2 [3] and polytetrafluoroethylene (PTFE) [28], have been used both as additives in lubricants and as solid lubricants. These particles tend to deposit, so their size and tribological properties decrease in the presence of moisture and oxygen, which leads to a limit of their applications [70]. Tests have been performed on the addition of nanoparticles with sizes between 2 and 120 nm in lubricants, as friction modifiers, to effectively reduce wear and friction. In particular, nanoparticles based on carbon compounds, metal, metal oxides, metal sulfides, metal borates, metal carbonates, rare earth compounds and SiO_2, have been tested [8], [75], [7] and their tribological performance as friction modifiers depends on the degree of crystallinity, size, shape, and concentration [78].

The additivation of vegetal oils is still at the beginning. For the most of additives, only mineral and synthetic oils have been studied. There are two trends regarding the additivation of vegetal oils:

- to use the same additives as for the above-mentioned oils,
- to formulate new additives based on the particular characteristics of vegetal oils.

The concentration of nanoadditive in the base oil strongly influences the tribological properties, but to determine the optimal value is quite difficult by theoretical methods. That is why it is recommended to do on laboratory tests. Because there are many tribological properties that can be affected by additives, the engineer must accept a compromise: optimize one parameter (one of great interest), improve other parameters and make the induced effects acceptable. For example, nanoadditives can reduce wear, but also may the value of the friction coefficient and the temperature in contact. Tests can adjust this system approach when performed with parameters in the actual application range.

There are also researchers who have included metal oxides in the category of extreme pressure additives [35], but due to their weak chemical activity on substrates and the fact that the layers are not continuous and stable in time, these additives could be considered rather as belonging to the category of friction and wear modifying additives.

Although many authors have written about the formation of a smooth, compact film formed on the worn surface, responsible for reducing friction and wear, recent reports and SEM investigations reveal that this formed film is not continuous, often just an unstable layer of powder, composed of nano-plates, laminated or not [15], [16], [85].

Tests on vegetal oils are reported in the literature, but the results are far from comparable and useful for industrial-scale applications. Information about the behavior of these vegetal oils, after testing on the 4-ball machine, is interesting, because it is possible to compare vegetal oils, additivated or not, with those already used, mineral or synthetic [39], [30], [12].

1.4. Mechanisms of nano additives for reducing friction and wear

Wu [84] proposed a model that takes into account the concentration of the additive (Fig. 1.2 and Fig. 1.3). Although the model was created for the use of TiO_2 as an additive in water, it can also be use to explain the behavior of lubricants with other nanoparticles (metal oxides, carbon-based materials etc.). The mechanism of lubrication with nanoadditives has also been described by other researchers [85], [16].

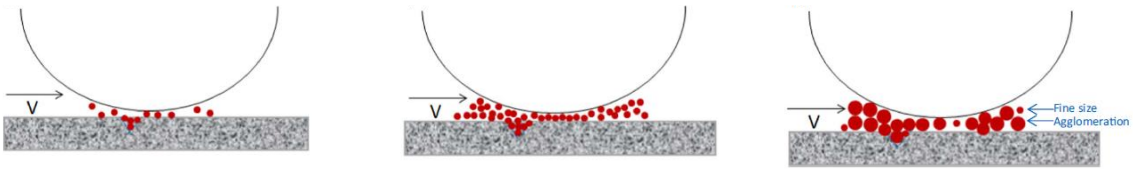

Fig. 1.2. Effect of particle size [84]

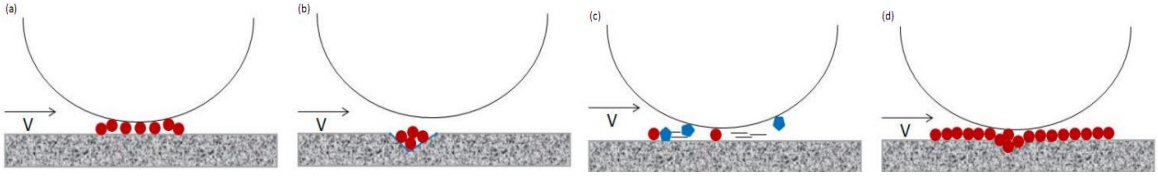

Fig. 1.3. Lubrication mechanisms when using nano particles in lubricants [84]

Figure 1.4. given SEM images of wear scars, of the tested balls on the 4-ball machine for rapeseed oil additivated with 1% TiO_2, at a sliding speed of 0.69 m/s and for loads F=100 N,F=200 N and F=300 N [16]; the dispersion of nanoparticles is not uniform, and some particles agglomerate, having dimensions of the order of microns.

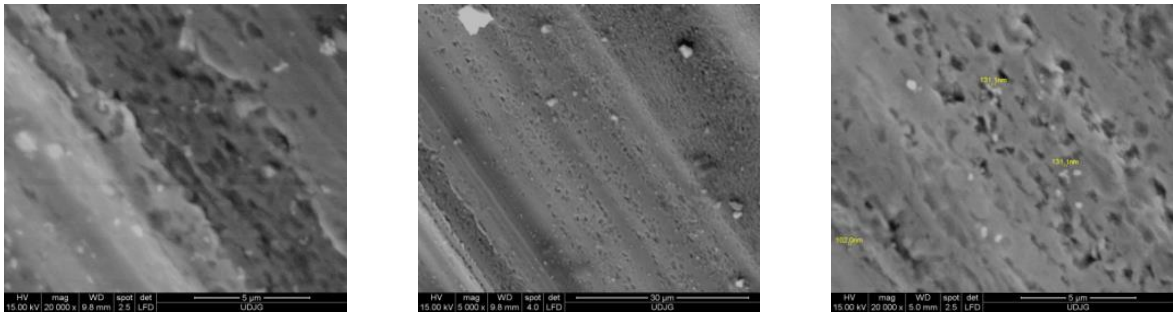

a) F=100 N b) F=200 N c) F=300 N

Fig. 1.4. Wear scars with particles of TiO_2, after testing the rapeseed oil with 1% TiO_2, at v=0.69 m/s [16]

Solid lubricants are added to the oils to reduce friction and wear. This group of friction modifiers includes carbon-based materials (fullerenes, nanotubes, graphite, graphene etc.), but also tungsten and molybdenum sulfides, fluorinated polymers [78]. Solid lubricants (micro or nano) help in the situation where the sliding surfaces have a rougher texture, "leveling" the profile of both surfaces. They are recommended in lubricants for mutual movements (in the case of the piston ring), producing a reduction in wear. They are generally added to lubricants that come in contact with surfaces with which high-pressure additives cannot react chemically, such as polymers and ceramic materials and some of their composites [66].

Vegetal oils have an excellent lubricity, much higher than that of mineral oil [6]. The polarity of vegetal oils improves its anti-wear characteristics, as they have an affinity for metals and protect the surface. Some refined, discolored and deodorized vegetal oils (RBD) have passed the wear tests by the test method on a hydraulic pump, according to ASTM D2882 and ASTM D2271 standards, in the natural state, without additives. These non-additivated oils decompose thermally due to their oxidative instability, but work well in wear tests [58].

1.5. Metal oxide nanoparticles in lubricants

Various metal oxides are used as additives in lubricants. The most commonly used would be TiO_2, CuO, Fe_3O_4, ZnO, Co_3O_4, and $Al2O_3$ [81], [68], [47], [42]. Their lubrication mechanisms are similar to those of nanomaterials containing metals, including the formation of tribo-films or adsorption films, the rolling effect and the agglomeration or repair effect. An example would be the use of spherical CuO and TiO_2 nanoparticles as an additive in lubricants, having a very good behavior in reducing friction and wear, especially for CuO nanoparticles [40]. The reduction of friction can be explained by the rolling effect, and the wear mechanism is associated with the deposition of CuO

nanoparticles on the friction surface, which can reduce shear stress and improve tribological properties. Table 1.2 shows several studies in which TiO_2 is used as an additive to reduce friction and wear and Table 1.3. presents studies using ZnO as additive.

The anti-wear behavior of the additive nanoparticles can be attributed to the tribo-agglomeration mechanism in the valleys of the texture.The nanoparticles are deposited on the friction surface and fixed on the surface texture.

Table 1.2. Research and publications with TiO_2 as an additive

Authors/ Year/ Reference	Lubricant			Tests				Results	
	Base oil	Additiv						Wear reduction	Friction reduction
		Size	Concen-tration	Tester	Load	speed	Oil tempe-rature	Observations	
[68]	mine-ral	20-25 nm	0.25wt%	4 balls	14,7 N	0.05 m/s	Room temperature	21%	
[86]	oil in water	30 nm	0, 0.5, 2, 4, 6 wt%	Ball on disk	50 N	50 mm/s	80 ºC	significantly reduced	
[34]	Water-based cutting fluid	20 nm	0,1-1,6 wt%	4 balls	147 N	1440 rpm		34.8%	From 0.17 to 0.04
[52]	Multigrade motor oil	10-25 nm	1.5 wt%	Pin on disk	40, 60, 90 N	0.5, 1 şi 1.5 m/s		significantly reduced	
[39]	Base oil API 1509	50-100 nm	0.1, 0.2, 0.3 0.4, 0.5 wt%	4 balls/ball on disk	100 N		75 ºC	reduced compared to the base oil	
[90]	Trimethyl propane ester/palm oil		0.1 wt%	4 balls	160kg	1200 rpm	Room temperature	11%	15%

Table 1.3. shows some studies in which ZnO is used as an additive to reduce friction and wear.

Authors/ Year/ Reference	Lubricant			Tests				Results	
	Base oil	Additiv		Tester	Wear reduction Load	Friction reduction speed	Oil temperature		
		Size	Concen-tration					Observations	
[69]	Mineral, PAO, sunflower, soybean	11.71 nm	0.5%	Back and forth movement	10 N		50 ºC	Efficient with mineral oil	
[47]	lubricant	4.04 nm	1.2 wt%	Pin on disk	392 N	1200 rpm	75 ºC	31.2%	9.9%
[57]		24 nm		Ball on disk	5 N	5 cm/s	25-400 ºC	Not significantly changes of COF	

In tribology, it has been anticipated that these metal oxide nanoparticles have good lubricating properties, when used as additives in lubricants for the following reasons:

- metal nanoparticles are so small that a stable colloidal dispersion in oils can be obtained by appropriate methods, which can avoid precipitation caused by gravity,
- when forming a stable, well-proportioned dispersion, the metal nanoparticles are more likely to be trapped on the friction surface,
- metallic nanoparticles can be deposited on the friction surface.

1.6. Conclusions

From the studied literature [69], [78], [5], [76], there is a research trend regarding the additivation of vegetal oils, especially for lubrication. The addition of nanoparticles (TiO_2, ZnO) may improve the tribological properties of vegetal oils. Friction is not always reduced, but the increase of the friction coefficient is acceptable because it is accompanied by a substantial reduction in wear. The focus should be done on the dispersion of the nanoadditive and the selection of dispersant.

The reported results are still inconclusive and the applications of these oils are based more on market inertia or practical user experience. Despite the benefits of using the additive nanoparticles, there are also challenges related to their applications, which could be investigated in future research:

- preparation and maintenance of homogeneous mixtures of particles and oils; the van der Waals force between the particles causes them to aggregate into solutions; therefore, various modification techniques for the stabilization of nanoparticles in vegetal oils should be investigated to produce physically and chemically stable lubricants,
- testing under appropriate conditions, closer to future applications,
- reporting results in a way that allows data to be compared and interpreted in order to introduce actual tribological systems.

The additivation of vegetal oils is still in its infancy, as the reported results are not effective yet, when these lubricants compared to the additivation of the classic alternative-mineral oils and even less, when compared to synthetic oils. But research needs to continue as these vegetal oils become an actual resource for basic lubricant stocks.

1.7. Research directions

Rapeseed oil is produced in Romania and is an environmentally friendly resource for oils.

The aim of the thesis is to improve the tribological behavior of nanoadditivated rapeseed oil, based on tests on the 4-ball machine through which the performance of the lubricants formulated by the author can be compared to other mineral or synthetic oils.

The author aims to:

- design a laboratory technology for additivating rapeseed oil with nanoparticles of ZnO and TiO_2,
- formulate a test plan that includes two regimes, normal operating regime and severe regime, based on a set of variables (nanoadditive concentration, sliding speed and load) on the 4-ball triboster.
- evaluate the tribological behavior by analyzing several tribological parameters (friction coefficient, wear scar diameter, the wear rate of the wear scar diameter, texture quality of worn surfaces by roughness parameters).

Chapter 3

Stress and strain assessment on the four ball system with the help of a simplified model

3.1. Elasto-plastic contact with normal load

The plasticity theory tried to bring the theoretical response of a solid body model closer to the actual response, to use it in evaluating the deformation processes, behavior of soils, wood and, more recently, composites, subjected to limit loads. Unlike Hooke's relation, that supposes a relation of direct proportionality between stress and strain, in the elasto-plastic field the relation between stress and strain is nonlinear, usually mathematically modeled on experimental data and of a simpler or more complex form, depending on the influencing factors taken into account (temperature, strain rate etc.). Given the multitude of materials, structures and demands, a valid general model is difficult to achieve and impractical. Therefore, in this study, the author evaluates the behavior of the material the balls are made of, with a bilinear hardening model, based on experimental data reported in literature [36], for the same steel grade, 100Cr6, hardened up to 65 HRC.

For hard steels, as is the case of ball bearing steel and taking into account experimental data, the yield strength can be considered identical to the elastic limit.

A hypothesis is very important when talking about an elastio-plastic contact, namely that the elastic properties are independent of the plastic behavior, which implies the cumulation of the elastic effect with the plastic one:

$$\varepsilon = \varepsilon^e + \varepsilon^p \tag{3.1}$$

where ε^e represents the elastic strain and ε^p represents plastic strain. At the same time, the modulus of elasticity will be considered as remaining constant.

The issue of elasto-plastic contact can be formulated by an elastic problem over which a plastic (residual) problem overlaps.

When the applied load causes stresses that exceed the proportionality or yield limit, in certain zones of the bodies in contact, a stress state occurs, for which the equivalent stress exceeds the elastic limit value of the material, resulting in:

- the appearance of a field with plastic strains, obviously remaining after unloading,
- the plastic imprint increases the contact conformability, and, thus, reducing the local stress,
- the change of the contact geometry leads to the change of the stress distribution on the contact surface and, implicitly, in the volume around it.

3.2. Models and simulations for sphere-sphere or sphere-plane contact

Existing studies [87] showed that, as compared to the elastic contact, the contact solution for the elasto-plastic contact has two main characteristics: the maximum contact stress was lower and the contact radius was larger as compared to simply elastic models.

Hardy [38] assumed that when, a plastic strain occurred in the contact area, the maximum contact stress tended to be constant. This implies the existence of a limit value of the maximum contact stress in the elasto-plastic contact, which is proportional to the yield limit of the materials in contact. In addition, Thornton [80] developed the methods adopted by Johnson [48] in studying the

impact between a sphere and a plane, and established a segmented model of contact stress distribution.

An example of elasto-plastic contact between two spheres is given based on Zhao's model [89], in the elasto-plastic domain, and the influences of material parameters, contact radius and normal external loads on the accuracy of the proposed method are discussed by comparing the differences between the numerical results by the finite element method and those obtained by the proposed method, which can accurately calculate the maximum contact stress and contact radius in the elasto-plastic contact; the relative errors, both of the maximum contact stress and of the contact radius, are within ± 5% [89].

The equivalent stress (von Mises stress) represents, in the case of the analyzed material, the transition from the elastic domain to the plastic domain, domains that have different mechanical properties and its value is given by the formula:

$$\sigma_{ech}^2 = \frac{1}{2}[(\sigma_{11} - \sigma_{22})^2 + (\sigma_{22} - \sigma_{33})^2 + (\sigma_{33} - \sigma_{11})^2 + 6(\sigma_{23}^2 + \sigma_{31}^2 + \sigma_{12}^2)] \quad (3.2)$$

where σ_{11}, σ_{22}, σ_{33} are the main stresses and σ_{12}, σ_{23}, σ_{31} are the shear stresses.

3.3. The proposed model

The model is a simplified isothermal model of the 4 ball tribotester. The simplification consists in the fact that the model is made up of only two balls, but the position of the balls is the actual position on the tribotester, the load being also applied in the vertical direction and offset by the second ball. The equivalence of the load on this model is done by the displacement printed on the upper ball (rotating ball) and the lower ball (stationary ball), a displacement identical to that obtained from the laboratory tests.

This vertical displacement is approach calculated as follows:

- the position of the contact between the upper and lower ball is determined,

- the displacement between the two balls in the direction of the centers is calculated,

- the projection of the displacement on the vertical axis is calculated; the displacement on the line of the centers of the two spheres is composed of the height of the cap corresponding to the average wear scar, as diameter of the cap (WSD), to which is added the depth of the wear scar, determined by 2D profiles, measured perpendicular to the sliding direction.

The model is run in Ansys (Explicit Dynamics) and the simulation has two stages:

1. the stage of loading of the two balls in static conditions,
2. performing a rotation or a part of rotation, under the load, so that the resulting scar during friction does not overlap with the initial imprint between spheres.

The simplifying hypotheses for this model are:

- isothermal regime, because temperature measurements in the oil bath at the end of the tests showed that the temperature did not exceed 90 ºC, which means that the properties of the hardened steel balls are not affected (ball bearing steel has a tempering temperature of about 300 ºC, up to this temperature; thus the structure and properties of the steel can be considered as not being thermally

influenced),

- the friction coefficient is specific to the boundary or mixt lubrication (COF = 0.08...0.15) as recording by testing,

- modeling without lubrication, as many of the tests, by the measured values of friction coefficient, denote the existence of a mixed regime and, therefore, a lower influence of a partial fluid film,

- perfectly smooth bodies in contact; this can be accepted in this simulation as very small values of the roughness parameters emerge from the profilometric study (see chapter 6),

- wear is not taken into account; this may influence the results of the simulation, but for the assessment of the stress and strain, in severe regime, wear may be neglected; the model can be further developed by taking into account wear. The 2D profilometric study in severe regime shows that the abrasive wear is more observable at low loads and the plastic strain is obvious without a severe abrasive wear, is observable at high loads (850 N, 900 N).

- an elasto-plastic constitutive model for the steel the balls are made of; studying the literature on test and models for hardened steels, the author opted for a bilinear-isotropic model with hardening, based on experimental data provided by [36].

Figure 3.1a presents the stress-strain curve for the AISI 52100 steel, given by Guo [Guo, 2002] and Fig. 3.1 b presents the stress-strain curve for the material model used in the simulation by the thesis author.

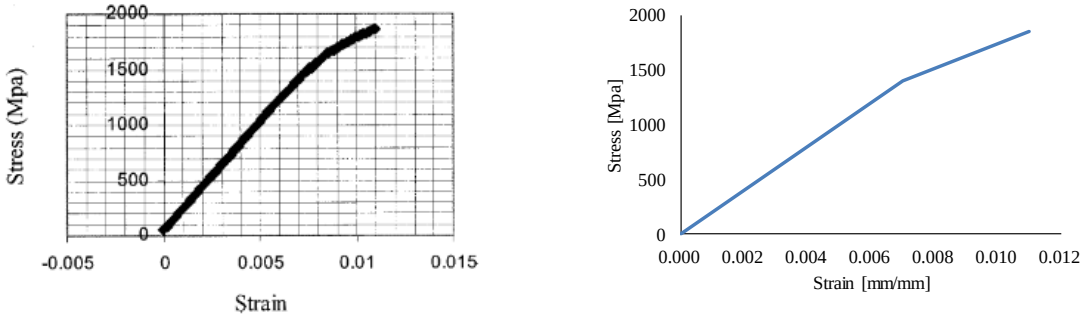

a) b)

Fig. 3.1. a) Stress-strain curve for AISI 52100 steel [36], b) stress-strain curve for the material model, as chosen by the thesis author

The author took into account plastic strains of the order of $3x10^{-3}$… $4x10^{-3}$ (mm/mm) on the model, because, on the stress-strain graph, the plastic strain is considered to start from approx. $5x10^{-3}$ (mm/mm) on the curve of the AISI 52100 material (Fig. 3.1).

The simulation has as variables the friction coefficient and the vertical displacement of the rotating ball, equivalent to the force recorded in the actual test (see Fig. 3.4-Fig. 3.6. and Table 3.3.).

The two spheres in contact are represented in Fig. 3.2 (a). Figures 3.2 (b) and (c) present details of the mesh. The author opted for a finer mesh network of the contact areas on the stationary ball and on a sphere sector corresponding to a band larger than the friction path on the rotating ball. The

number of nodes is 29390 and the number of elements is 155259. The transition ratio between elements is 0.272, while the growth rate of the elements is 1.2. Table 3.1 gives the constitutive model of the ball material proposed by the author, with its properties. Table 3.2 gives the values of the characteristic points on the strain-stress bilinear hardening model for the ball steel.

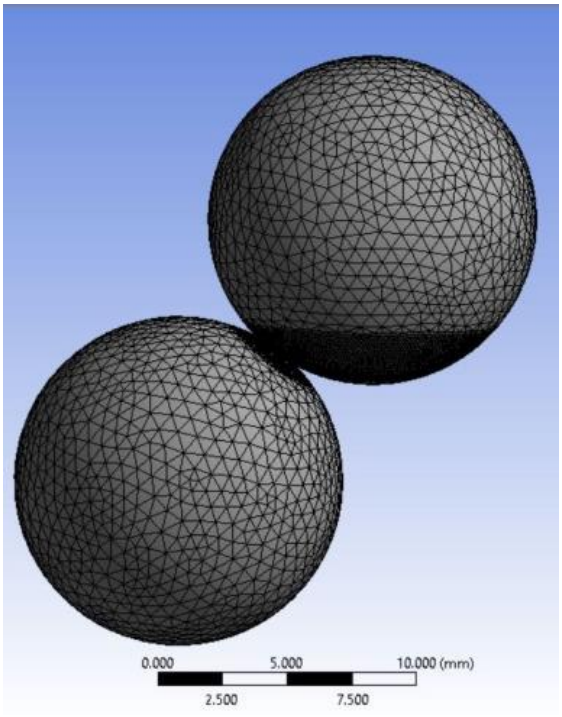

a) model mesh (overview)

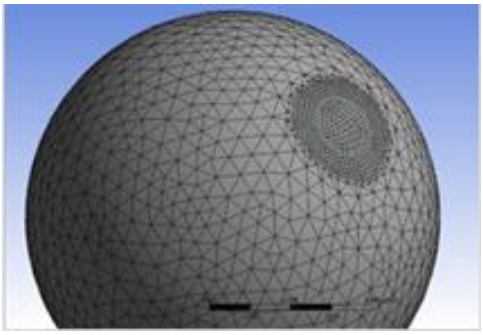

b) fixed (stationary) ball

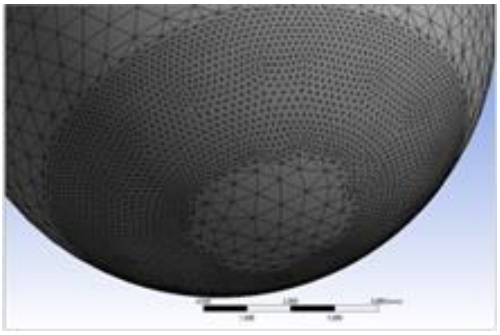

c) rotating ball

Fig. 3.2. Details of contact area mesh

Table 3.1. Material properties (for the model proposed by the author)

Properties	Values
Density [kg·m^{-3}]	7850
Young modulus [MPa]	$2 \cdot 10^5$
Poisson coefficient	0.3
Volum modulus [MPa]	$1.6667 \cdot 10^5$
Shear modulus [MPa]	$0.76923 \cdot 10^5$

Table 3.2. The characteristic points on the strain-stress curve for ball steel constitutive model

Stress [MPa]	Strain [mm/mm]
1	0
1400	$7 \cdot 10^{-3}$
1850	$1.1 \cdot 10^{-2}$

The simulation stages are:

- stage 1, in which a constant-sloping load is applied on the two balls until the displacement in

the z direction of the model is sufficiently close to the actual displacement of the four-ball system,

- stage 2, which consists of performing a complete (360º) for lower loads, or incomplete (300º) rotation, for higher loads, depending on the load (there is no overlapping of the friction path).

Figure 3.3 presents the evolution of maximum values of equivalent stress (von Mises), for the entire simulation on static load + rotation (a) and for the rotation only (b).

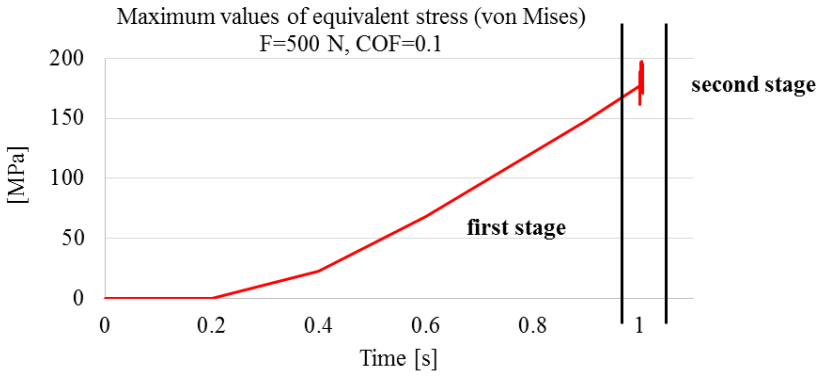

a) Entire time interval for the simulation

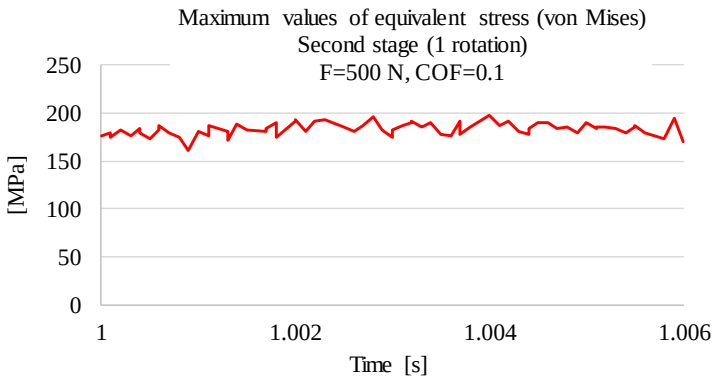

b) Second stage of the simulation

Fig. 3.3. Identification of the simulation stages, here being represented the value of the maximum stress for F=500 N, COF=0.1 (equivalent load to z=0.0065 mm)

The first step of the simulation consists of the static loading of the balls when the force is applied, from each case, from F=500 N to F=900 N, increasing up to the value considered equivalent to the displacement z of the balls in the vertical direction. After the end of this stage, the second one follows, which consists of starting the rotation of the upper ball. It performs a complete rotation in 1.006 seconds (corresponding to the test sliding velocity of 0.53 m/s or 1400 rpm).

In the equilateral triangle $\Delta O_1O_2O_3$ (Fig. 3.4), the height, is given by the formula:

$$H = \frac{O1O2\sqrt{3}}{2} = \frac{2r\sqrt{3}}{2} = 10.985 \text{ mm} \tag{3.3}$$

where O_1O_2=2r.

In ΔMPO_4, $\measuredangle MPO_4 = \measuredangle NO_1O_4 = \alpha$, and $\beta = 180° - (90° + \alpha)$, (3.4)

where

$$\alpha = \arccos\frac{1.15\,r}{2r} = \arccos 0.575 = 54.90\,° \tag{3.5}$$

and r is the radius of the ball, r =6.35 mm. It results β=35.10°

The vertical displacement of the rotating ball, z, (Fig. 3.5) is calculated using the formula

$$z = 2\delta \sin\alpha \tag{3.6}$$

Displacement z became:

$$z = 2\delta \sin 54.90° = 1.636\,\delta \tag{3.7}$$

$$\delta = \frac{z}{2\sin\alpha} \tag{3.8}$$

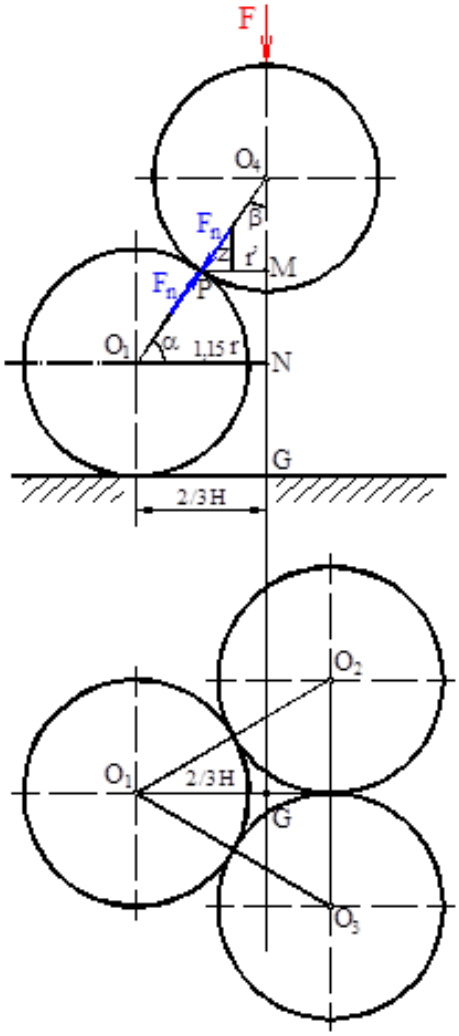

Fig. 3.4. The model geometry

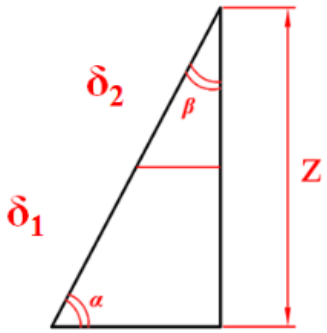

Fig. 3.5. Components of the vertical displacements

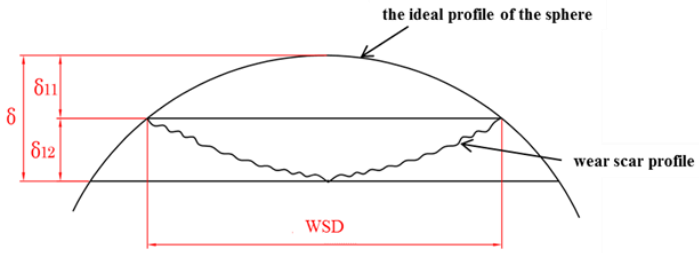

Fig. 3.6. Depth of wear scar, measured on the 2D profile, perpendicular to the sliding direction

In Table 3.3 (measured values for z), δ_{11} is the depth of the wear scar measured on the 2D profile of the ball, δ_{12} is the height of the spherical cap (Fig. 3.60, which is calculated with the relation:

$$A = \frac{\pi(WSD)^2}{4} = 2\pi r, \tag{3.9}$$

and the result will be:

$$\delta = \frac{\pi(WSD)^2}{8\pi r} = \frac{(WSD)^2}{8r} \tag{3.10}$$

The centers of the three non-rotating balls form an equilateral triangle $\Delta O_1O_2O_3$. The weight center of the equilateral triangle, denoted by G, is at the intersection of its heights, at 2/3 of the peak and at 1/3 of the base. The height of the equilateral triangle was noted with

$$O_1G = \frac{2}{3}H = 1{,}15r \tag{3.11}$$

The movement of the balls in the direction of their centers is considered to be a sum $\delta=\delta_{11}+\delta_{12}$ where δ_{11} and δ_{12} are the changes of the simplified ball profiles on the radial direction. In turn, each movement consists of two components:

- the depth of the wear scar measured on the 2D profile, obtained perpendicular to the sliding direction (Fig. 3.8),

- the height of the spherical cap, calculated as the average value for WSD, as measured for the force taken into account in the actual test.

The simulated cases have as variable COF and the vertical displacement of the rotating sphere, which was introduced as a value of the vertical displacement taking into account the actual deformation of the balls.

$$\delta=\delta_{11}+\delta_{12} \tag{3.12}$$

where δ_{11} and δ_{12} are the depths of the wear scars on the two balls in the direction of normal force in contact, δ_1 being the depth of the wear scar in the direction of contact on ball 1, and δ_2 being the depth of the wear scar on the rotating ball, the ball 2; the wear mark on the rotating ball is a circular ring.

The displacement of the rotating ball shall be calculated as the projection on the vertical direction of displacement δ and the angle α, between the vertical direction and the direction of application of the force on the two balls (Fig. 3.5).

Because δ_{11} and δ_{12} are difficult to be measured, they are calculated by considering the WSD, as the diameter of a spherical cap of height δ_{11} and δ_{12}, as measured from tests and 2D profilometry, respectively:

$$\delta_{11} = \frac{\pi(\mathrm{WSD})^2}{4}\frac{1}{2\pi R} \tag{3.13}$$

$$\delta_{12} = \frac{\pi(WSW)^2}{4}\frac{1}{2\pi R} \tag{3.14}$$

where WSD is the average diameter of the wear scar and WSW is the width of the wear scar on the rotating ball, as measured from 3D profilometry.

The geometry of the model is the same, but the displacement of the approach balls towards each other and the friction coefficient are changed. For the same value of δ, three cases are run, each with a different value for the friction coefficient.

Table 3.3. Measured and adopted values for z

Load	WSD	δ_{11} (profile depth as midline)	δ_{12} (height of cap with WSD base)	δ_1	$2\delta_1$	z	z value applied in simulation
[N]	[μm]						
500	354	1.5	2.466	3.96685	7.933701	6.48	6.5
600	426	2.2	3.572	5.772362	11.54472	9.44	9.5
700	687	12	9.290	21.29073	42.58146	34.83	35
850	2582	220	131.234	351,2347	702.4694	574.62	575
900	2692	230	142.654	372,6548	745.3096	609.66	610

Table 3.3 shows the average diameters of the wear scars (WSD), the depth of the profile δ_{11}, obtained from the measurements and geometric parameters, so that the displacement z can be applied in the model. z represents the calculated values of the displacement, the last column of the table being the values applied in the simulations, approximated to the first decimal figure.

Figure 3.7 gives the curve for the displacement z and it is observed that up to 800 N, the value of the displacement slightly increases, but from 850 N. The displacement has higher values, the very high jump being done between 800 N and 850 N.

Figure 3.8 presents 2D profiles on the non-rotating ball of the wear scar, perpendicular to the sliding direction, for different loads, from the smallest analyzed load, F=500 N, to the highest analyzed load, F=900 N. Each profile has its scale, imposed by the soft [92].

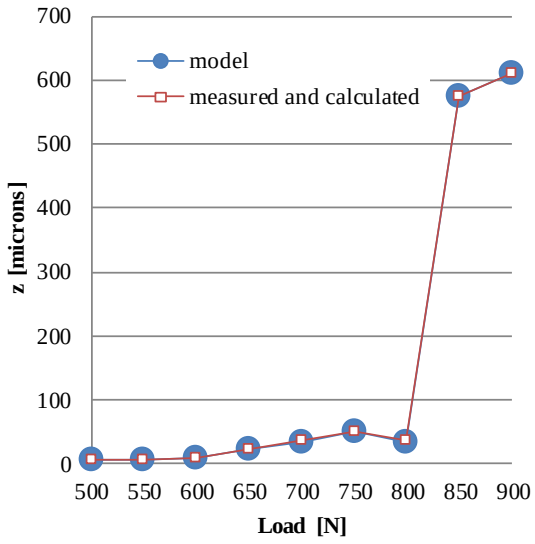

Fig. 3.7. The value of the vertical displacement of the balls, corresponding to the force applied in the vertical direction, in actual tests

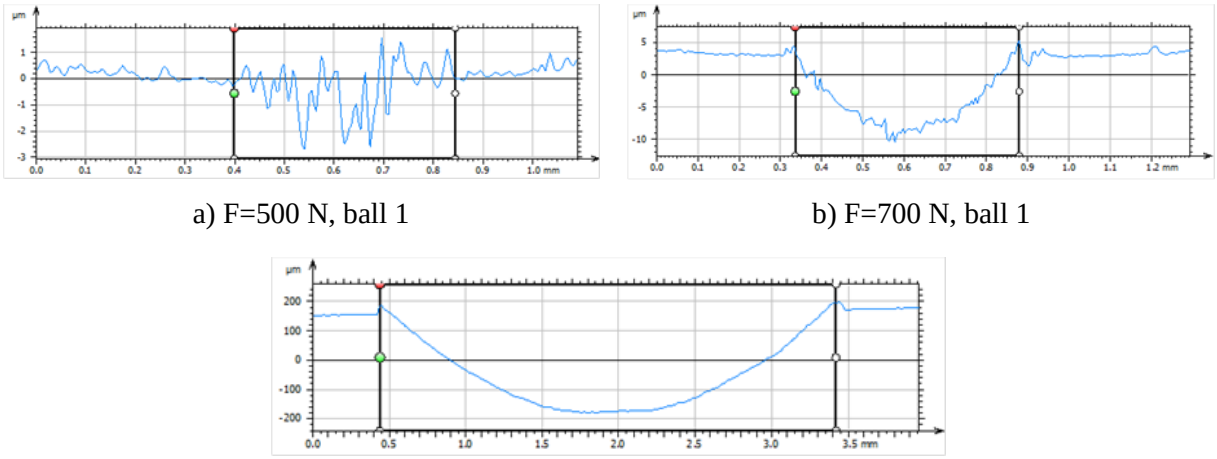

a) F=500 N, ball 1 b) F=700 N, ball 1

c) F=850 N, ball 1

Fig. 3.8. Typical profiles of the wear scar on a 2D profile, measured perpendicular to the sliding direction, for the stationary ball

It is observed that, for F=500 N and also for F=700 N, the shape of the profile indicates a very small depth of the wear scar, the profile revealing rather superficial abrasive wear. For the force F=700 N to F=900 N, a much greater scar depth is observed, without excessive abrasion on the surface, which would suggest a strong plastic strain and a lower intensity of abrasive wear.

3.4 Simulation results

3.4.1. The influence of the COF value on the state of stress and strains

The simulation of sliding ball was done for the following cases: one case without friction (COF=0) and two cases with friction (COF=0.08 and COF=0.1). For each case, the maximum equivalent stress is analyzed, the distribution of stresses and total and plastic strains at the end of rotation are discussed, comparing to the actual values obtained for the wear scars.

Figure 3.9 shows the evolution of the maximum elastic strain in time, for two values of the applied loads, for the stage with relative movement between the balls.

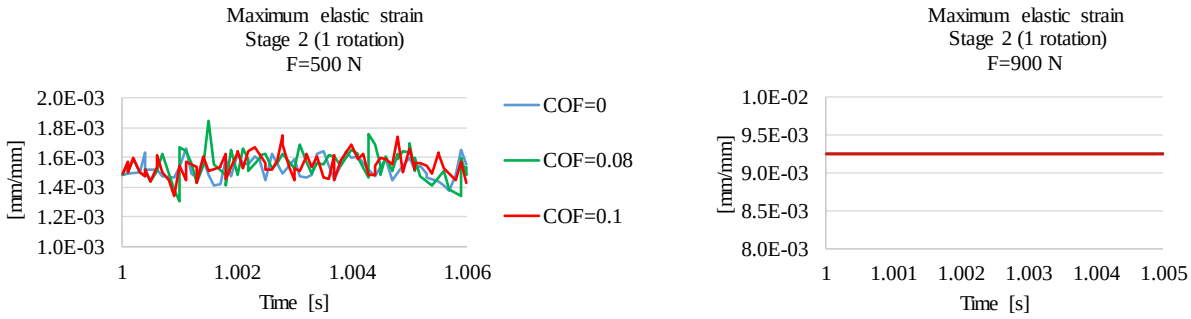

a) F=500 N (δ=6.5 μm) b) F=900 N (δ=610 μm)

Fig. 3.9. The evolution of the maximum elastic strain, on the stationary ball, in time, for the two values of the applied load

According to the theory presented in [27], [14], the total strain can be considered the algebric sum of elastic strain and plastic strain. Therefore, the components of the total strain for the second stage of the simulation the sliding of the two balls, will be further analyzed.

For F=500 N, maximum value of the elastic strain oscillates in a narrow range, characteristic for a sliding contact.

For F=900 N, for all values of COF, it can be seen the maximum elastic strain remains constant, which means that the material has exhausted its linear elasticity domain and entered the plastic domain. The elastic part has a similar behavior regardless of the value of the friction coefficient. The rotating ball pushes the material creating a material threshold in front of the scar, over which it must pass. This process is specific only to the elastic domain of the material. On the first rotation, several peaks of maximum elastic strain were observed, especially for COF=0. For F=900 N, it is observed that the values of maximum elastic strain are constant, suggesting that the maximum total strain will have a plastic component, this being logically based on the overlap of elastic and plastic effects, as explained by Frunză [27] in his work.

The maximum plastic strain values are given in Fig. 3.10. At the load F=500 N, the value of the maximum plastic strain at the end of the rotation is ordered proportionally to the friction coefficient. So, the highest value after a rotation on the non-rotating ball is for COF=0.1.

Due to the lack of friction, the material in front of the contact may be more strongly deformed.

Already, at F=500 N, the maximum plastic strain exceeds the value of 1/1000; the load of 500 N is not recommended for mixed system operation with a friction coefficient between 0 and 0.1. The introduction of the friction coefficient makes the plastic strain more uniform.

The analysis of the simulation results will be done by comparing the values of plastic strain to measured ones. It is observed that the modeling makes possible to notice very small values of plastic strain difficult to measure (bellow 10^{-3} mm/mm). On any image with strain state, values between $3x10^{-3}$… $4x10^{-3}$ mm/mm will be taken into account for measuring the strain countur on the model.

The higher friction coefficient causes an increase in plastic strain. The plastic strain may have close values, not necessarily in the order of increasing the friction coefficient, but the differences are of the order of 10^{-5}, which is a very small value.

The values of the plastic strain already exceed 1/1000 of the ball diameter, so, F= 500 N is not in the load range for normal regime, already representing a severe regime. The strain already appears at the first rotation, when the load is applied on the balls at rest, before the rotation, as it happens experimentally. The slight oscillations of the friction coefficient obtained experimentally can be explained by the small variations of the elastic and plastic strains in time.

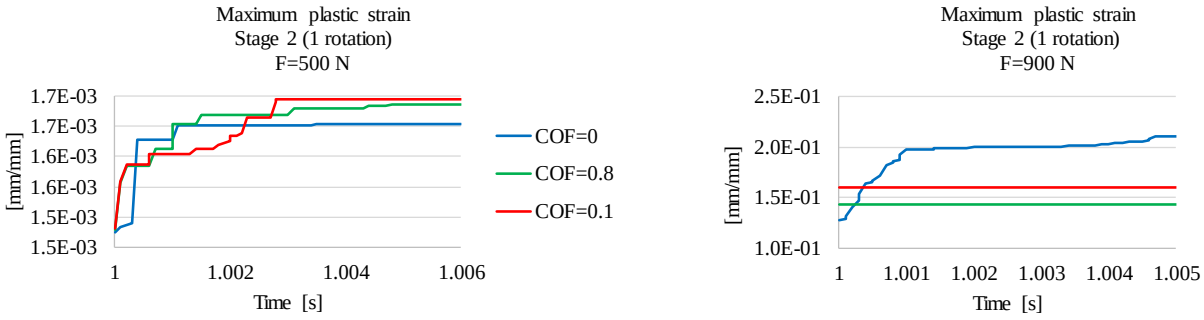

a) 500 N b) 900 N

Fig. 3.10. Evolution of maximum plastic strain, on the fixed ball, in time, for Stage 2 – one rotation

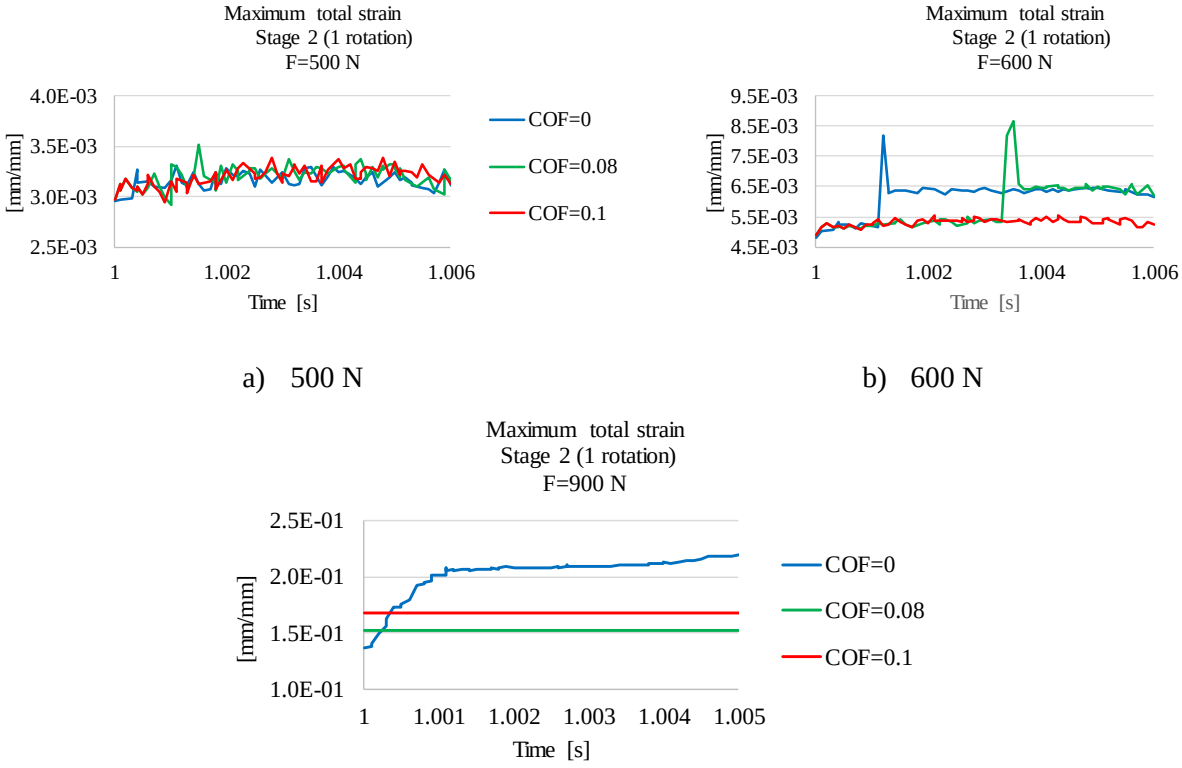

a) 500 N b) 600 N

c) 900 N

Fig. 3.11. Evolution of maximum total strain, in time, stage 2 - one rotation

The maximum total strain in time is shown in Fig. 3.11 and it is based on the principle of overlapping effects, adding the elastic strain and the plastic strain. In the first phase, the material exhausts its elastic strain, then enters in the field of plastic strain, with $\varepsilon_{total} = \varepsilon_{elastic} + \varepsilon_{plastic}$.

The analysis of the maximum values of the equivalent stress (von Mises) is given in Fig. 3.12.

At F=500 N, the range of variation of maximum von Mises stresses (Fig. 3.12) is about the same, regardless of the value of friction coefficient. At F=600 N, when the ball has done its imprint and must rotate, a maximum appears. Two stress peaks were observed, of about the same value (approximately 500 MPa) for COF=0 and COF=0.08. These could be explained by the fact that the upper ball has

already imprinted the lower ball and in rotation, it must pass over the edges of the imprint. The maximum values of the equivalent stress for F=500 N and F=600 N do not exceed the yield strenght. The peaks of maximum equivalent stress correspond to the peaks of maximum total strain.The stress also does not imply a substantial imprint of the wear scar.

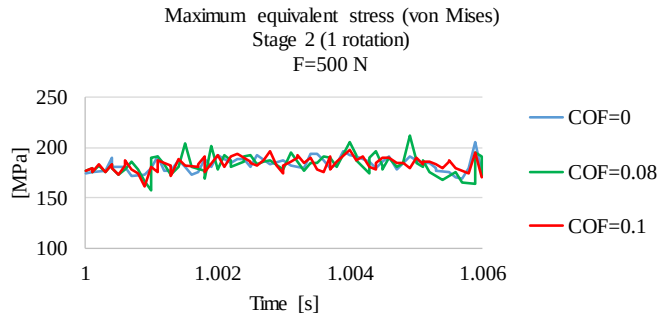

a) 500 N

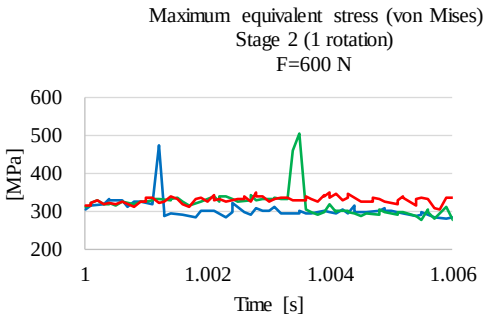

b) 600 N

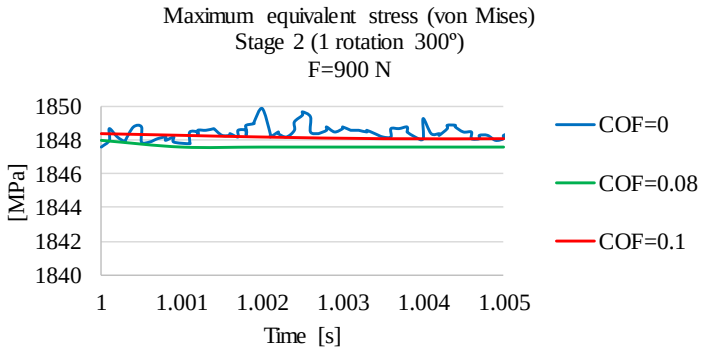

c) 900 N

Fig. 3.12. The evolution of the maximum equivalent stress in time, stage 2 – one rotation

For F=900 N, the stress is constant because the wear scar increases by plastic deformation. For higher values of the friction coeficient, a smaller variation of the stress is observed. The variation of the maximum values of the equivalent stress for the case without friction is 0.119% of the minimum value recorded for this case.

$$\frac{\sigma_{max}-\sigma_{min}}{\sigma_{min}} \cdot 100\% \tag{3.15}$$

Table 3.4 presents the calculated values of the displacement, the average diameters of the wear scars, measured with the help of an optical microscope, but also on the model for all applied forces. Table 3.5 gives the maximum and minimum values of equivalent stresses (von Mises) and their variation for the simulated cases, having as variables the force and the friction coefficient.

The percentage variation of maximum equivalent stress during rotation is the ratio between the variation of equivalent stress and the maximum equivalent stress and it is calculated by the formula:

$$\Delta\sigma_{\%} = \frac{\Delta\sigma}{\sigma_{max}} \cdot 100 \tag{3.16}$$

where $\Delta\sigma$ is the difference between the maximum value of the equivalent stress (σ_{max}) and the minimum value obtained for the equivalent stress (σ_{min}).

Table 3.4. Measured wear scar diameters, displacement value and average variation of WSDs

Case	Load on actual system [N]	z [mm]	Measured WSD (average for one test) [mm]	Measured on the model [mm]	Average variation [%] $(WSD_{real}-WSD_{model}).100/WSD_{real}$
1	500	**0.0065**	**0.354** (0.298…0.389)	**0.4** (0.390…0.410)	-13
2	600	**0.0095**	**0.426** (0.397…0.423)	**0.440** (0.420…0.455)	-3
3	700	**0.035**	**0.687** (0.63…0.744)	**0.700** (0.680…0.720)	-2
4	850	**0.575**	**2.582** (2.5…2.65)	**2.750** (2.6…2.8)	-7
5	900	**0.61**	**2.692** (2.569…2.883)	**2.800** (2.7…2.9)	-4

Table 3.5. The variation of equivalent maximum stresses, depending on the load and COF

Load [N]	COF	σ_{max} [MPa]	σ_{min} [MPa]	$\Delta\sigma$[MPa]	$\Delta\sigma_{\%}$ [%]
500	0	205	170	35	17.07
	0.08	210	158	52	24.76
	0.1	197	161	36	18.27
900	0	1850	1833	17	0.91
	0.08	1848	1833	15	0.81
	0.1	1848	1830	18	0.97

3.4.2. Shear stress analysis

External tangential stress must be taken into account in frictional contacts ($\tau_f=\mu\sigma$). These loads change the state of shear stress.

In Figure 3.13 the shear stress for F=500 N, related to the reference planes are presented, τ_{xy}, τ_{yz} and τ_{xz}, the notation corresponding to the chosen coordinate system, the same for all the run cases. In the first column, there are images with the shear stresses and their values for the simulated case without friction and, in the second column, the shear stresses for the friction case, the value of the friction coefficient being 0.1.In Figure 3.14, for F=900 N, values of tangential stresses, in the case without friction and, in the case with friction, for the reference planes, namely τ_{xy} and τ_{yz}, are almost identical. In contrast, for the reference plane xz, the values of tangential stresses are higher for the friction simulation those in the case with COF=0.

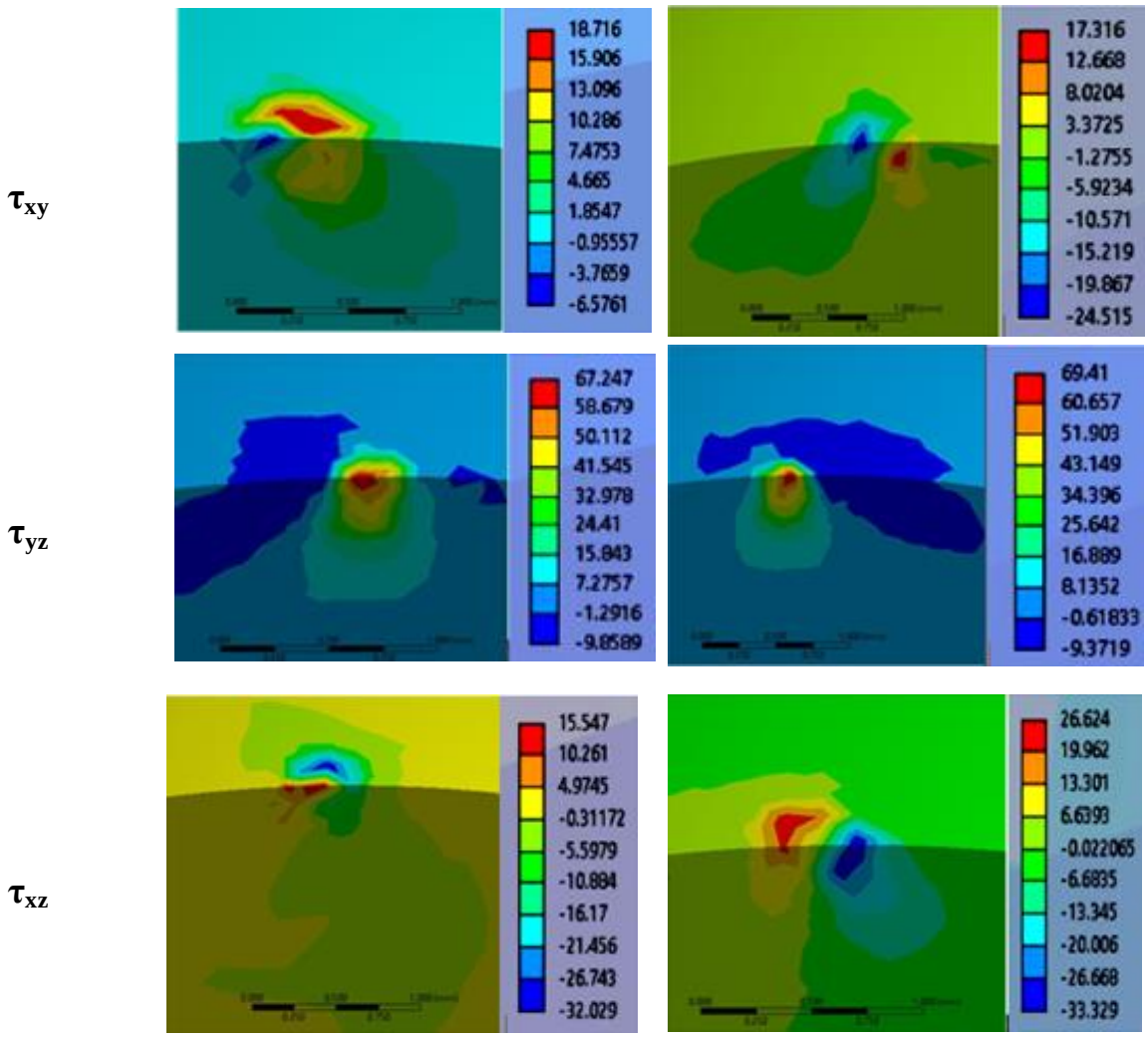

Fig. 3.13. Shear stresses for F=500 N

Analyzing Fig. 3.14, it is observed that the values of the shear stresses, for the force F = 900 N and zero friction coefficient, are a little bit higher than the shear stresses for the case with friction, for all the analyzed shear stresses.

If there is no friction, τ_{xy} retains some symmetry, but the values are higher, τ_{xymax}= 875 MPa.

When friction is simulated (COF=0.1=constant), the distribution for τ_{xy} changes, the maximum area is asymmetricized and the concentration appears in the half front of the contact and right in front of it. For F=900 N, the difference between the maximum shear stress values for the simulated extreme cases (COF = 0 and COF = 0,1) is:

$$\Delta\tau_{xy} = \frac{\tau_{xy(COF=0)} - \tau_{xy(COF=0.1)}}{\tau_{xy(COF=0)}} = \frac{875-681}{875} \cdot 100 = 22\ \% \qquad (3.17)$$

as compared to the value for COF=0.

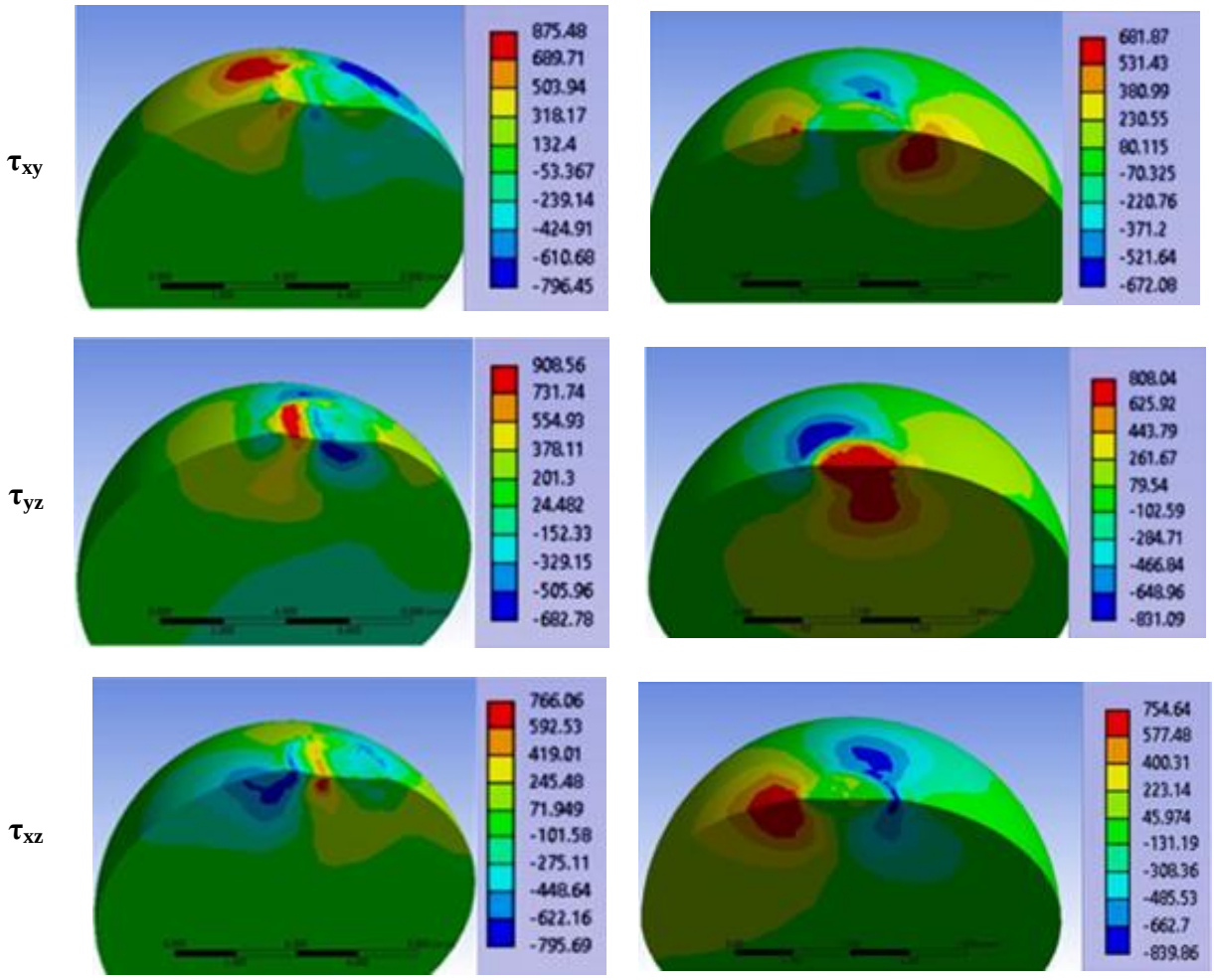

Fig. 3.14. Shear stresses for F=900 N

τ_{xz} has the lowest values as compared to the other shear stresses, but with the smallest variation

$$\Delta\tau_{xz} = \frac{\tau_{xz(COF=0)} - \tau_{xz(COF=0.1)}}{\tau_{xz(COF=0)}} \cdot 100 = \frac{766-754}{766} \cdot 100 = 1.56\ \% \tag{3.18}$$

The area of distribution of maximum values appears in front of the contact, just outside it, which would explain the strong plastic strain in front of the contact.

τ_{yz} has high values for the case without friction, $\tau_{yz\ (COF\ =\ 0)}$=908 MPa as compared to the same shear stress taking friction into account, $\tau_{yz\ (COF\ =0.1)}$=808 MPa.

The highest difference for τ_{yz} is given in the formula:

$$\Delta\tau_{yz} = \frac{\tau_{yz(COF=0)} - \tau_{yz(COF=0.1)}}{\tau_{yz(COF=0)}} \cdot 100 = \frac{908-808}{908} \cdot 100 = 11.01\ \% \tag{3.19}$$

3.4.3. The influence of load on the behavior of the model

Figure 3.15 presents the evolution in time of the maximum values of von Mises stress. In the first stage of static loading of the simulation, in the time interval (0-1), for the case without friction and for the case with friction (COF=0.08 and COF=0.1) at lower loads, F=500 N and F=600 N, the values

of the equivalent maximum stress vary in the same range, from 0 to 500 MPa. The graphs for these cases are very similar, the stress values not exceeding the value of the yield limit. For F=700 N, for both cases with friction, but also for the case without friction, the oscillation interval is about the same, the maximum value of the equivalent stress reaching up to 1500 MPa.

For F=850 N and F= 900 N, the maximum value of the equivalent stress reaches the value of 1850 MPa.

The same situation is in the second stage of the simulation, between 1-1.005 seconds, where it is noticed the same oscillation intervals for the maximum equivalent stress, with the mention that, for F= 600 N some peaks appear, a sign that the material is still in the elastic field.

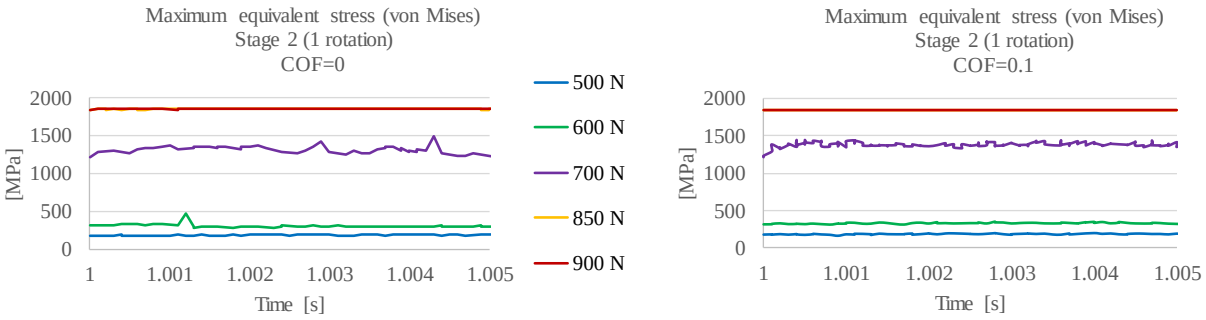

a) COF=0 b) COF=0.1

Fig. 3.15. The influence of the friction coefficient on the evolution of maximum equivalent stress in time, stage 2-one rotation

In Fig. 3.16, the influence of the load on the state of elastic strain is given.

In the second stage of simulation (the rotation), peaks of elastic strain, for F=600 N and F=700 N are observed, are observed, resulting from the local deformation of the material.

In cases with friction, a scratch of the graph of maximum values of elastic strain for F=600 N and F=700 N is observed. For F=850 N and F=900 N, the graphs are perfectly superimposed on each other (Fig. 3.16).

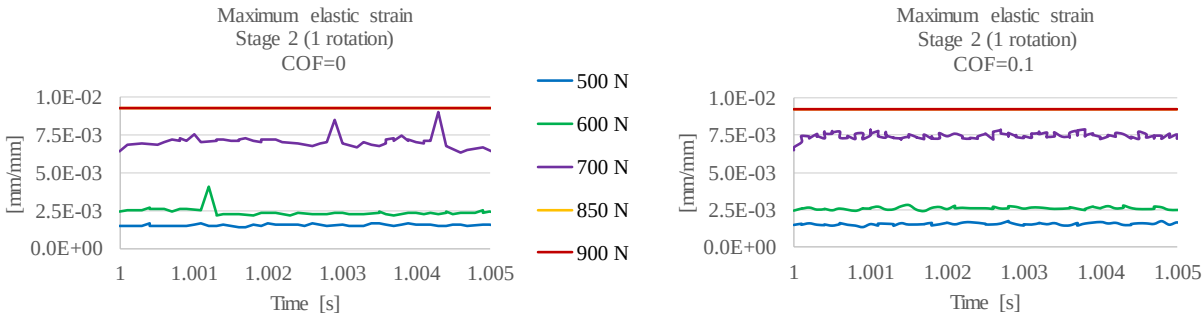

a) COF=0 b) COF=0.1

Fig. 3.16. Influence of COF on the distribution of maximum elastic strains, stage 2 - one rotation

Figure 3.17 shows the influence of load on maximum plastic strain. If it is analyzed the forces of 500 N, 600 N and 700 N, it is noticed a similar evolution, for the case where there is no friction, and for the case with friction, for both stages of the simulation. However, for F=700 N, slightly higher values of maximum plastic strain are observed those for the loads F=500 N and F=600 N.

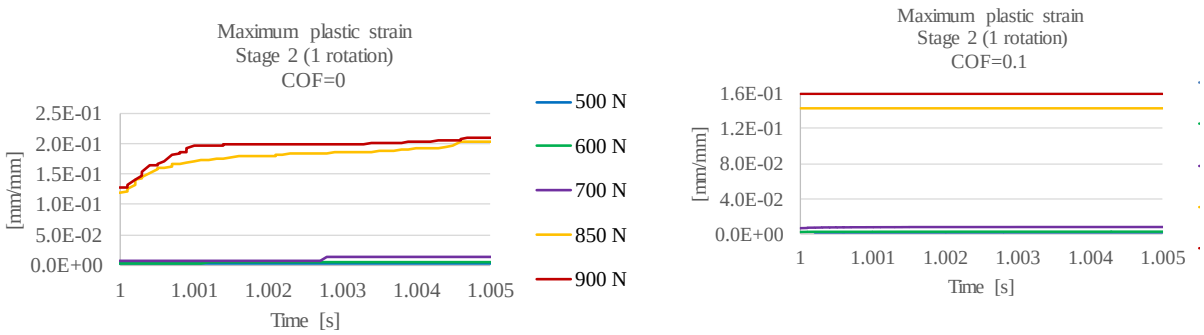

a) COF=0 b) COF=0.1

Fig. 3.17. Influence of COF on the state of maximum plastic strain, stage 2 - one rotation

At high loads, much higher values of plastic strain are observed, reaching $2.5x10^{-1}$ mm/mm for the case without friction, in the first stage of simulation. Even in the second stage of the simulation, the maximum plastic strain is higher in the case without friction that in the case where COF≠0.

Figure 3.18 shows how the friction coefficient influences the distribution of equivalent stresses at the end of the rotation. Only the cases for COF=0 and COF=0.1, for the load F=500 N, were analyzed. The equivalent stresse values for both simulated cases are relatively similar.

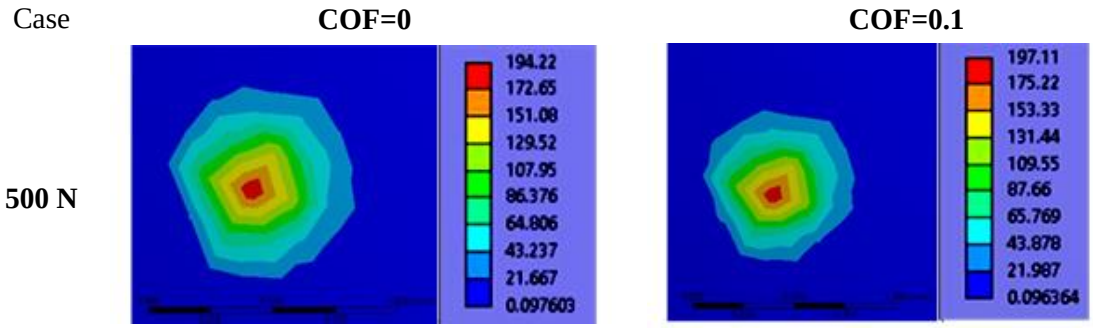

Fig. 3.18. Influence of the friction coefficient on the distribution of equivalent stresses (in MPa), on the stationary ball, for F=500 N. The rotating ball performed an angle of rotation equal to 360º

For F=700 N, the values of the maximum equivalent stress reach~1042.7 MPa for the stationary bal land it is obvious that equivalent stress is near the yield limit (Fig. 3.19)

In the case without friction (Fig. 3.20), but also in case with friction, for F=900 N, values of the equivalent maximum stress is 1843.7 MPa, but in the elasto-plastic domain.

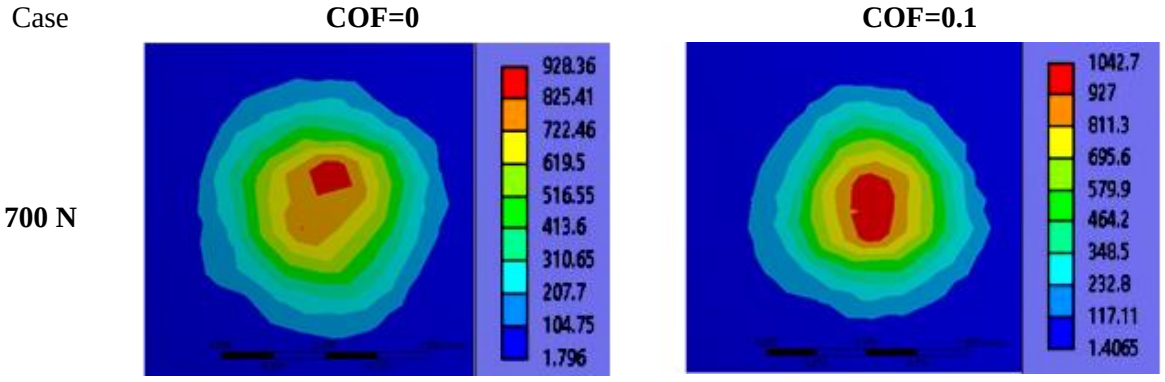

Fig. 3.19 Influence of the friction coefficient on the distribution of equivalent stresses (in MPa), on the stationary ball, for F=700 N. The rotating ball performed an angle of rotation equal to 360º

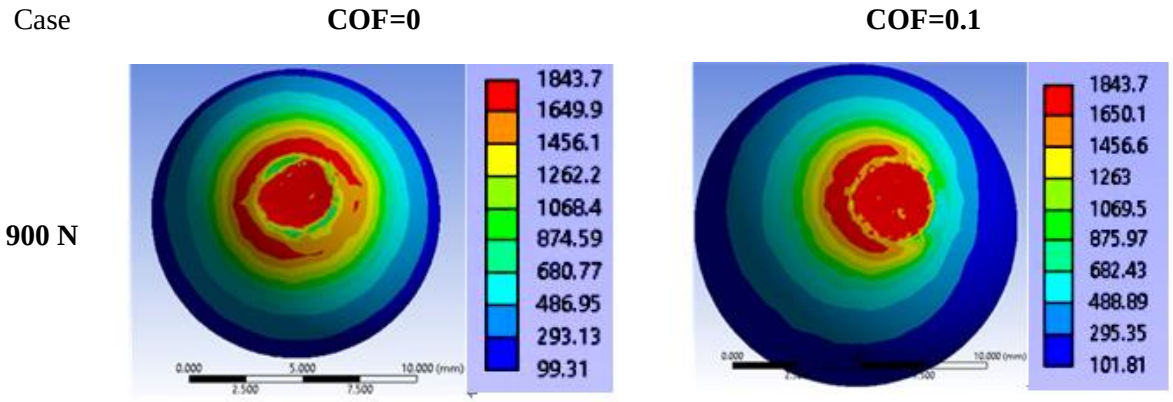

Fig. 3.20. The influence of the friction coefficient on the equivalent stress distribution (in MPa), for F = 900 N. The rotating ball performed an angle of rotation equal to 300º, (stationary ball)

Figure 3.21presents wear scars, virtually re-built with the Mountains SPIP 8.1 software, for ball 1, non-rotating, of a set of balls tested in non-additivated rapeseed oil. The testing was done for loads of 500 N, 600 N, 700 N, 850 N and 900 N, and the sliding speed was 0.53 m / s. The testing time was 60 s, and the test regime was severe. Wear scars are similar to those determined on the ball, in the sense that the wear scars on the fixed ball are not symmetrical, the explanation being the position of the balls in the tribotester and the sliding direction, and for high loads, the profilometry shows strong plastic strains accompanied by the formation of outline.

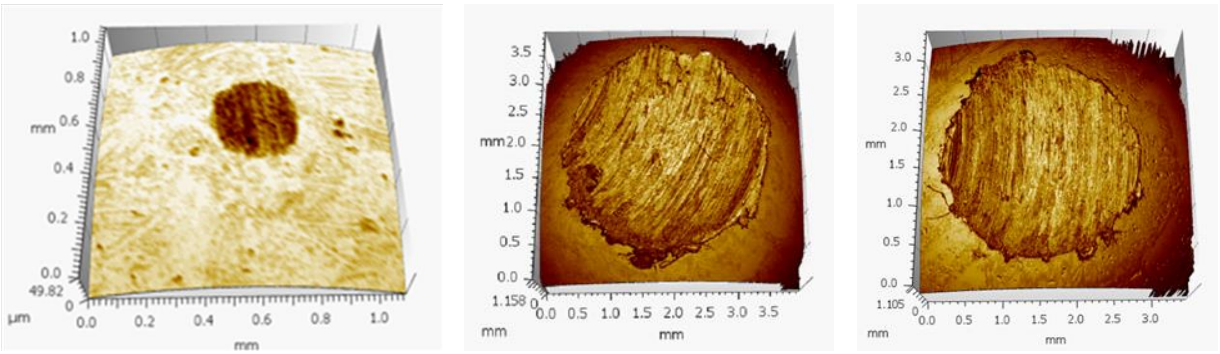

a) F=500 N b) F=850 N c) F=900 N

Fig. 3.21. Wear scars, virtual re-built with the Mountains SPIP 8.1 software, on the stationary ball

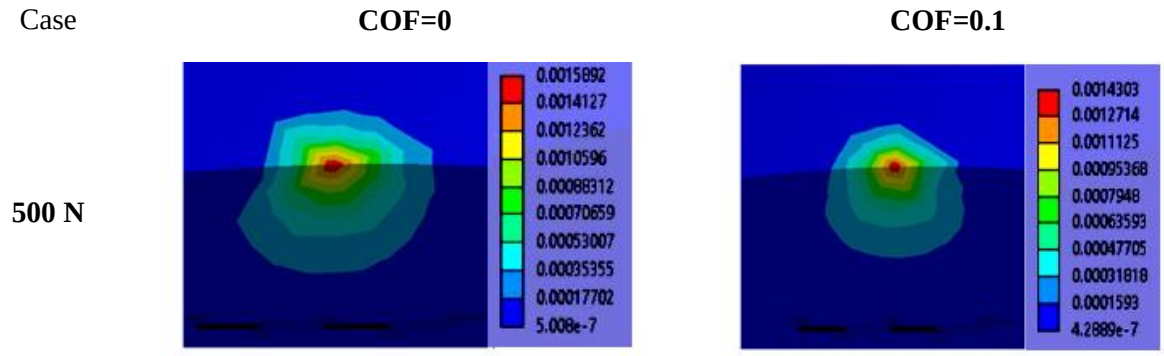

Fig. 3.22. Influence of the friction coefficient on the distribution of the elastic strain (mm/mm),for F=500 N. The rotating ball performed an angle of rotation equal to 360º

Figure 3.22 shows the influence of the friction coefficient on the state of elastic strain, for the load of 500 N, in the case without friction, as in the case with friction. Very small values of elastic strains are observed for the case of the analyzed force. Starting with F=700 N, the values of plastic strain increase slightly (Fig. 3.23) and they are observed on the rotating ball and on the fixed ball, for the cases without friction, but also for the case with friction. In Fig. 3.24, where the load is F=900 N, it can be observed that the values of elastic strain have almost doubled as compared to the cases discussed above, for the case with COF=0, but also for the simulation with COF=0.1.

In the second stage of the simulation, the constancy of the maximum value of the elastic strain for the load F=900 N (Fig. 3.24) is observed, in the case of friction and in the case without friction. This can be explained by the fact that the material comes out of the area of linear elasticity.

Figure 3.25 shows the influence of the friction coefficient on the distribution of plastic strain (mm/mm) for the load F=500 N. The rotating ball performed an angle of rotation equal to 360 º.

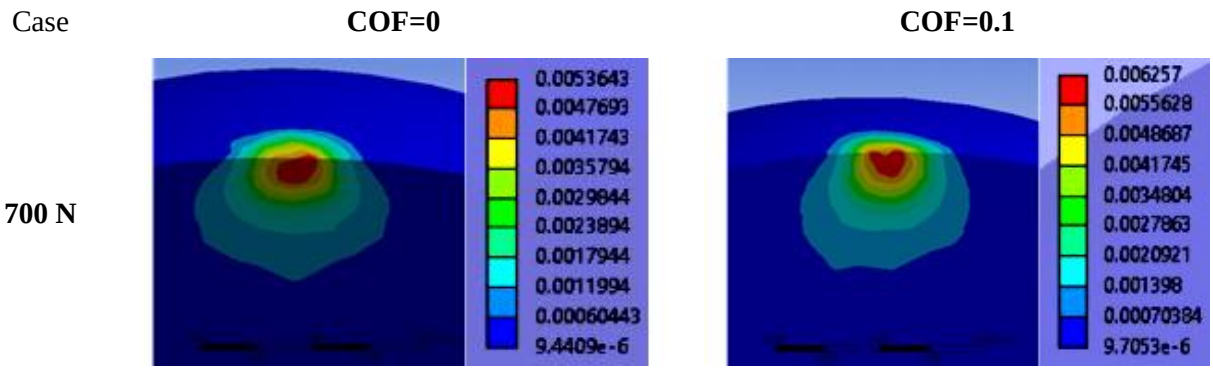

Fig. 3.23. Influence of the friction coefficient on the distribution of the elastic strain (mm/mm), for F=700 N. The rotating ball performed an angle of rotation equal to 360º

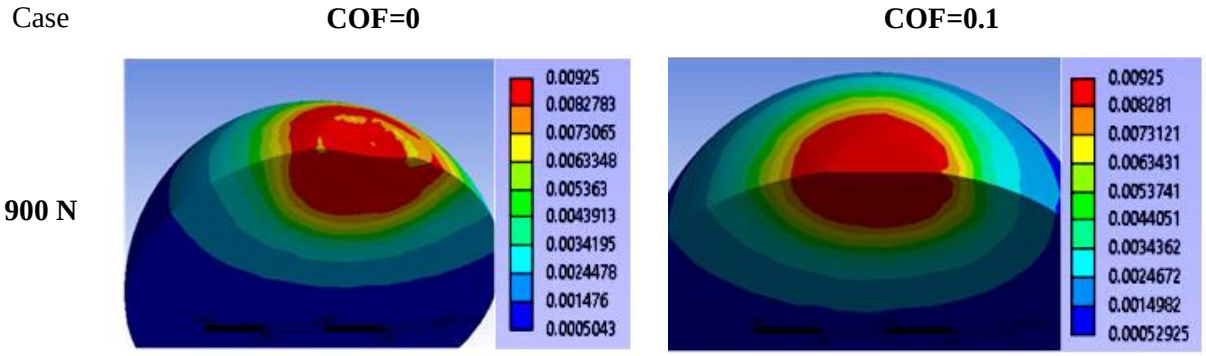

Fig. 3.24. Influence of the friction coefficient on the distribution of the elastic strain (mm/mm), for F=900 N. The rotating ball performed an angle of rotation equal to 300°

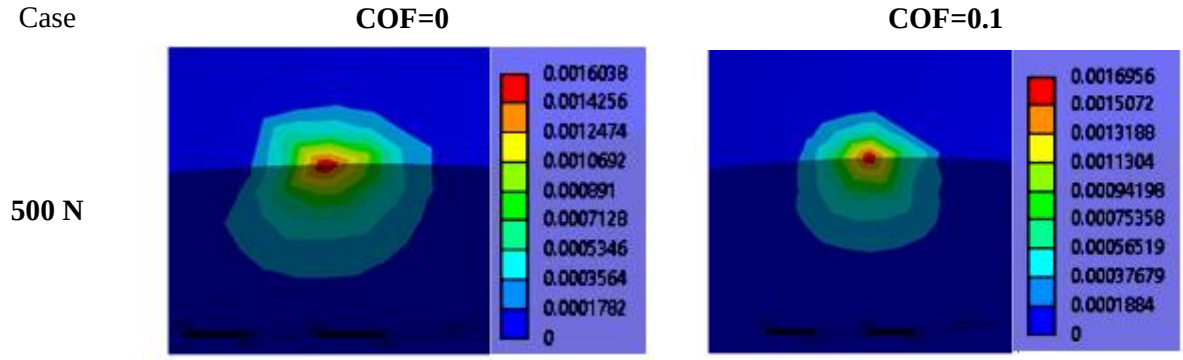

Fig. 3.25. The influence of the friction coefficient on the distribution of plastic strain (mm/mm) for the F=500 N. The rotating ball performed an angle of rotation equal to 360º

Figure 3.26 shows the influence of the friction coefficient on the state of plastic strains, when the load acting on the rotating ball is F=900 N. The values of plastic strain have increased significantly as compared to the situation analyzed previously and much higher values of plastic strain were obtained for the case COF=0.

For the simulation at this load, higher values of plastic strain on the stationary ball stand out as

compared to the values obtained on the rotating ball, especially in the case without friction.

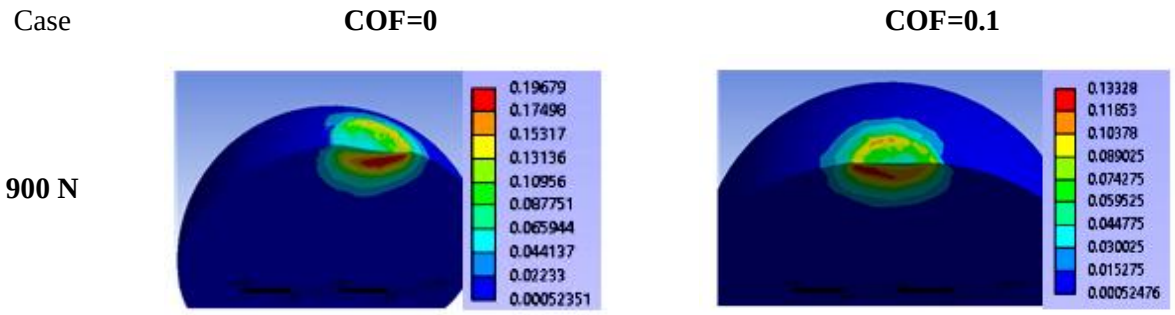

Fig. 3.26. Influence of the coefficient of friction on the distribution of plastic strain (mm/mm), for F=900 N. The rotating ball performed a rotation equal to 300º (stationary ball)

In Fig. 3.27, the total strains are presented and how they were influenced by the friction coefficient (for COF=0 and COF=0.1). The simulation was performed for a load F=500 N in two situations. In the first situation, there was no friction and in the second, a friction coefficient equal to 0.1 was taken into account. The figure shows the distributions of total strains, for the second stage, rotation for an angle of 360°. It can be seen that the values of the total strain are quite small.

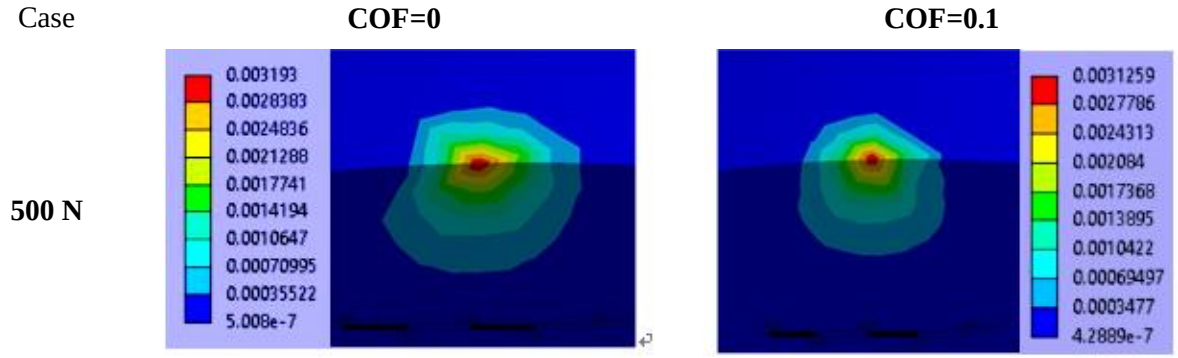

Fig. 3.27. Influence of the friction coefficient on the distribution of the total strain (mm/mm), for F=500 N. The rotating ball performed an angle of rotation equal to 360º (stationary ball)

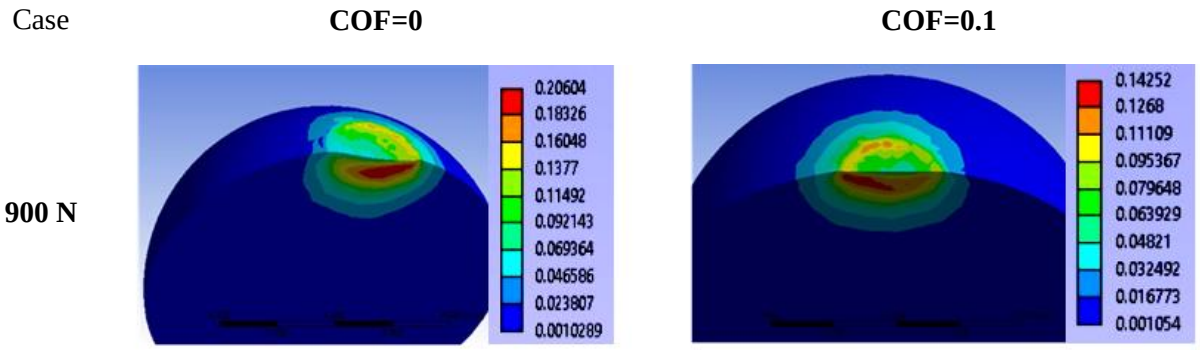

Fig. 3.28. Influence of COFon the total strain distribution (mm/mm) on the stationary ball, for F=900N. The rotating ball rotates for an angle of 300º

The influence of the friction coefficient on the distribution of the total strain is shown in Fig. 3.28, in which, the applied load is 900 N. Higher values of the total strains are observed on the stationary ball in case COF=0.

Figures 3.29 and 3.30 present images with isolines of plastic strains, for the simulated loads F=500 N and F=900 N, in case without friction, but also in case with friction. Isolines of 0.0007 mm/mm (for F=500 N) and 0.06 mm/mm (for F=900 N), approximatively correspond for the average value of WSD.

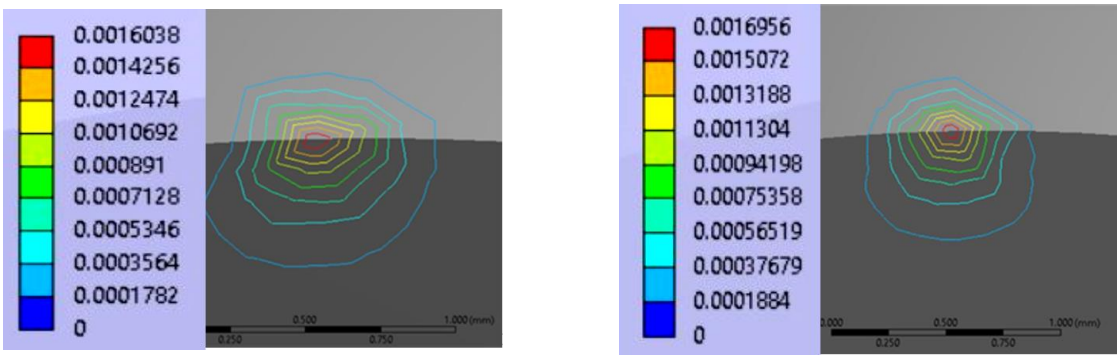

a) COF=0 b) COF=0.1

Fig. 3.29. Distribution of plastic strains, for F=500 N (isolines) in mm/mm

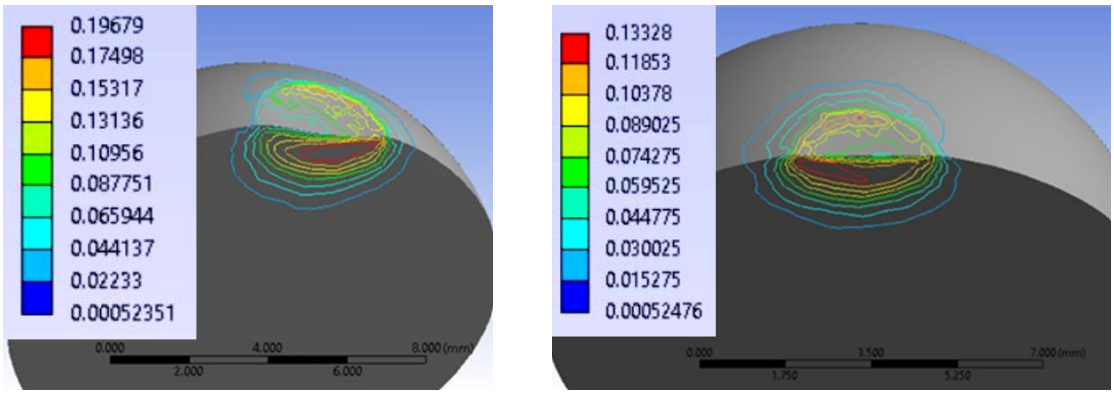

a) COF=0 b) COF=0.1

Fig. 3.30. Distribution of plastic strains, for F=900 N (isolines) in mm/mm

3.5. Conclusions

The model is original and it is based on experimental findings and studied literature [89], [49], [59]. The simulation is done in two steps. The first step consists of the static loading on the two balls (extracted from the four ball model and based on a calculated and measured aproach corresponding to each load in severe regime), and in the second step, a partial rotation (300°), or complete rotation

(360°) is done. The material constitutive model takes into account experimental data obtained on the same steel grade, 100Cr6, with the same quality in terms of hardness, Young modulus and equivalent plastic strain at break**.**

The model is useful for evaluating the stress and strain distributions, so that a working range for test parameters and the transition from normal regime (acceptable load in operation) to a severe regime (by identifying maximum stresses) can be evaluated. Qualitatively, the model highlights the ellipsoidal shape of the wear scar due to the influence of the friction load and the sliding movement.

In this model, wear is not simulated and surfaces in contact are perfectly smooth, but in reality, abrasive wear dominates in the normal regime, in the severe regime being predominant plastic strain processes (similar also in simulation) and the adhesive wear that is not highlighted by simulation.

Equivalent stress values obtained from simulation may be useful by comparing the contact fatigue limit for the ball material.

Chapter 4
Laboratory formulation of lubricants and test methodology on the four ball machine

4.1. Lubricants testing on the four-ball tribotester

The lubricant is considered to be a body that acts between the surfaces of a friction coupling and can be intentionally placed or exists naturally to reduce friction and/or wear. The main properties of a lubricant are: anti-wear and anti-corrosion properties, resistance to oxidation, thermal stability, high viscosity index, increase of system efficiency, evacuation of heat generated by friction.

The presence of lubricant is absolutely necessary for the friction zones to be functional and for this reason, the lubricant is not considered a auxiliary element of the tribosystem [23].

For laboratory tests, the characterisation of a lubricant would be done by the tribological properties determined on the four-ball machine.

The test is useful because several lubricants tested under the same conditions can be compared, the characteristics of the additives can be checked and the percentage of additive concentration and base oil nature can be included in parametric evaluation, as required by the beneficiaries.

In order to formulate a new lubricant, the final step should include testing it in conditions close to, or similar to normal operating conditions. The tests must be repeated and the tested parameters should be as numerous as possible and on realistic ranges.

Testing on the 4-ball tribostester is recommended by researchers for its simplicity [17], [32], [72].

The tribotester consists of three stationary balls, which are pressed by a fourth ball in rotating motion. In general, the quality of a lubricant is assessed by the size of the wear scars generated on stationary balls.

The 4-ball tribotester (Fig. 4.1) is composed of a drive shaft in a vertical position, which has at its lower end a conical device (1), which helps to fix the rotating ball (2). The rotating ball rests on the three stationary balls, which are fixed by a nut (4) and a conical piece (5). The entire stationary ball fastening system is installed on a pressure bearing, which facilitates vertical rotation and loading. A force is applied by means of a lever on the fastening system of the three stationary balls. When the upper ball rotates, a friction moment appears, which acts also on the stationary ball clamping system.

The lubricant to be tested is inserted into the cup where the three stationary balls are located. The amount of lubricant is about 8-10 ml and then, other 3 ml is added to entirely cover the balls.

The balls used for testing were supplied from SKF; they are made of chrome steel, with a diameter of 12.7 mm ± 0.0005 mm, according to the ISO standard 683-17: 2014, they are finely grinded and have a high hardness (62...65 HRC) and a high quality surface (Ra=0.02...0.03 μm).

4.2. Tribological parameters measurable by tests on the four-ball tribotester

This subchapter analyzes the texture parameters on the wear scars on the stationary balls.

The evaluation of the wear parameters is done with the following parameters:

- the wear scar diameter for the three stationary balls (WSD); it is calculated by making the arithmetic mean of six measured diameters, two for each ball, the first diameter being measured along the sliding direction, the second being perpendicular to the first measured diameter,
- the wear rate of wear scar diameter w(WSD).

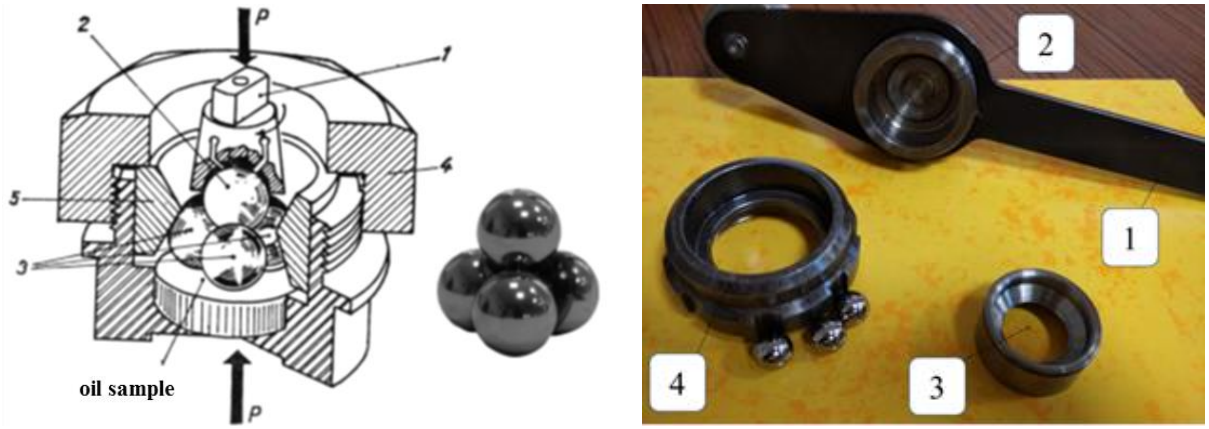

a) 1 – rotating ball cup, 2 – rotating ball, 3 – stationary balls, 4 – nut, 5 – fixing ring for the stationary balls

b) 1 – arm for loading, 2 – spherical seat for loading, 3 - fixing ring for stationary balls 4 – nut

Fig. 4.1. The main components of the 4-ball tribotester

The friction coefficient

The friction force was measured by the author using an assembly consisting of a tensometric bridge (mounted between the arm of the four-ball tribotester frame and the arm of the fixing cup), a system that acquires the transmitted data and on a computer (Fig. 4.2)

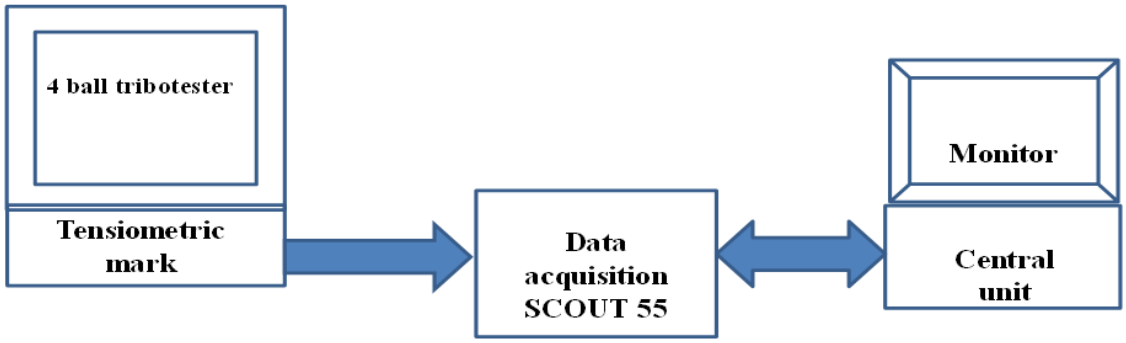

Fig. 4.2. Scheme assembly containing data acquisition system

4.3. Obtaining lubricants based on rapeseed oil and nanoadditives TiO_2 and ZnO. Laboratory methodology.

The lubricants tested in this study are based on rapeseed oil, supplied by Expur Company from Bucharest, without additives or additivated with nanomaterials based on metal oxides (ZnO and TiO_2), in different concentrations (0.25 wt%, 0.5 wt% and 1.0 wt%). The fatty acid composition of the analyzed rapeseed oil is presented in Table 4.1 and was performed at Expur Bucharest, using a chromatograph.

The additives used in this doctoral thesis (Fig. 4.3) were provided by PlasmaChem [PlasmaChem, 2016] and have the following properties:

- ZnO: average particle size ~14 nm, specific surface area ~30 m²/g,
- TiO_2: average particle size ~21 nm, specific surface area ~50 m²/ g

The dispersion of additives in the base oil is an issue that needs to be addressed for this type of anti-wear additives. Taking into account the fact that the tested rapeseed oil is a complex of fatty acid triglycerides (Table 4.1), the author proposes a way to obtain a better dispersion.

Tabel 4.1. Typical composition in fatty acids of the rapeseed oil

Fat acid	Symbol	Concentration, %wt
Myristic acid	C14:0	0.06
Palmitic acid	C16:0	4.6
Palmitoleic acid	C16:1	0.21
Heptadecanoic acid	C17:0	0.07
Heptadecenoic acid	C17:1	0.18
Stearic acid	C18:0	1.49
Oleic acid	C18:1	60.85
Linoleic acid	C18:2	19.9
Linolenic acid	C18:3	7.64
Arachidic acid	C20:0	0.49
Eicosenoic acid	C20:2	1.14

The steps followed in laboratory method were:

- mixing the nanoadditive (mechanical mixing) with an equal mass of guaicol, for a period of 20 minutes; the dispersing agent (guaicol) is compatible with the vegetal oil used as based oil, but also with the used additives,

- gradually adding of the rapeseed oil, which has been previously measured to obtain 200 g of lubricant,

- stirring with a magnetic homogenizing device for 1 hour,

- sonication + cooling of 200 g lubricant for 5 minutes with the help of sonicator Bandelin HD 3200; the lubricant is heating at approximately 70 °C; this step of sonication + cooling is repeated 5 times for obtaining a total sonication time of 60 minutes. The parameters of sonicating regime are: frequency 20 kHz ± 500 Hz and power 100 W, in continuous regime.

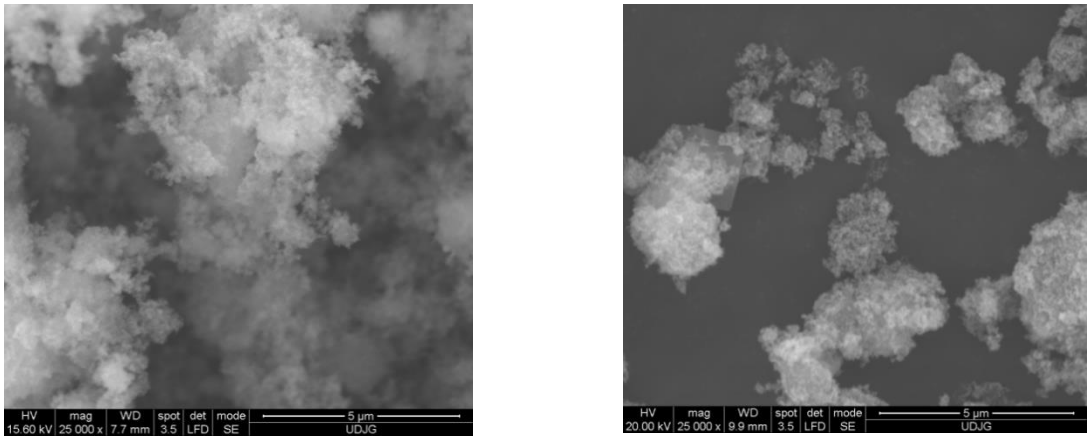

a) TiO_2 b) ZnO

Fig. 4.3. SEM images of the nanoadditives

4.4. Test campaign on the four-ball tribotester

The test parameters for each tested lubricant were:

a) in normal regime

- load - 100 N, 200 N and 300 N,

- sliding velocity - 0.38 m/s, 0.53 m/s and 0.69 m/s, corresponding to the rotational speeds of the four ball main shaft of, 1400 rpm and 1800 rpm respectively,

- test time - 60 minutes (±1%),

- the concentration of additive in the formulated lubricants is 0.25%, 0.50% and 1% (wt),

b) in severe regime
- load - from 500 N to 900 N (in steps of 50 N),
- sliding velocity - 0.53 m/s, corresponding to a rotational speed of 1400 rpm,
- test time - 1 minute (±1%),
- the concentration of the additive in the formulated lubricants is also 0.25%, 0.50% and 1% (wt).

Wear scars diameters were measured using an optical microscope.

Figure 4.4 shows the schematic representation of the tests performed by the author and the test regimes. Each test was repeated twice.

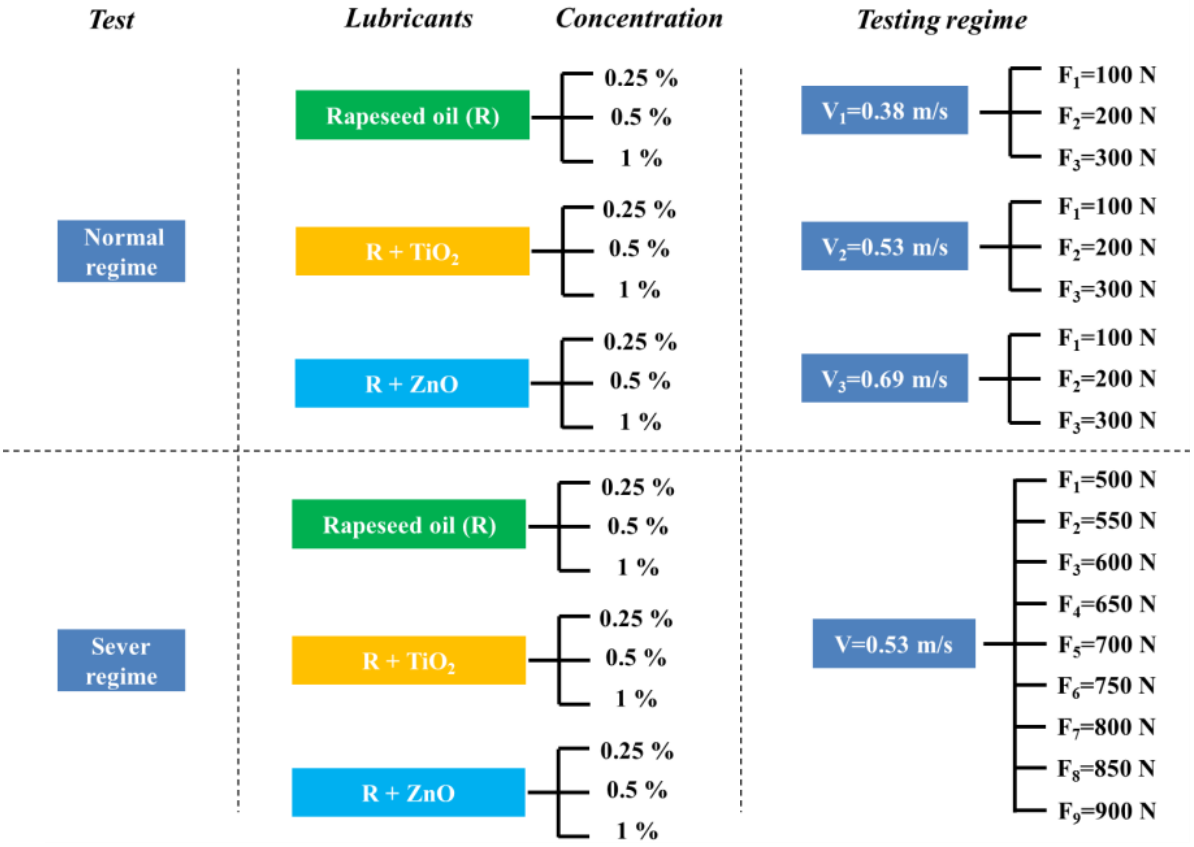

Fig. 4.4. Schematical representation of the test campaign performed by the author and the test regimes.

4.5. Conclusions

Based on the documentation analysed by the author on the additivation of vegetal oils with friction and wear modifiers, the author chose crude rapeseed oil as the base oil and as friction and wear modifiers, TiO_2 and ZnO. The author of this study took over the technology of mixing/dispersing nanoparticles from previous works [16], [30], carried out within the Research Center „Mechanics and Tribology of Surface Layers" of „Dunărea de Jos" University of Galați. The formulation of nanoadditivated lubricants was based on a sonication and alternative cooling regime, repeated several times (3-5 times), after which the lubricant obtained with different concentrations of additive was subjected to a test campaign. Unlike many other scientific reports on lubricant testing, which focused on a single test regime, this thesis aimed to test newly formulated lubricants in normal and severe regimes. This new approach made possible to highlight the role of nanoadditives in the severe regime, in which, although they did not form a continuous film, they still led to the protection of contact surfaces and the reduction of the WSD, a characteristic parameter of tests on the four ball machine.

Chapter 5
Tribological behavior of formulated lubricants on the four-ball tribotester. Experimental results

5.1. The investigated tribological parameters

A very important thing is to establish a test methodology to evaluate a lubricant from a qualitative and quantitative points of view.

Tribological tests can be grouped into: severe regime tests and normal operating regime tests.

In this chapter, the following tribological parameters were analyzed:

- **the friction coefficient**, COF, more precisely the values of this parameter during a test; an instantaneous value, at time t, the average value during the whole test (in normal regime, the duration of the test was 1 hour, recording 7200 values, two samples per second and in severe regime the test had a duration of 1 minute) and the interval in which the friction coefficient varies during the test,
- **the wear scar diameter**, WSD, is a specific parameter to four-ball tribotester. The wear scar diameter represents the arithmetic average of the six diameters of the measured wear scars, two on each stationary ball,
- **wear rate of wear scar diameter**, w(WSD)

$$w(WSD) = \frac{WSD}{F \times L} \text{ [mm/N·m]} \quad (5.1)$$

where WSD is the average wear scar diameter for a test, F is the applied load on the four ball machine, L is the sliding distance ($L = v \cdot t$, v being the sliding velocity and t, the test duration).

The sliding distances L are different due to the duration of a test in normal operation (1 hour), but with different velocities:

L_{1000} (v =0.38 m/s) =1378.8 m, L_{1400} (v=0.53 m/s)=1933.2 m, L_{1800} (v =0.69 m/s)=2487 m.

5.2. Friction assessment for non-additivated rapeseed oil

Friction was discussed in this paper by:

- qualitative assessment of the evolution of the COF in time,
- the average of friction coefficient values recorded in one hour and the range of scattering values for two tests.

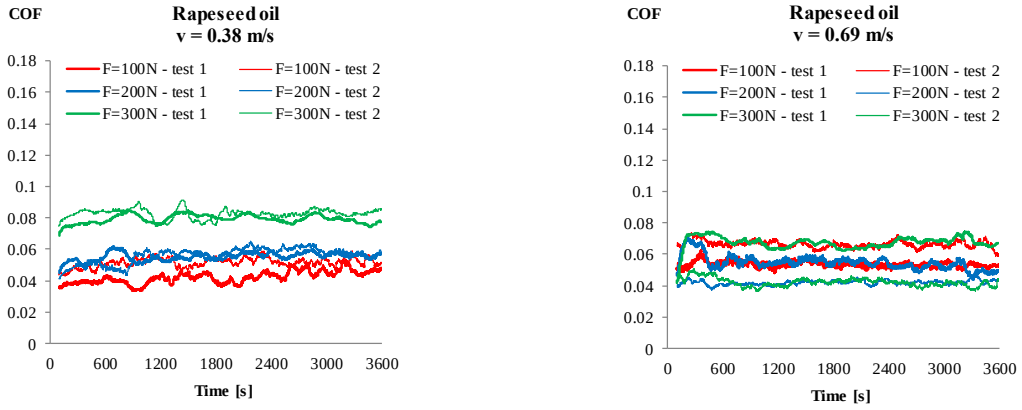

Fig. 5.1. Evolution of COF in time, as a function of load and speed, for two tests with the same parameters (F, v), for rapeseed oil

The graphs in Fig. 5.1 are done using a moving average of 200 values. The author chose this representation to highlight the friction coefficient trend evolution over 1 hour test, for which 7200 values were recorded (2 values per second).

The graphs show how the increase in speed led to the agglomeration of the curves in a narrow interval. If, at a speed of 0.38 m/s, COF is between 0.04 and 0.09, at a speed of 0.69 m/s, the friction coefficient is between 0.05 and 0.08. COF of rapeseed oil is less sensitive to load at high speeds. The formation of a film is observed at high speeds, as values are very low.

5.3. Wear assessment for non-additivated rapeseed oil

Wear was evaluated by two characteristic parameters of the four-ball tribotester:

- wear scar diameter, WSD,
- wear rate of wear scar diameter, w(WSD).

Figure 5.2 shows the evolution of the wear scar diameter for the rapeseed oil, tested at different loads and sliding speeds. An increase of WSD values is observed with increasing load and sliding speed. The highest value of WSD was obtained for the load F=300 N, at the speed v = 0.69 m / s.

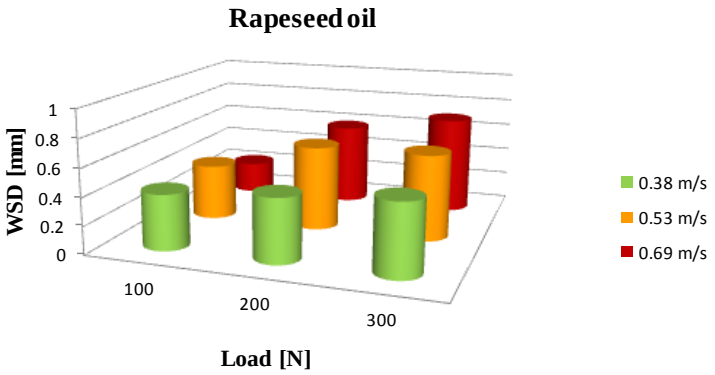

Fig. 5.2. The evolution of WSD for rapeseed oil

Even if the sliding distances differ, the trend of the evolution of WSD is the same, but increasing and almost linear, which means that the tests did not show a change in wear processes.

The wear rate of wear scar diameter (Fig. 5.3) is a very important wear parameter because it is calculated for the same test duration, but at different sliding distances and the results could be compared.

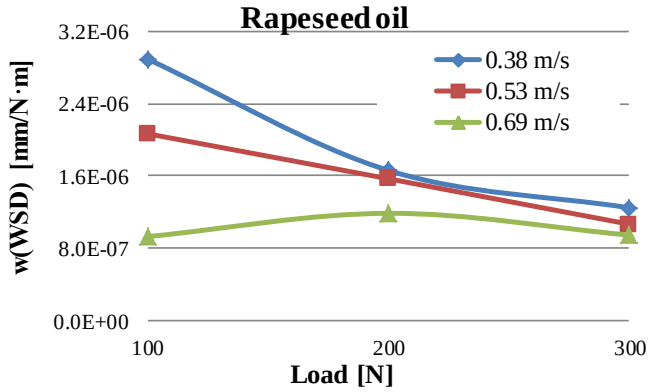

Fig. 5.3. Wear rate of WSD for rapeseed oil

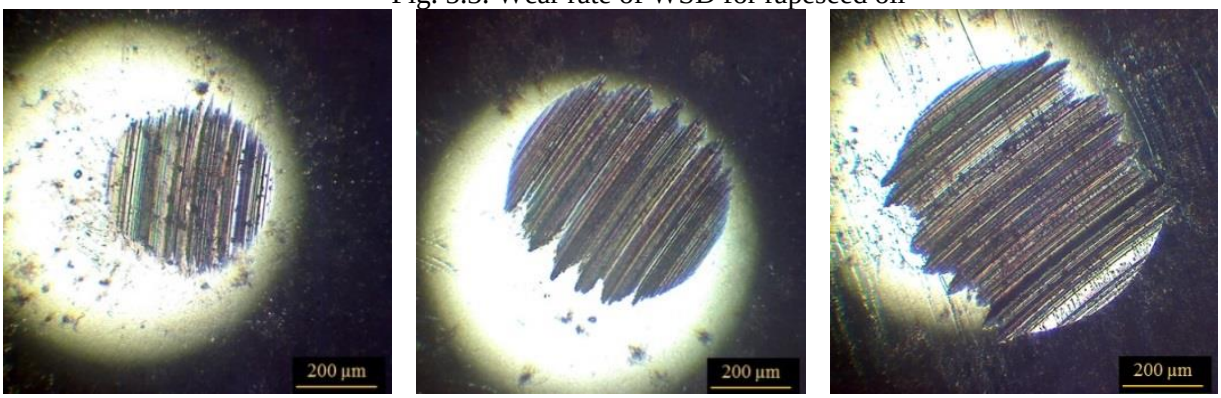

F=100 N F=200 N F=300 N

Fig. 5.4. Wear scars obtained on testing with non-additivated rapeseed oil and v=0.69 m/s

Figure 5.4 shows wear scars for the non-additivated rapeseed oil test, for v=0.69 m/s: the wear scar increased with load, also highlighting the evolution of the abrasive wear process. At F=300 N, there are more tear zones than in the case of smaller loads, 100 N and 200 N.

5.4. Lubricants additivated with TiO_2

Friction coefficient for rapeseed oil additivated with TiO_2

When adding 1% TiO_2 in rapeseed oil (Fig. 5.5), it is observed the scattering of the friction coefficient, this being higher at the intermediate speed of 0.53 m/s.

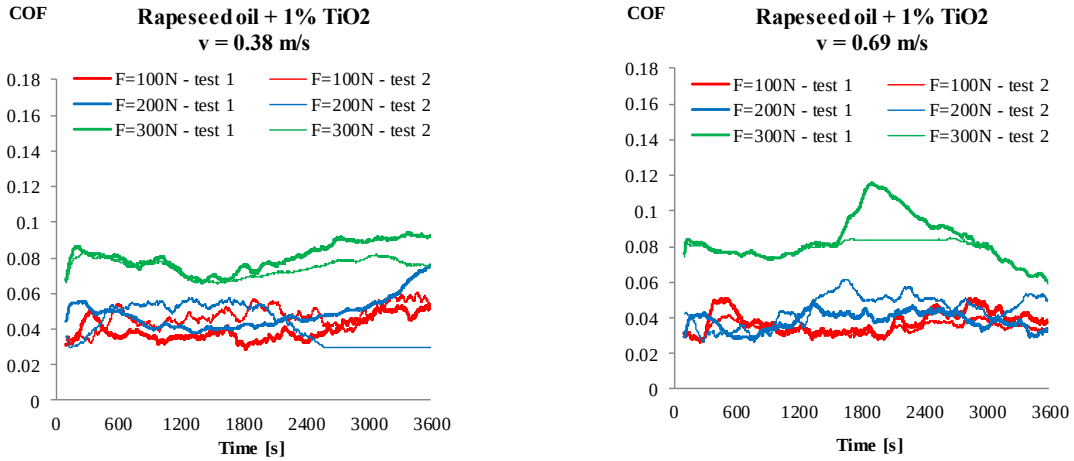

Fig. 5.5. The evolution of COF for the lubricant additivated with 1% TiO_2

In Fig. 5.6, average values of friction coefficient for rapeseed oil additivated with TiO_2 are shown. In general, the highest value of the friction coefficient is given by high load and low speed, in agreement with the hydroelastodynamic lubrication theory [22]. Lower values than those for the neat rapeseed oil are charcateristics for the additivated oil only for load F=100 N, but not under higher load, F=300 N.

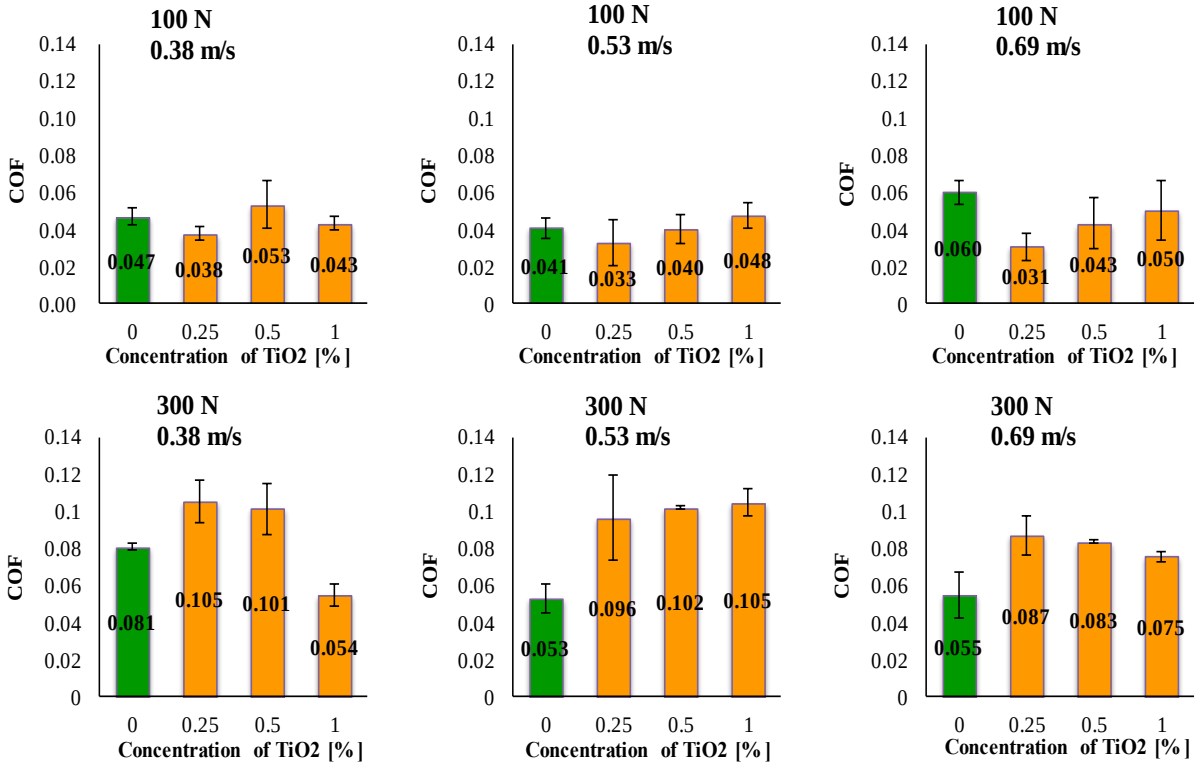

Fig. 5.6. Mean values and spread range of COF, for two tests performed with the same parameters (F, v, C), for rapeseed oil additivated with TiO_2 (F-load, v-sliding velocity, C-additive concentration)

Wear assessment

Figure 5.7 shows the average wear scar diameter for TiO_2 lubricants. It is observed that the wear scar diameter increases with the load, the highest values being obtained at high loads.

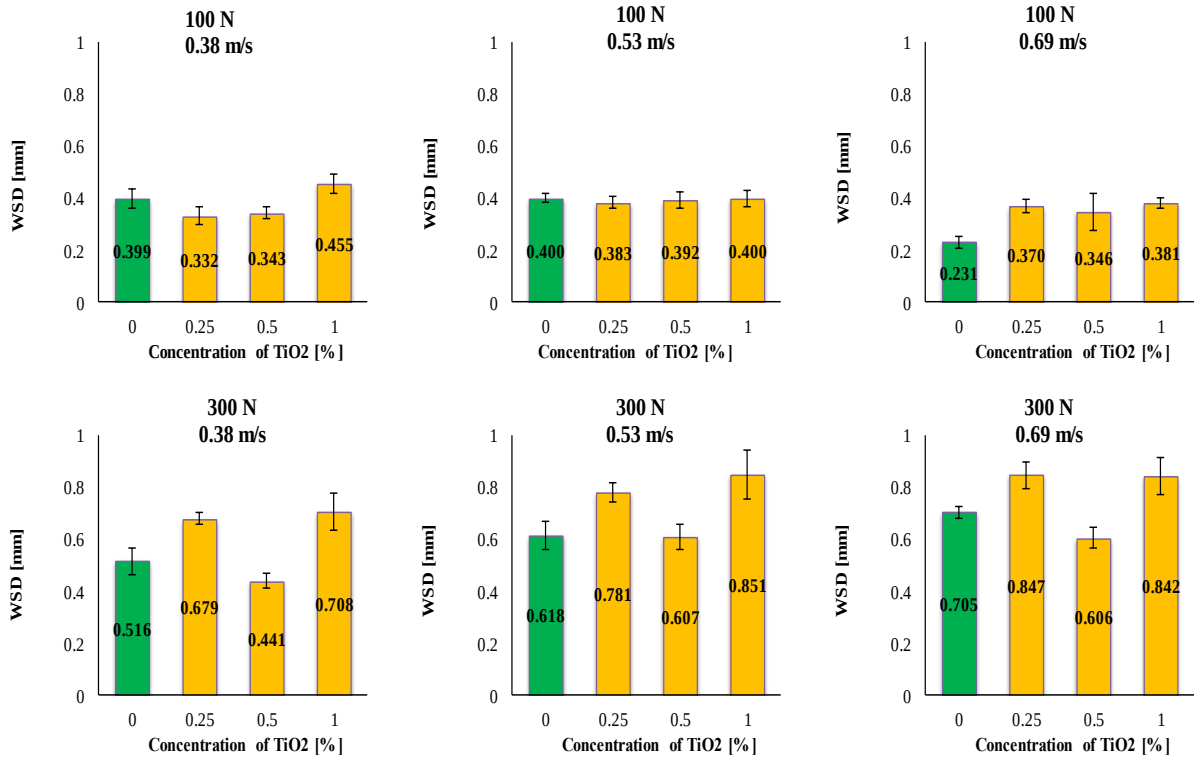

Fig. 5.7. WSD for additivated lubricants with TiO_2

The influence of the additive on wear is beneficial, especially at low sliding speeds, 0.38 m/s, which means that, below this speed, the particles remain in contact and protect the surface.

In Fig. 5.8 the images with the wear scars, measured under the optical microscope are given.

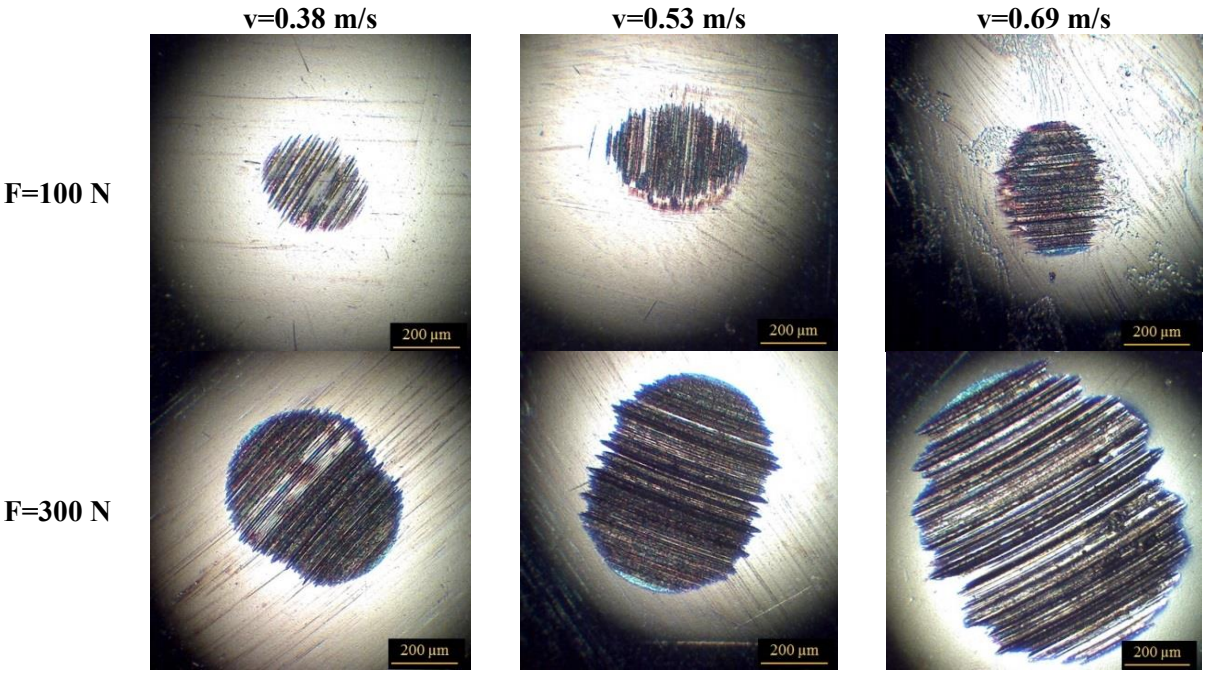

Fig. 5.8. Images of the wear scars of rapeseed oil+1% TiO_2

Analyzing the images, one may notice that wear scars remain small under F=100 N, but for F=300 N abrasive wear is intense especially under v=0.69 m/s, meaning the regime is mixt or with boundary lubrication.

Wear rate of wear scar diameter

The wear rate of wear scar diameter helps to determine the influence of nanoadditive concentration. From the graphs in Fig. 5.9, it is observed:

- a decrease of w(WSD) with load for all concentrations and speeds, for additivated lubricants,
- the slope of the speed dependency is smaller for the same load,
- the additivation with this friction and wear modifier would be justified in the field of high load for all speeds.

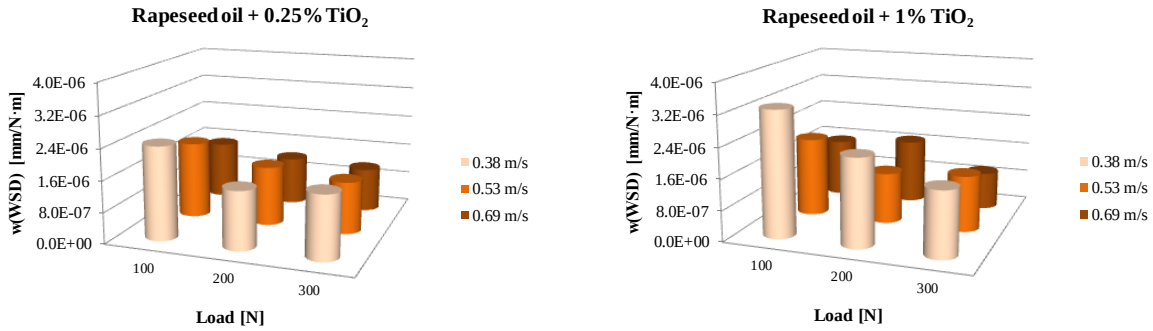

Fig. 5.9. Wear rate of WSD, depending on the test regime (F, v) and the TiO_2 concentration

5.5. Lubricants additivated with ZnO

For the rapeseed oil additivated with 1% ZnO (Fig. 5.10) a scattering of the friction coefficient values is observed. ZnO addition increases the friction coefficient at low speeds, and the spreading intervals are larger. Addition with 1% ZnO is not appropriate for decreasing COF, but if the wear parameters are analyzed, the increase of the friction coefficient is accepted.

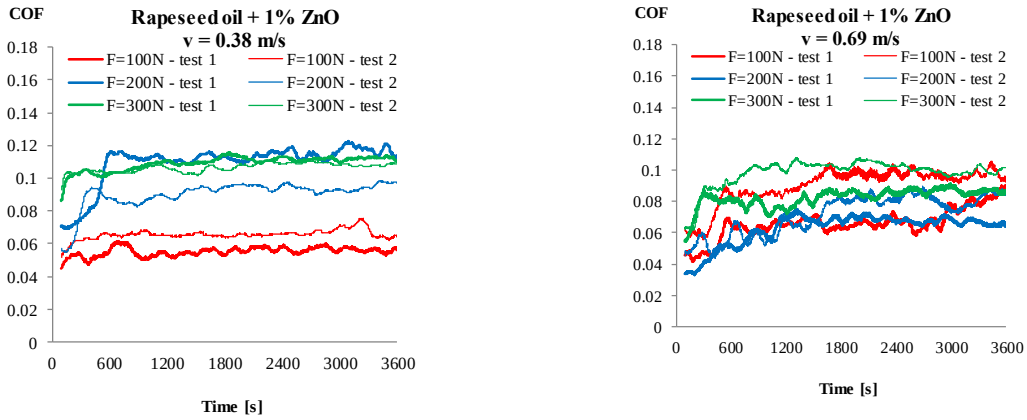

Fig. 5.10. The evolution of COF for the additivated lubricant with 1% ZnO

In Fig. 5.11, average values of friction coefficient for rapeseed oil additivated with ZnO are shown. Two tests with the same parameters were performed (load, sliding velocity and additive concentration), for rapeseed oil and rapeseed oil additivated with ZnO nanoparticles.

It can be seen from the graphs that no smaller average COF values were obtained for non-additivated rapeseed oil as compared to those for rapeseed oil.

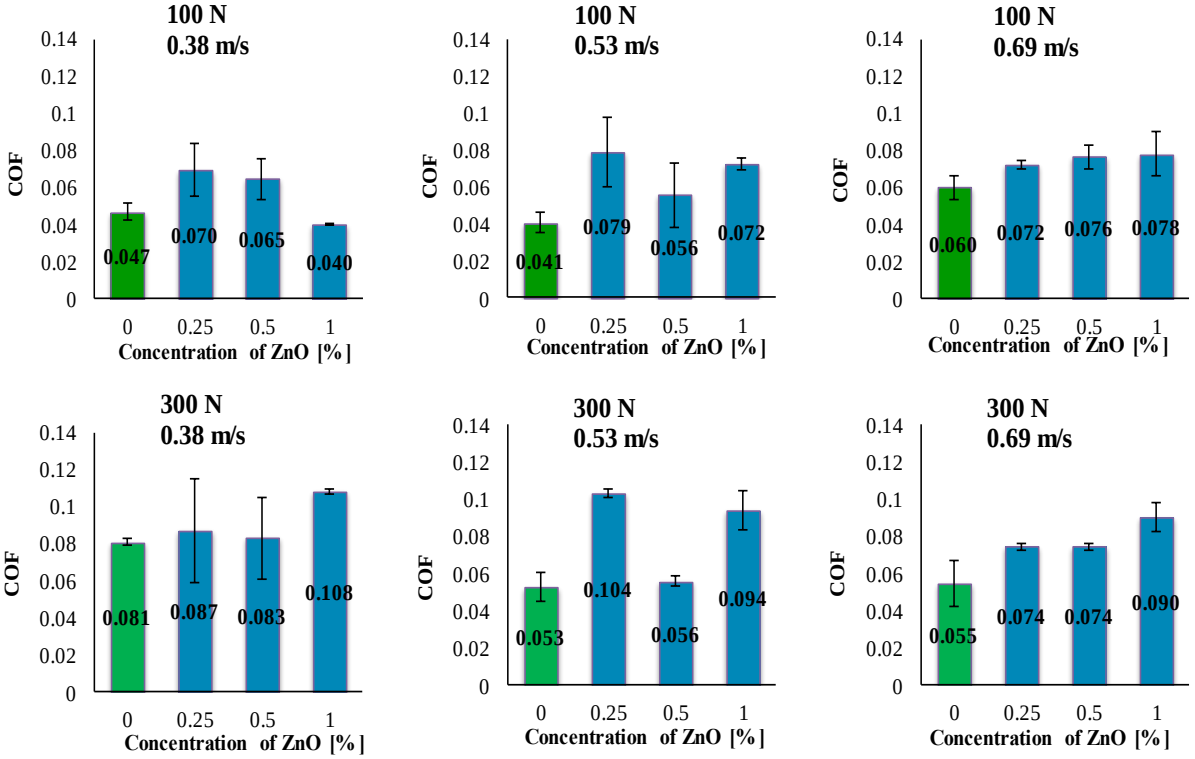

Fig. 5.11. Average values and spread range of COF, for two tests performed with the same parameters (F, v, C), for rapeseed oil additivated with ZnO

Wear parameters

The author agrees with the conclusion of the researcher Shahnazar [69] that ZnO nanoparticles could reduce wear by deposition on sliding surfaces, but from SEM images (Fig. 5.12), it is observed that ZnO does not form a protective film on the surface, as other researchers stated.

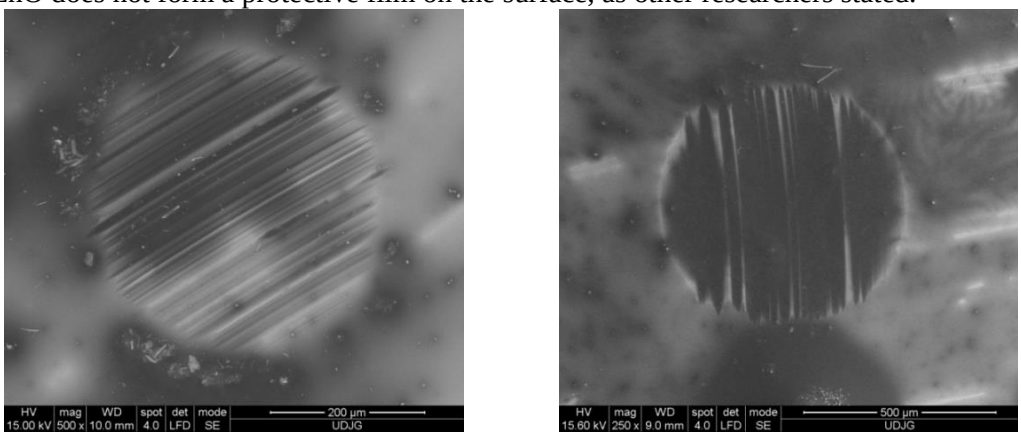

a) F=100 N, v=0.38 m/s b) F=300 N, v=0.69 m/s

Fig. 5.12. SEM images of wear scars for rapeseed oil additivated with 1% ZnO

At all tested regimes, the average values of the wear scar diameters are obtained in a narrow range and the spreading intervals are not large either (Fig. 5.13), but the differences are too small to highlight a trend and influence of the additive or test regime. In other words, wear is less sensitive to speed and load. This type of nanoadditive could be recommended where could be a variable load and speed regime.

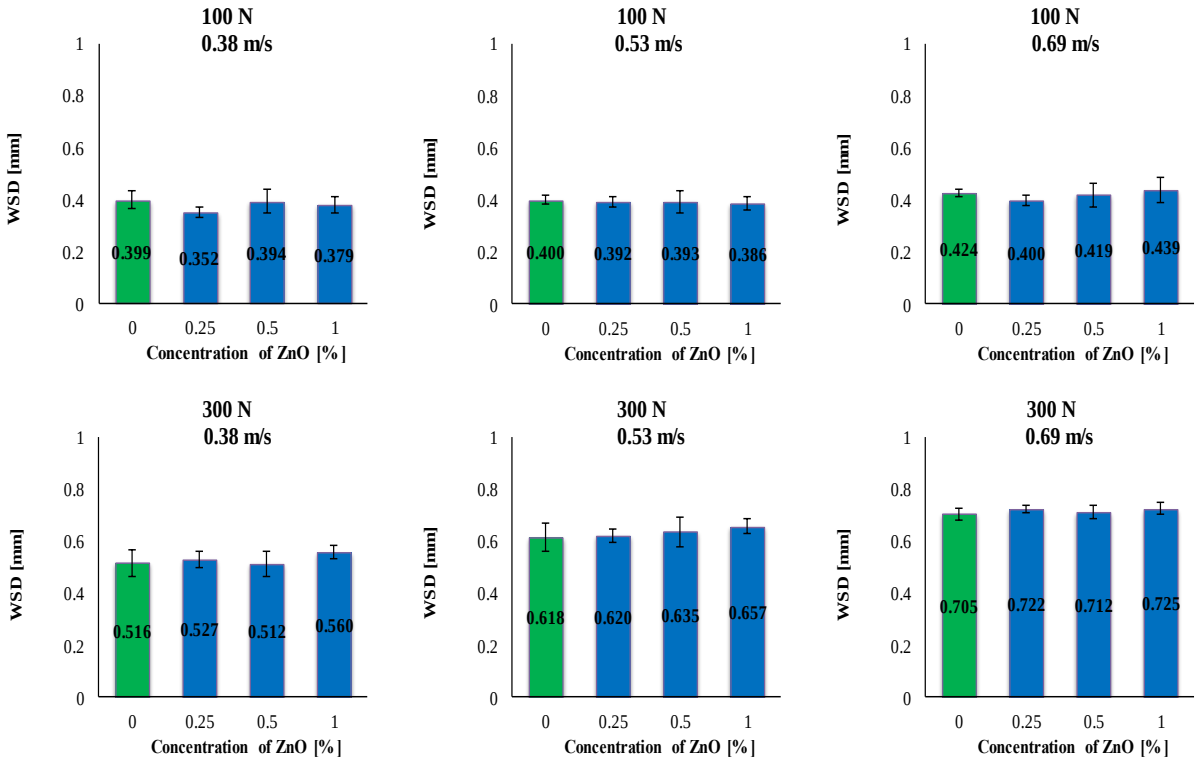

Fig. 5.13. Average wear scar diameter for additivated lubricants with ZnO

In Fig. 5.14 images of the wear scars, from the optical microscope, from rapeseed oil additivated with 1% ZnO, are given. It is observed that there is not a significative difference between the images of the wear scars, fact confirmed by the graphs of the wear scars diameter (Fig. 5.13).

Wear scars increase with increasing load, at the highest loads having the largest wear scars for the case where rapeseed oil it is additivated with ZnO nanoparticles.

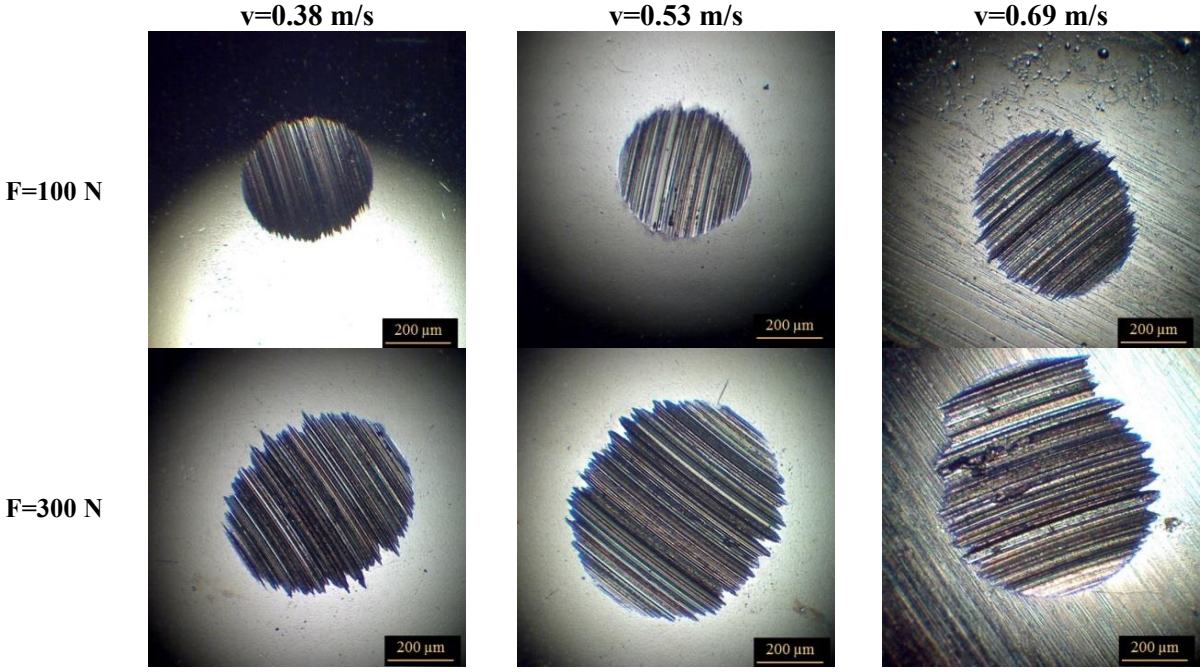

Fig. 5.14. Images of the wear scars of rapeseed oil+1% ZnO

Wear rate of the wear scar diameter

From Fig. 5.15, it is observed that there is a high wear rate at low loads and speeds. When increases the load, the wear rate of the wear scar diameter decreases. This means a more intense abrasive wear, which occurs when the lubricant does not form a film and/or if the additive cannot protect the surface.

Analyzing the graphs, it can be seen that the wear rate of the wear scar diameter has a tendency to decrease with the increase of the load. For the load F=300 N, the wear rate of the wear scar diameter is not greatly influenced by the speed. The graphs have the same trend and they are similar in terms of appearance regardless of the percentage of nanoadditive concentration.

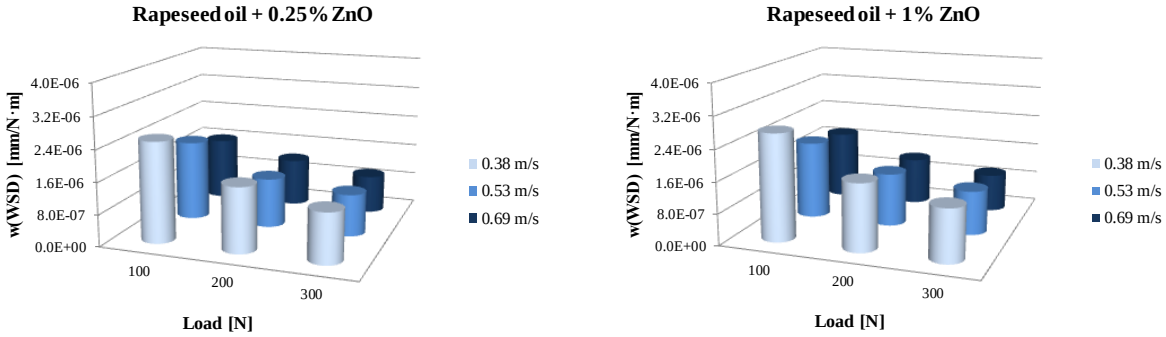

Fig. 5.15. Wear rate of WSD, depending on the test regime (F, v) and the ZnO concentration

5.6. Temperature in lubricant bath at the end of the test

A summary of the experimental data regarding the temperature in the lubricant bath at the end of the test is given in Fig. 5.16 and Fig. 5.17.

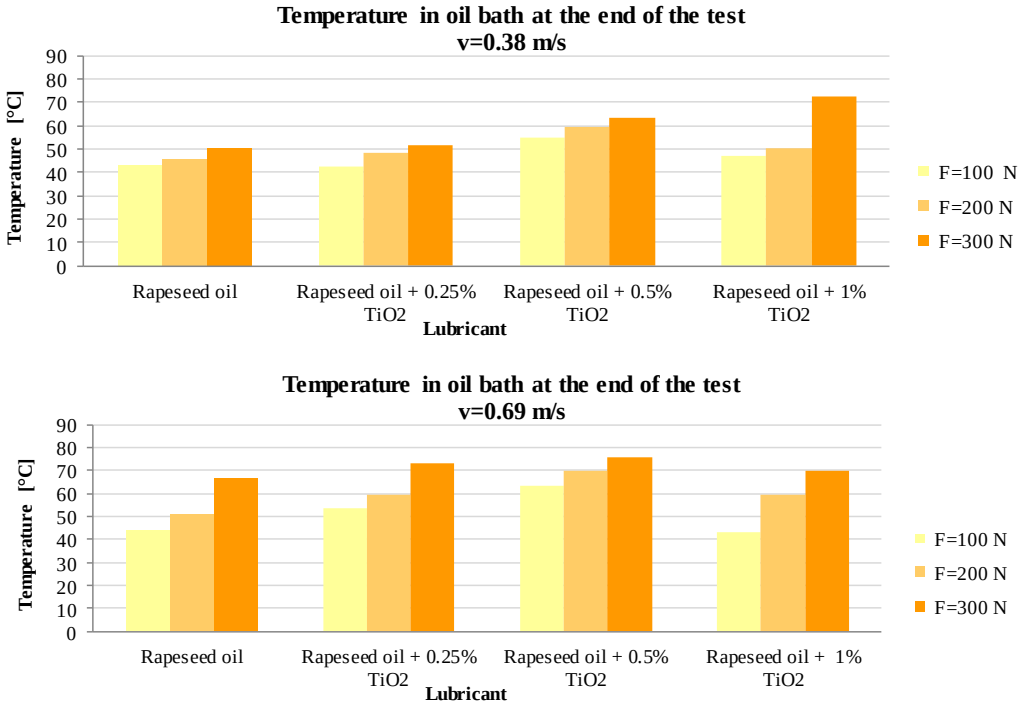

Fig. 5.16. Temperature in lubricant bath, at the end of the test, for lubricants additivated with TiO_2 nanoparticles

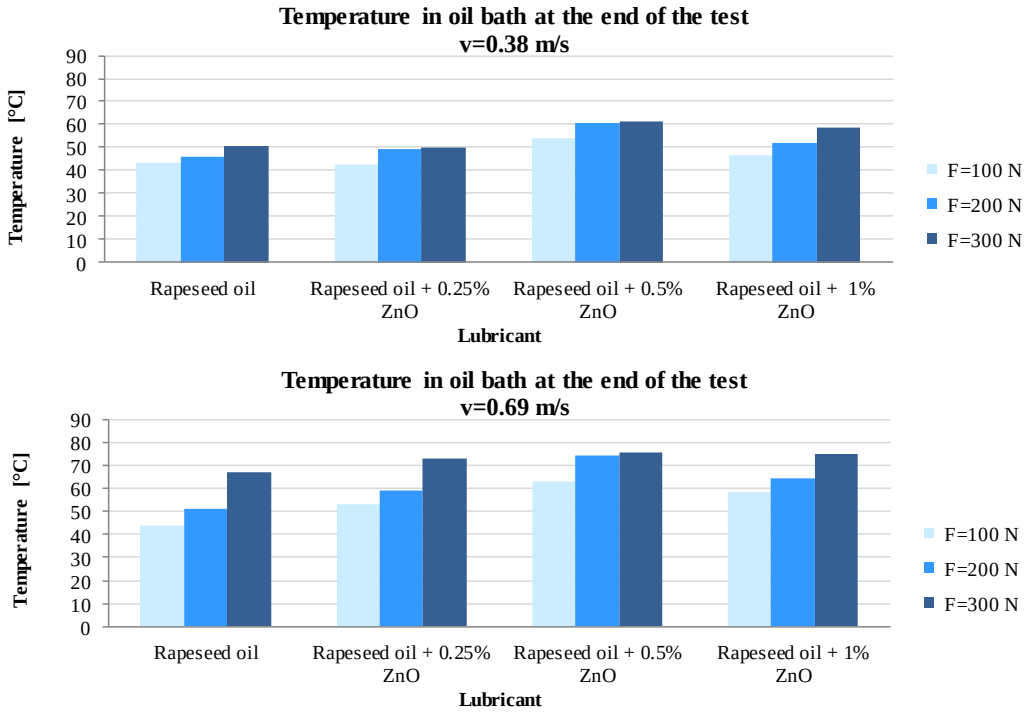

Fig. 5.17. Temperature in lubricant bath, at the end of the test, for lubricants additivated with ZnO nanoparticles

The difference between the final temperature at the end of the test, is small for low regimes (v=0.38 m/s), and the temperature value is in the range of 43-55 ºC. For the sliding speed, v=0.69 m/s, the temperature values are distributed over a longer interval.

For most severe regimes, the final temperature recorded for rapeseed oil is 70 ºC.

For rapeseed oil additivated with 1% TiO_2, the temperature at the end of the test, for v=0.38 m/s is in the range 72-82 ºC and for the speed v=0.69 m/s, the temperature is 70,2 ºC (Fig. 5.16).

Rapeseed oil with 1% ZnO has a higher temperature, between 50-60 ºC for speed v=0.38 m/s and for v=0.69 m/s the temperature is in the range of 60-77 ºC. Additional heat generation can be explained by the friction of Zn particles, rolled in contact (Fig. 5.17).

5.7. Analysis of experimental results by maps of tribological parameters

5.7.1. The use of maps in the analysis of tribological parameters

The maps in this study were done in Matlab R2016a, using a spline interpolation and the surfaces are "required" to include experimental data. A point on a wear map is a test for a set of parameters.

Maps of the friction coefficient were done with average values of the two tests, performed with the same parameters, maps of the wear rate of the wear scar diameter under the same conditions and maps for the temperature in the lubricant bath with the value at the end of the test. These were useful in assessing trends and determining test regimes.

5.7.2. The friction coefficient analysis

On such a wear map, the relationships between the different dominant wear mechanisms can be highlighted, which are observed to occur when COF changes its trend.

For the rapeseed oil additivated with ZnO, it is observed that, at the speed v=0.38 m/s, COF does not have a clear tendency of dependence on the load and the concentration of the nanoadditive (Fig. 5.18).

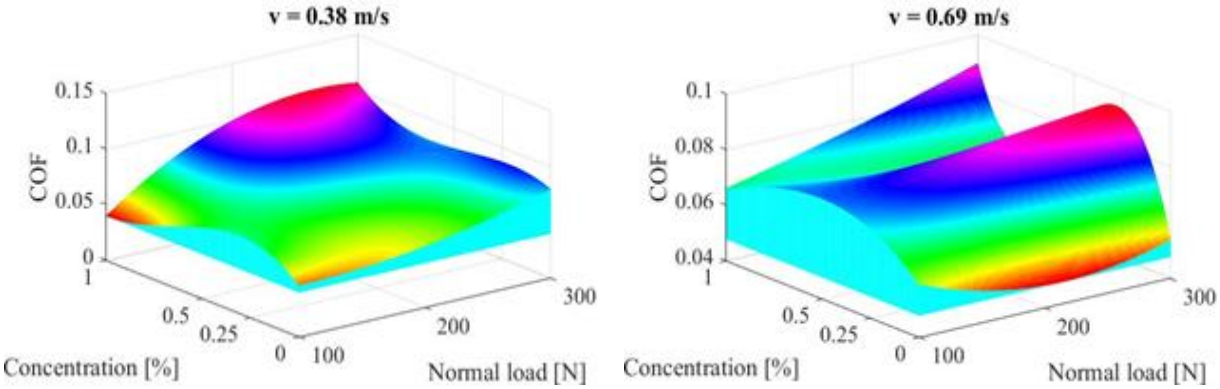

Fig. 5.18. COF maps for tested lubricants additivated with ZnO

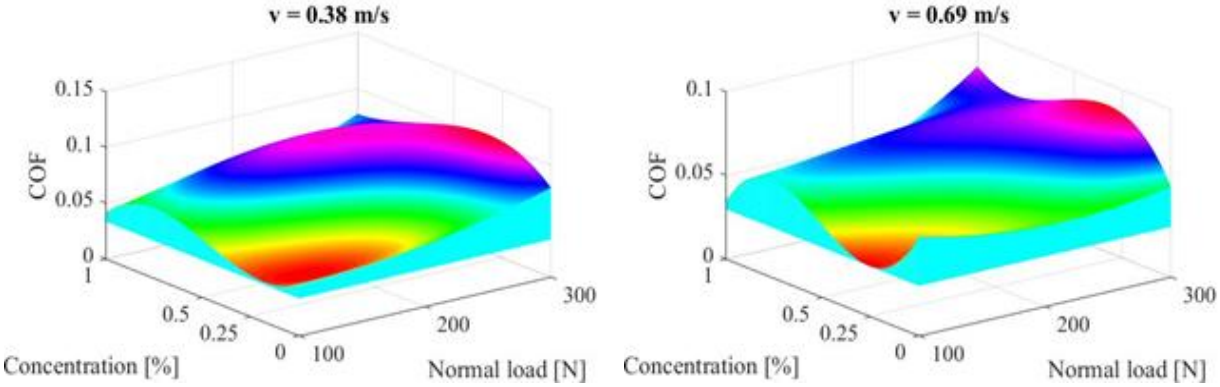

Fig. 5.19. COF maps for tested lubricants additivated with TiO_2

For rapeseed oil additivated with TiO_2, the friction coefficient is higher at a speed of 0.69 m/s and the load F=300 N, exceeding the value of 0.1 (Fig. 5.19).

5.7.3. Wear parameters

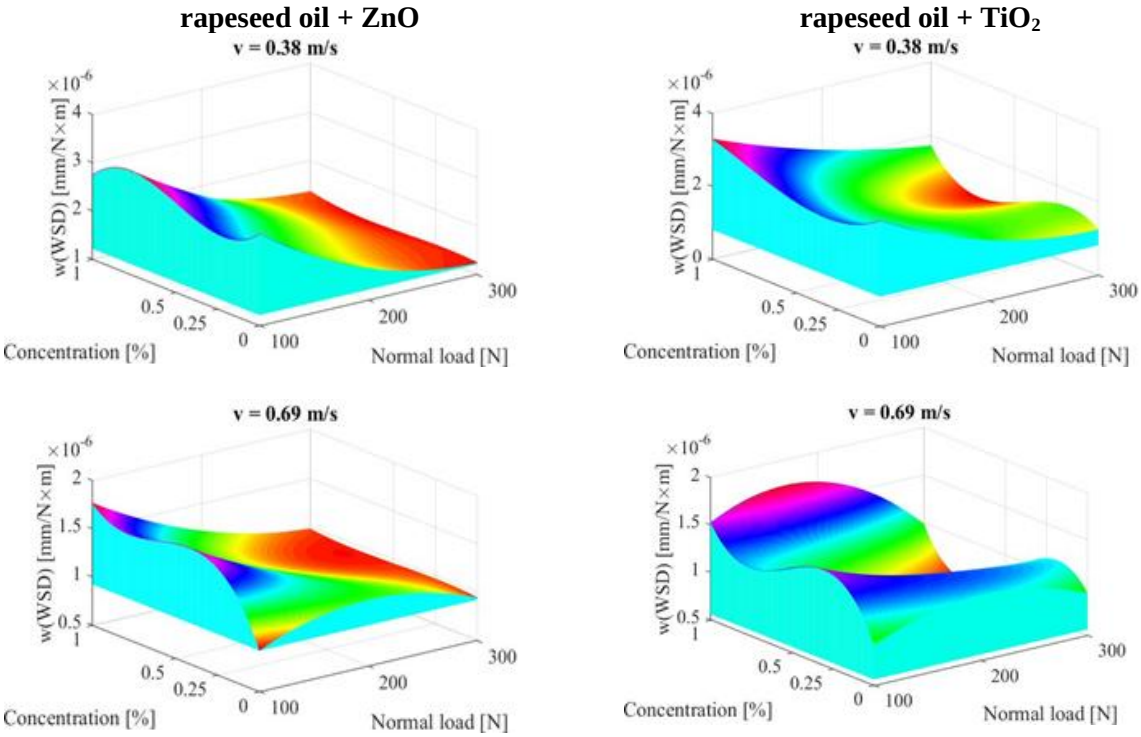

Fig. 5.20. w(WSD) maps for tested lubricants

The influence of the quality of the additive is manifested not by the minimum value, but by the area of the map domain for which minimum values of w(WSD) are obtained.

Figure 5.20 shows maps of w(WSD) for each tested speed. It is observed that, regardless of the nature of the additive, at the concentration of 1% and the least severe regime (F=100 N, v=0.38 m/s) the highest values of the wear parameter were obtained.

It would result that, at low loads, the nanoadditive is not pressed and maintained in the contact profile; in this case, it favors the increase of wear by alternating areas in direct contact and by hindering the circulation of fluid (for cooling the contact).

5.7.4. Temperature in lubricant bath

Figure 5.21 shows the maps for the evolution of end test temperature in the lubricant bath, for rapeseed oil and rapeseed oil additivated with TiO_2 and ZnO. 0 means zero concentration of additive, that is the rapeseed oil.

The highest temperature values were obtained for the non-additivated rapeseed oil.

In conclusion, the additives tested by the author increased the temperature of the additive lubricants as compared to rapeseed oil, in any regime, but the increase does not lead to the oxidation zone of rapeseed oil (~ 140 ºC).

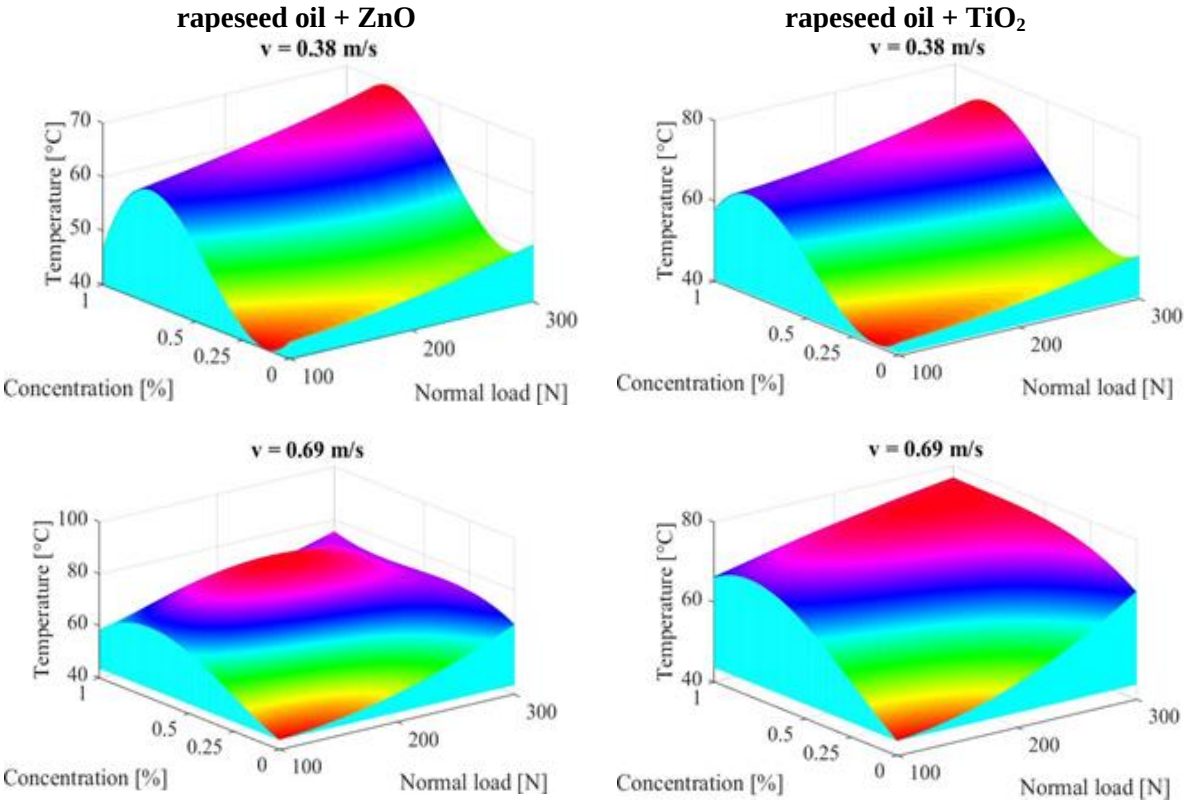

Fig. 5.21. Maps for temperature in oil bath for tested lubricants

5.8. Severe regime tests

5.8.1. Test parameters for lubricants in severe regime

In the case of severe regime, wear and friction are influenced by some properties of the boundary layers formed on the surface of materials. These continuous layers block the contact between the elements.

The test parameters for tested lubricants in severe regime are:

- load - from 500 N to 900 N (step increase of 50 N),
- sliding speed - 0.53 m/s, corresponding to a rotational speed of1400 rpm,
- test time - 1 minute (±1%),
- the concentration of the additive in the formulated lubricants is 0.25%, 0.50% and 1% (wt).

5.8.2. Friction coefficient

In severe regime tests, the friction coefficient reaches extreme values that can lead to seizures.

For the rapeseed oil (Fig. 5.22), large variations of the friction coefficient are observed until the second 15 of the test, after which the values have not large variations. This means that the surface destruction or sudden processes that occur at high loads occur in the first period of the test, not towards its end.

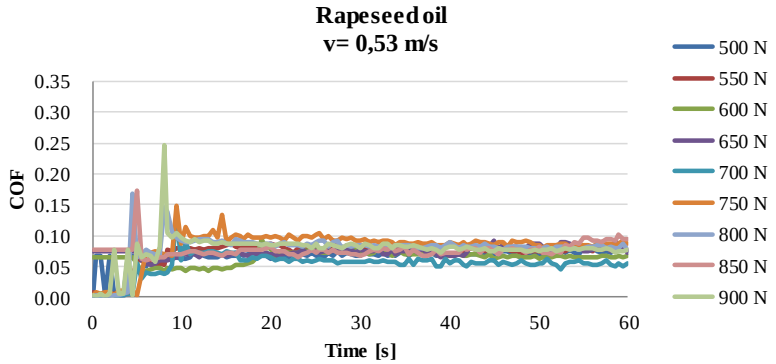

Fig. 5.22. The evolution of COF for rapeseed oil, in severe regime

Figure 5.23 gives the evolution of the friction coefficient for the case of rapeseed oil additivated with 1% TiO_2, in severe regime. There is an increase of the friction coefficient and a rifling of it in the first 10-15 seconds, but after that the values become stable around 0.10...0.13.

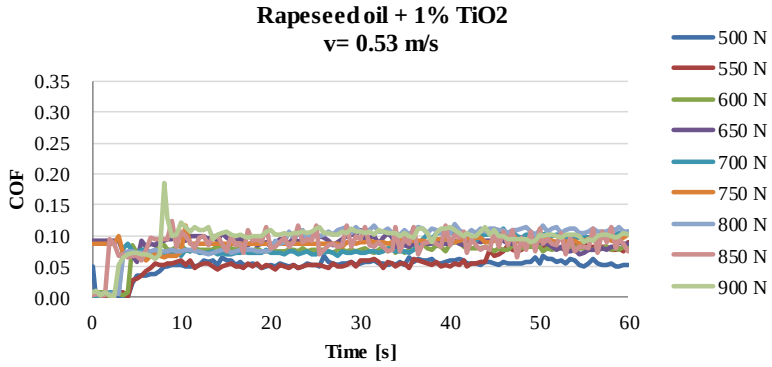

Fig. 5.23. The evolution of COF for rapeseed oil additivated with 1% TiO_2, in severe regime

Figure 5.24 gives the evolution of the friction coefficient for the case of rapeseed oil additivated with 1% ZnO, in severe regime. COF has very high values at the beginning of the test, after which it goes to the value of 0.1, which means a mixed lubrication regime. It means that, at the beginning of the test, there are major changes (plastic strains and abrasive wear) that generate the large wear scars. COF oscillations last up to 30 s.

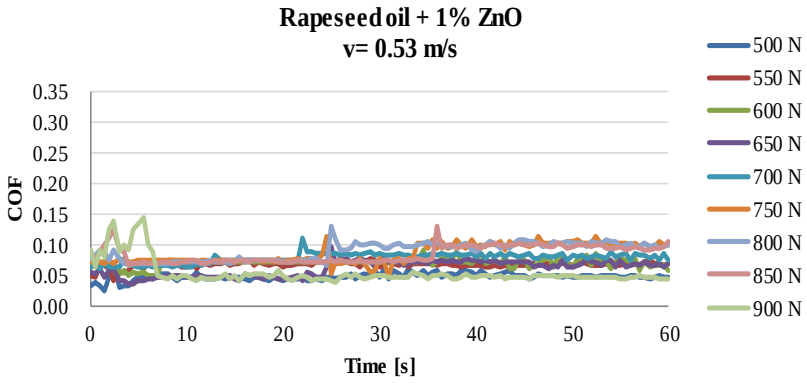

Fig. 5.24. The evolution of COF for rapeseed oil additivated with 1% ZnO, in severe regime

In Fig. 5.25, the values of the average friction coefficients for the rapeseed oil and rapeseed oil additivated with TiO_2 and ZnO nanoparticles are given.

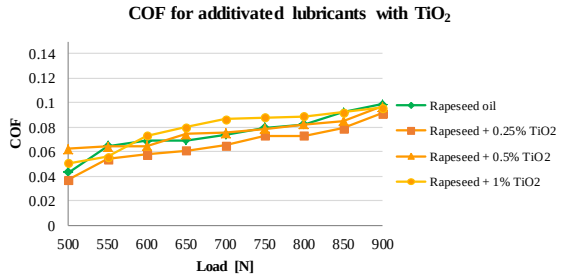

a) Lubricants additivated with TiO_2

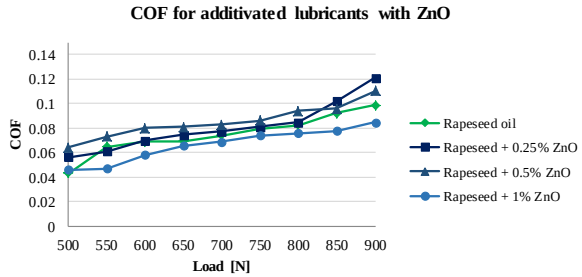

b) Lubricants additivated with ZnO

Fig. 5.25. Average values of friction coefficients

For the lubricants additivated with TiO_2, the graph aimed to compare COF values. No conclusive result was obtained from the representation; it is not possible to determine which of these friction coefficients is better, because the values are crowded around the value of 0.1, on average.

In the case of rapeseed oil additivated with ZnO, higher COF values were obtained for the lubricants additivated with 0.25% and 0.5% additive. In the severe regime, the average of the friction coefficients does not reflect the destruction processes on the tested balls.

5.8.3. Wear scar diameter (WSD)

The load-wear curve is a very important characteristic for tests performed in a severe regime because the shape of the curve and the wear scar diameter values reveal if the lubricant behavior is adequate.

Figure 5.26 shows the average values of the wear scar diameter for rapeseed oil and rapeseed oil additivated with TiO_2 and ZnO nanoparticles.

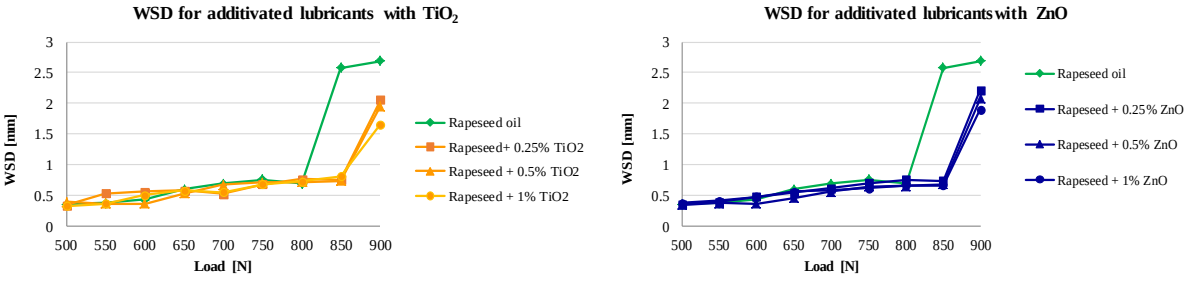

a) Lubricants additivated with TiO_2 b) Lubricants additivated with ZnO

Fig. 5.26. Average values of WSD for rapeseed oi land rapeseed oil additivated with TiO_2 and ZnO

Very high values (~3 mm) are observed for the non-additivated rapeseed oil and for the rapeseed oil additivated with 0.5% TiO_2. For the additive concentration of 0.25% and 1%, the WSD values are much smaller, reaching almost 2 mm for the lubricant additivated with 0.25% TiO_2. The best performance had the rapeseed oil additivated with 1% TiO_2.

For the non-additivated rapeseed oil and for the one additivated with ZnO nanoparticles, at F=500 N and F=550 N, the WSD values are almost identical, which means that the lubricants tested under these loads behave similarly to the normal working regime. From 550 N to 800 N (inclusive), all tested lubricants followed a similar curve with slightly larger slope lines. Starting with 850 N, the curve becomes different, the higher slope being obtained for the non-additivated rapeseed oil. The lubricant with a higher concentration of additive (1% ZnO) continues the previous trend, which means that the lubricant can withstand much higher loads than other lubricants. Between 850 N and 900 N, the slope of each lubricant is different. The best tribological behavior had the lubricant with 1% ZnO.

Figure 5.27 presents images with wear scars, measured with an optical microscope, for rapeseed oil and rapeseed oil additivated with 1% TiO_2 and 1% ZnO.

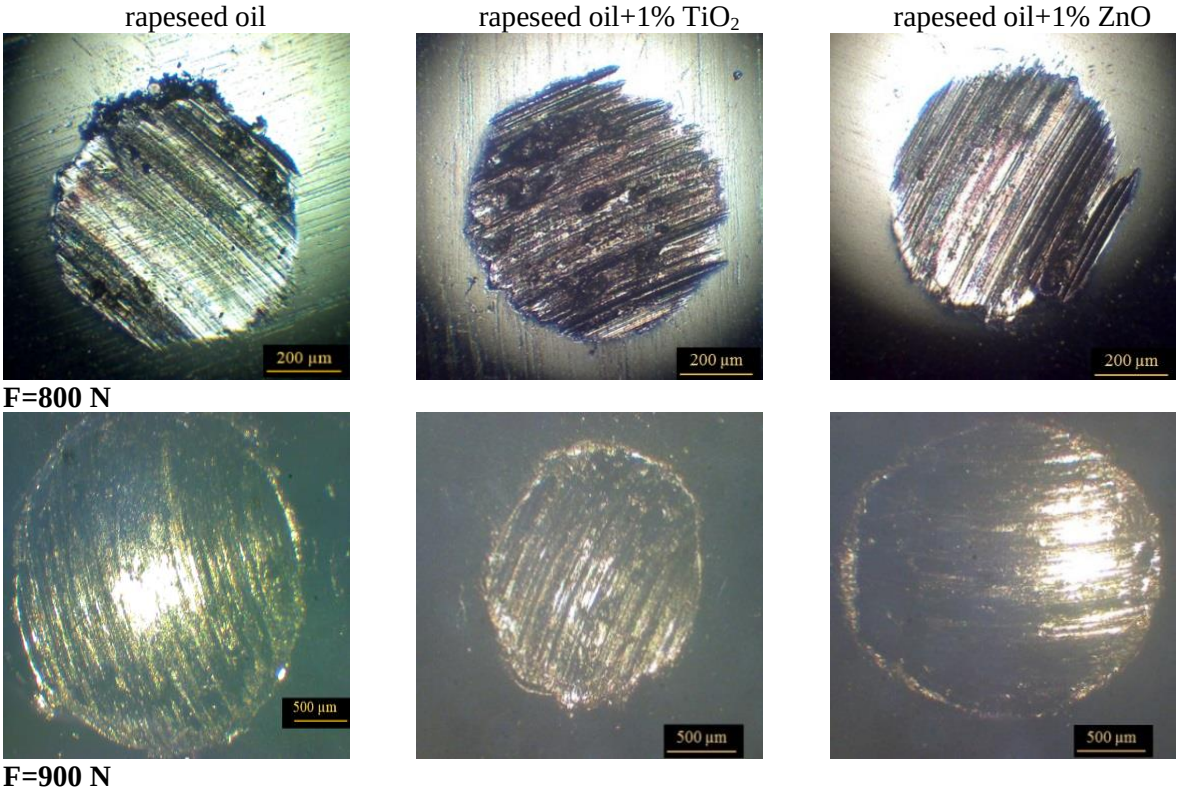

Fig. 5.27. Wear scars measured with an optical microscope

5.8.4. Temperature in the lubricant bath, at the end of the test

The temperature of rapeseed oil and rapeseed oil additivated with TiO_2 and ZnO nanoparticles, in the lubricant bath, was analyzed in Fig. 5.28.

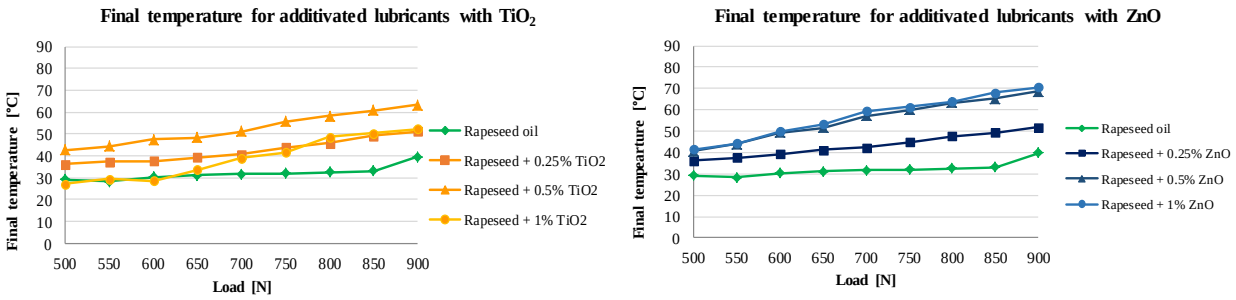

a) Lubricants additivated with TiO_2 **b)** Lubricants additivated with ZnO

Fig. 5.28. The evolution of temperature in the lubricant bath

The lowest temperature values are obtained, at the end of the 1 minute test, in the severe regime, for rapeseed oil (between 30 °C-40 °C).

In the case of the additivation of rapeseed oil with TiO_2 nanoparticles, the highest temperature at the end of the test was recorded for rapeseed oil additivated with 0.5% TiO_2 (exceeding 60 °C).

For rapeseed oil additivated with ZnO, an increase of temperature for the lubricants additivated with 0.5% and 1% ZnO nanoparticles is observed. In the case of heavy loads, even accidentally, the temperature will rise and the cooling system of the device must maintain the temperature below the value of the oxidation temperature of vegetal oils (~140 °C).

The additional heat generation could be explained by the friction of the ZnO particles, rolling in contact.

5.9. Conclusions on the tribological behavior of the formulated lubricants

The research focused on the tribological study of rapeseed oil and rapeseed oil additivated with ZnO and TiO_2 nanoparticles.

At high sliding speeds, for non-additivated rapeseed oil, a fluid film is noticed duet o the low values of COF in normal regime. The friction coefficient of rapeseed oil is less sensitive to load at high speeds.

It is noted that rapeseed oil additivated with 1% ZnO and 1% TiO_2 did not improve the value of the friction coefficient, but the additivation of rapeseed oil was efficient in reducing wear.

Chapter 6
Roughness parameters analysis for wear scars for rapeseed oil with nanoadditives on the four-ball machine

6.1. 2D and 3D parameters of the surface texture

For the analysis of the worn surface quality, from the studied documentation [73], [71], [19], [20], [31], [62], [50], [65], [74], the following directions of investigation are outlined:

- a comparison must be done between the 2D/3D parameters, using a method for sampling the 2D parameters and the areas investigated for the 3D parameters,
- the study and the tests should be analyzed in order to fiind a correlation between the evolution of the texture parameters and the functional parameters,
- the study should be done for both surfaces of the triboelements.

Average arithmetic deviation of the profile, Ra or of the surface, Sa [μm]

$$Sa = \frac{1}{M \cdot N} \sum_{j=1}^{N} \sum_{i=1}^{M} \left| z(x_i, y_j) \right| \tag{6.1}$$

$$Ra = \frac{1}{M} \sum_{i=1}^{M} \left| z(x_i) \right| \tag{6.2}$$

where $z(x_i)$ is the height of the rated profile, at any position (x_i), i=1...M.

Average arithmetic deviation of the profile, Ra, or of the surface, Sa, is the most used parameter in profilometric studies.

The maximum surface/profile height, St/Rt is the distance between the highest peak and the deepest valley in the investigated area.

If working with unfiltered raw profiles relative to a reference line/surface:

$$Rt = (|Rp| + |Rv|) \tag{6.3}$$

$$St = (|Sp| + |Sv|) \tag{6.4}$$

Functional parameters

In the 2D analysis, these parameters can be defined from the load-bearing length curve and in the 3D analysis they can be defined from the load-bearing area curve. The curve described by the functional parameters is called Abbott-Firestone curve and characterizes the surface bearing capacity.

These parameters also have suggestive names: Rpk - "zone of asperity heights" or contact region (in this zone, in the wear process, the peaks of asperities are deformed and/or detached in contact with the conjugate surface), Rk - the "core" of the texture, "the load bearing core" in service, Rvk - "the valley area" or "lubricant retention area".

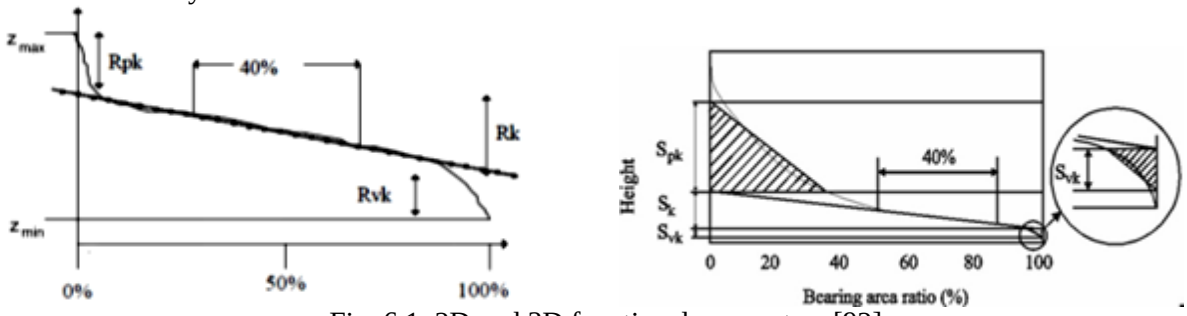

Fig. 6.1. 2D and 3D functional parameters [92]

6.2. Methodology for recording the texture of wear scars

6.2.1. Surface texture evaluation methodology

For surface quality assessment, the NANOFOCUS μSCAN laser profilometer, from the "Ştefan cel Mare" University of Suceava, was used. This is an optical non-contact profilometer for measuring surface microtropography, with a measuring area of 150 mm x 200 mm, a vertical measurement range of 1.00 μm to 18 mm, a vertical resolution of 25 nm [NanoFocus AG μScan®]. Mountains SPIP program [92] was used to process the results. The 3D parameters were calculated for each wear scar of the three stationary balls and the average, maximum value and minimum value were calculated. The measurement step is the same for 3D and 2D investigations: 5 μm. Line spacing for 3D measurements is also 5 μm. 2D and 3D parameters are the average of three measurements, that is, three profile lines,

perpendicular to the sliding direction, on each wear scar.

The linear profiles must be perpendicular to the sliding direction, so they are one of the axes of the selected ellipse delimiting the wear scar. 3D parameters are calculated for all z(x,y) values measured on the investigated area (wear scar).

Figure 6.2 presents a wear scar, virtually rebuilt with Mountains SPIP 8.1, on a ball of a test with rapeseed oil and a regime F=100 N and v=0.69 m/s. The wear scar was „cut" from the originally recorded image, the ellipse of the trace being in accordance with the measurements obtained under the optical microscope.

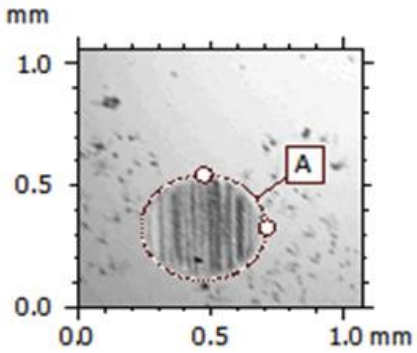

Fig. 6.2. Selecting wear scar area as an ellipse. Rapeseed oil, F=100 N, v=0.69 m/s

For each wear scar, for the measurement and calculation of the parameters, the steps described below are followed (Fig. 6.3).

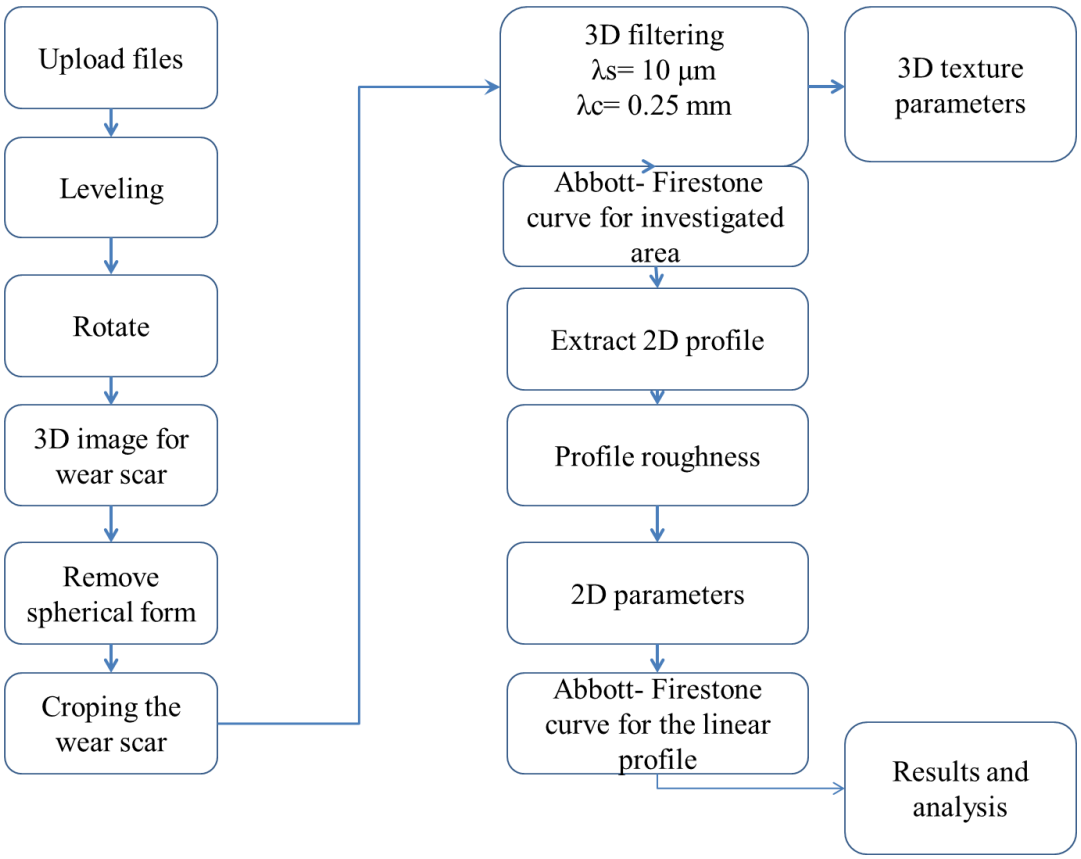

Fig. 6.3. Measuring and calculating roughness parameters with Mountains SPIP 8.1

The parameter values depend on the applied filters. The following filters were kept constant for this study: λs=10 μm and λc=0.25 mm, taking into account recomandations from [93], [94].

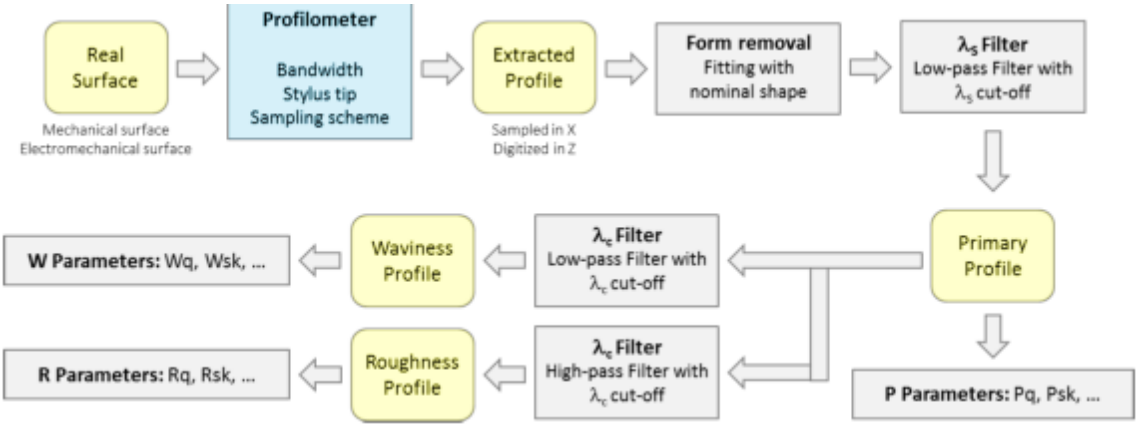

Fig. 6.4. Measurement diagram on an optical profilometer [10]

6.3. Study of the worn surface texture of the balls, with 3D profilometry

6.3.1. 3D parameters for initial surface of the ball

Figure 6.5 shows a virtualy rebuilt image, obtained with the Mountains SPIP 8.1 program, of the investigated area of 1500 µm x 1500 µm for a ball, using the non-contact profilometer.

Table 6.1 gives characteristic values for the surface of the balls.

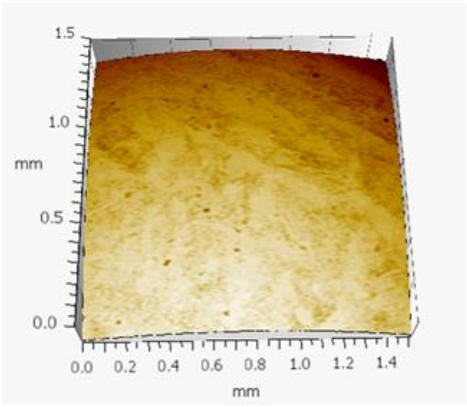

Fig. 6.5. Virtual image of the initial surface of the ball

Table 6.1. Characteristic values for the initial surface of the ball

	2 µm	**5 µm**	**20 µm**
Sa [µm]	0.1938	0.206	0.2261
Sq [µm]	0.2984	0.313	0.3188
Ssk	0.3077	-0.203	0.3124
Sku	12.58	19.17	6.359
Sv [µm]	3.617	6.027	1.351
St [µm]	8.334	10.03	3.314
Sp [µm]	4.717	4.001	1.963
Spk [µm]	0.4733	0.474	0.4863
Sk [µm]	0.4193	0.484	0.5795
Svk [µm]	0.4604	0.486	0.4180

Taking into account the information in Fig 6.5 and Table 6.1, the characterization of the initial (non- worn) surface texture of the balls can be as follows:

- very rare high asperities (St=10.03 µm),
- fine finished surface (Sa=0.206 µm),

- plateau with bumps resulting from the technological peculiarities of obtaining the surface of the balls (Ssk= −0.203, Sku =19.17).

The Abbott-Firestone curve (Fig. 6.6) is often used to evaluate the behavior of a surface with a certain degree of roughness under load and motion to evaluate the "blockage" retain of a quantity of lubricant in the texture valleys [11], [21].

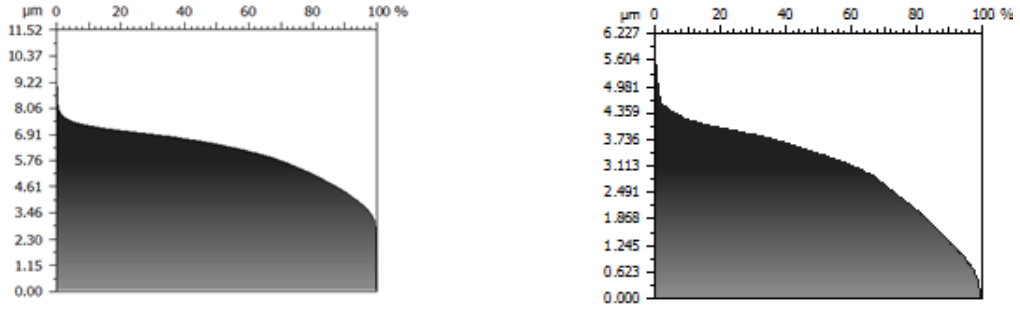

a) 5 µm step **b) 20 µm step**

Fig. 6.6. Abbott-Firestone curve for non-worn ball texture, with different reading steps

Analyzing the shape and characteristic values of the Abbott-Firestone curve, a very large difference is observed between the 20 µm step scan and the smaller step, 5 µm. The author did the profilometric study with 5µm step between lines and points, on each line.

6.4. Analysis of 3D parameters for worn ball scars in normal and severe regime

6.4.1. Normal operating regime

Amplitude parameters

Average arithmetic deviation of the surface, Sa [µm]

In Fig. 6.7, the parameter Sa is presented, after testing with non-additivated rapeseed oil and additivated with TiO_2 and ZnO, at the loads of 100 N, 200 N and 300 N, and sliding speed of 0.38 m/s and 0.69 m/s.

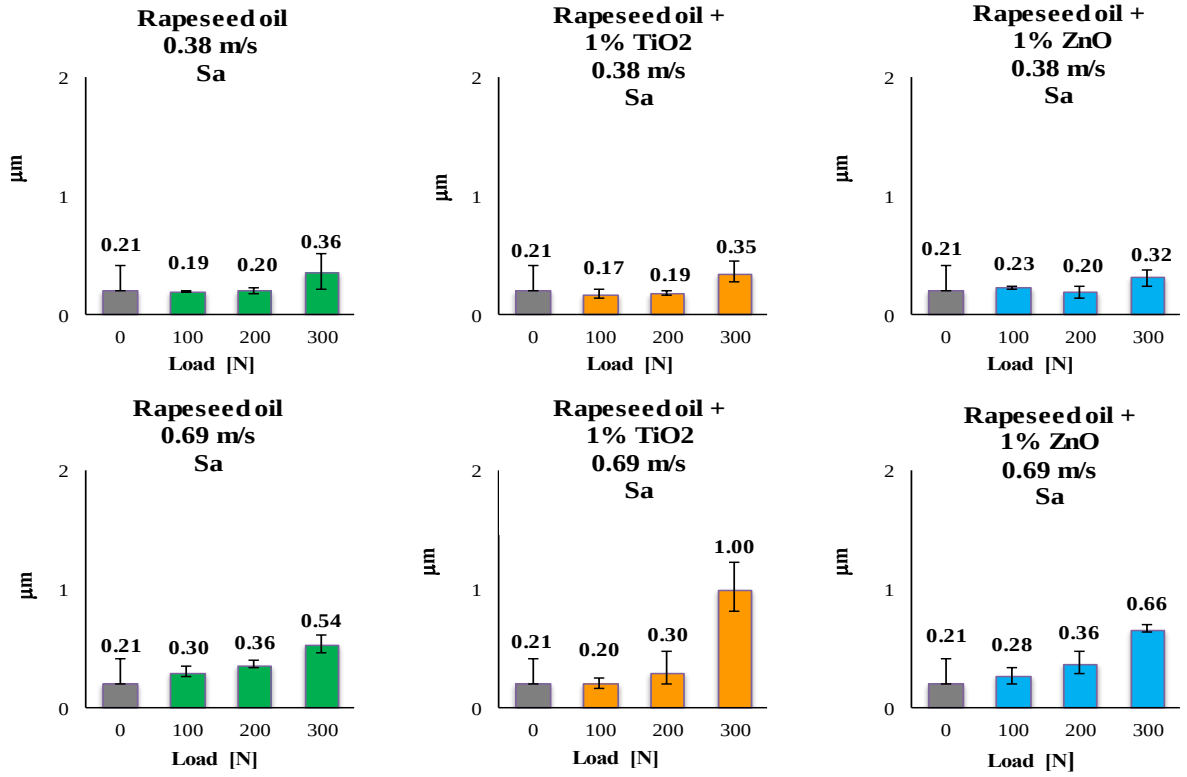

Fig. 6.7. The evolution of Sa parameter for normal regime

The mean values of Sa appear to be linearly dependent on the load. At lower speed, the degradation of the ball surface evolves after a lower slope for the transition from F=100 N to F=200 N. A slight increase of Sa is observed for each load, at any of the sliding speeds. At the lowest speed (v=0.38 m/s), for non-additivated rapeseed oil and for rapeseed oil additivated with 1% TiO_2, a slight decrease is observed due to the very fine run-in (only the peaks of the roughness wear). For other speeds and loads, the average roughness increases slightly but the surfaces could be still used.

The maximum surface height, St [µm]

In Fig. 6.8, the evolution of St parameter is presented. At the lowest forces, F=100 N and F=200 N, the values of St are lower as compared to the values obtained for F=300 N, for all tested sliding speeds and for the additivated rapeseed oil, where much higher values were obtained.

St is an important parameter, especially in the lubricated contact tribology, because high heights of profile, although very rare, destroy the lubricant film, and can change the regime from an EHD regime to a mixt regime, which leads to a sudden increase in the friction coefficient.

Sa does not provide information about the spatial structure and does not differentiate between valleys and peaks of surface texture. Malburg [55] also appreciated the quality of the surface through the ratio $\xi_{(Sa,St)}$, defined as:

$$\xi_{(Sa,St)} = \frac{St}{Sa} \tag{6.5}$$

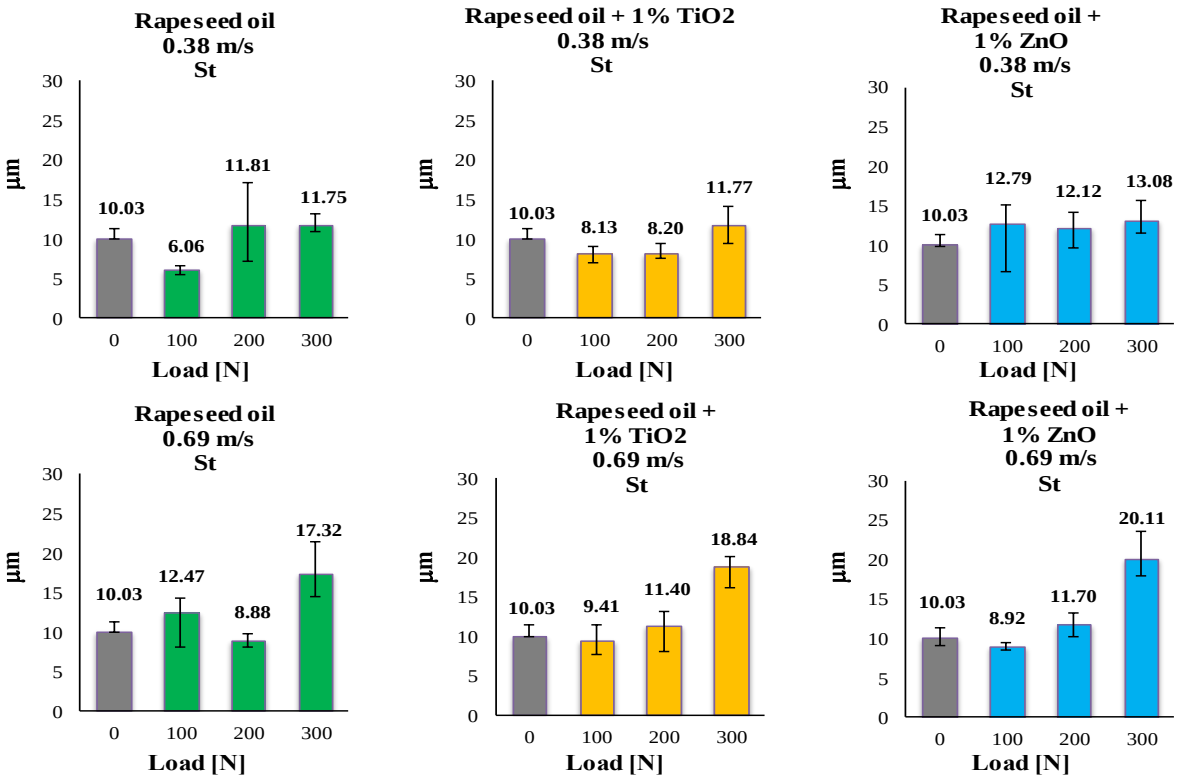

Fig. 6.8. The evolution of St parameter, as a function of sliding speed, load and additivation of rapeseed oil

The author considered that this ratio should also be taken into account when studying worn surfaces. In their case, a small value of the mentioned ratio can indicate a good quality of the worn surface, and a continuation of the operation of the tribosystem in good conditions. A high value can characterize an area with peaks and/or valleys (rare or not), but very high, which implies an aggressive wear process, at least in the area of the existence of the singular maximum of the heights of the asperities.

Table 6.2 gives the values of the parameters Sa, St and the ratio of these two parameters, St/Sa, for non-additivated rapeseed oil and the rapeseed oil additivated with 1% TiO_2 and 1% ZnO, respectively, for all loads applied at sliding speeds of 0.38 m/s and 0.69 m/s

Table 6.2. The values of the parameters Sa, St and the ratio of these two parameters, St/Sa

	0.38 m/s			**0.69 m/s**		
	100 N	**200 N**	**300 N**	**100 N**	**200 N**	**300 N**
St	6.06	11.81	11.75	12.47	8.88	17.32
Sa	0.19	0.2	0.36	0.3	0.36	0.54
$\xi_{(Sa,St)}$	31.89	59.05	32.63	41.56	24.66	32.07
	0.38 m/s			**0.69 m/s**		
	100 N	**200 N**	**300 N**	**100 N**	**200 N**	**300 N**
St	8.13	8.2	11.77	9.41	11.4	18.84
Sa	0.17	0.19	0.35	0.2	0.3	1
$\xi_{(Sa,St)}$	47.82	43.15	33.62	47.05	38	18.84
	0.38 m/s			**0.69 m/s**		
	100 N	**200 N**	**300 N**	**100 N**	**200 N**	**300 N**
St	12.79	12.12	13.08	8.92	11.7	20.11
Sa	0.23	0.2	0.32	0.28	0.36	0.66
$\xi_{(Sa,St)}$	55.6	60.6	40.87	31.85	32.5	30.46

Analyzing Fig. 6.9 for ξ, there is a decreasing trend of the parameter for the highest speed, but the values cannot be clearly framed in a speed and load dependent relationship.

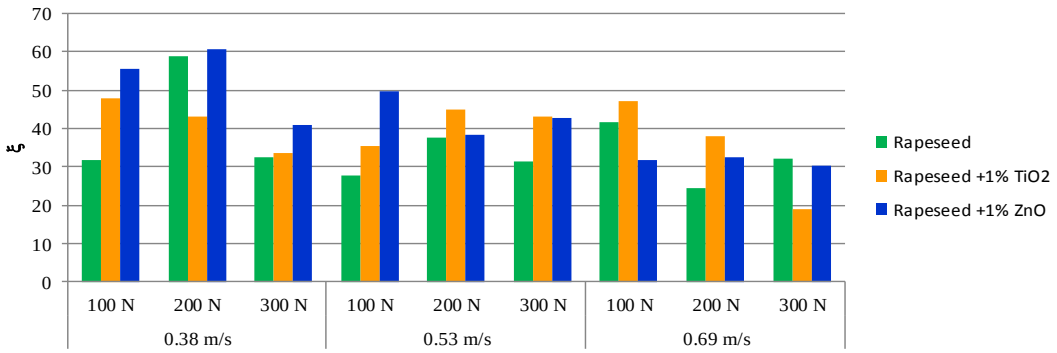

Fig. 6.9. The evolution of $\xi_{(Sa,St)}$ parameter as a function of sliding speed, load and additive nature

For the non-worn ball, the value of the parameter ξ was calculated:

$$\xi_{St/Sa} = \frac{10.03}{0.206} = 48.68 \tag{6.6}$$

3D functional parameters

In Fig. 6.10, the analyzed functional parameters are represented as their sum, Svk+Sk+Spk. In the graphs, the value 0 represents the non-worn surface of the ball.

The analysis of these parameters is important because they indicate how the components of the texture evolve (the peak area which is also the area of light wear, the area of the core resistance and the area which influences the lubricant retention in the contact).

The increase of Spk indicates an abrasive wear, observable also in photos, the decrease of Sk means the decrease of the texture layer resistance and the increase of Svk shows that the wear has extended to the bottom of the texture.

For the lubrication with rapeseed oil, a linear increase of the sum of the functional parameters with a higher slope to a higher speed, is observed.

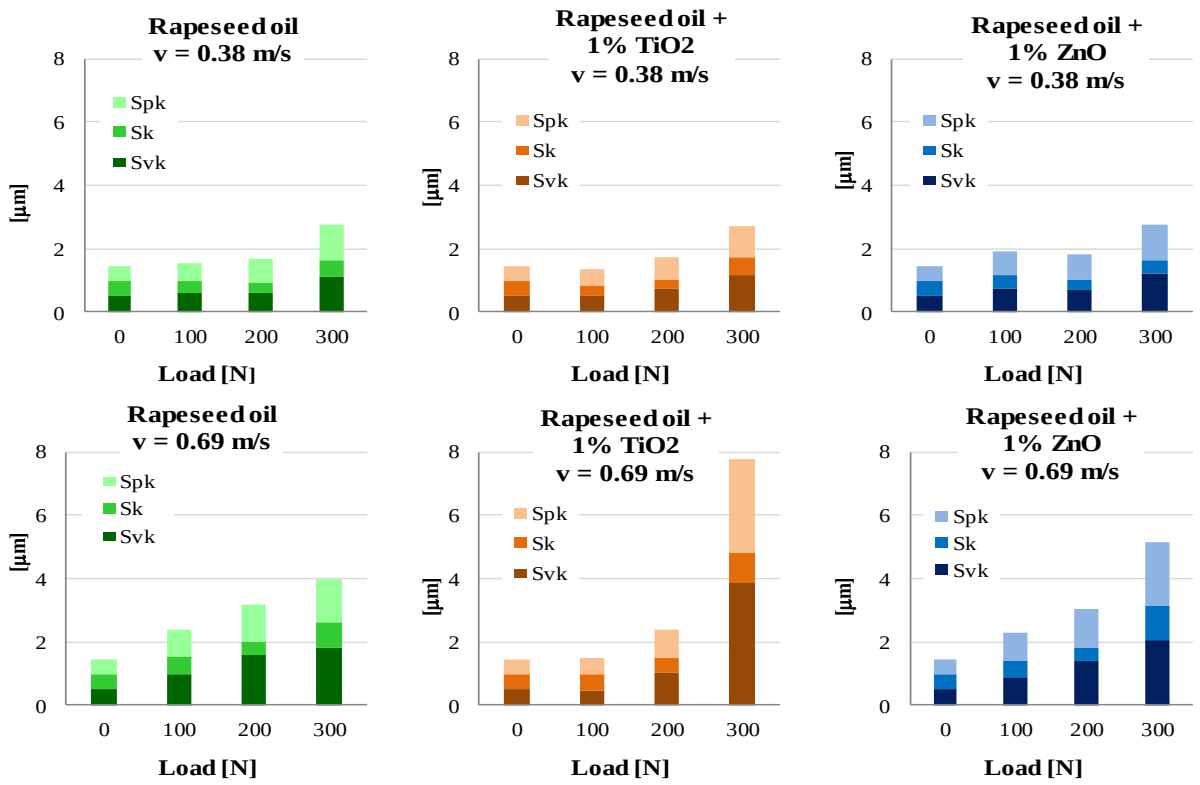

Fig. 6.10. Sum of 3D functional parameters (Spk+ Sk+ Svk), depending on the load and sliding speed

A similar evolution has the rapeseed oil additivated with 1% TiO_2, but the big changes of the functional parameters are observed only at F=300 N, which means that, for the other loads, the additive favors maintaining the texture and even finishing it because the sum of the functional parameters does not increase much from the initial value. A dramatic change is observed only for the extreme regime (F=300, v=0.69 m/s), which implies a severe regime of wear (abrasive, but possible of adhesion, also).

For rapeseed oil and rapeseed oil additivated with 1% ZnO, the sum of the functional parameters has an increase proportional to the load, the increase is proportional on all intervals, which would reflect wear without process change (no adhesive wear occurs, that would have increased the sum of the functional parameters).

6.4.2. Severe regime

From documentation [10], [21], the analysis of the roughness parameters for the severe regime is an original idea that can be capitalized in the sense of clearer delimitation and on the criterion of surface quality of the working regime accepted by the tribosystem (balls + lubricant + working regime).

Amplitude parameters

Average arithmetic deviation of the surface, Sa [µm]

Figure 6.11 presents the evolution of Sa parameter in the severe operating regime. Sa parameter expresses, as an absolute value, the difference in height of each point compared to the arithmetic mean of the surface. This parameter is generally used to evaluate the surface roughness.

The tendency to increase the roughness in the severe regime is lower for rapeseed oil up to the load of 900 N.

For nano-additivated lubricants have the same trend, but with a slightly steeper slope and for the 900 N, the arithmetic mean deviation of the surface texture increases sharply.

From the point of view of quality surface, the severe regime does not produce dramatic change at 900 N, but the wear scars increase a lot.

In the case of additivated lubricants, the surface quality changes a lot. The value of Sa parameter increases sharply at F=900 N.

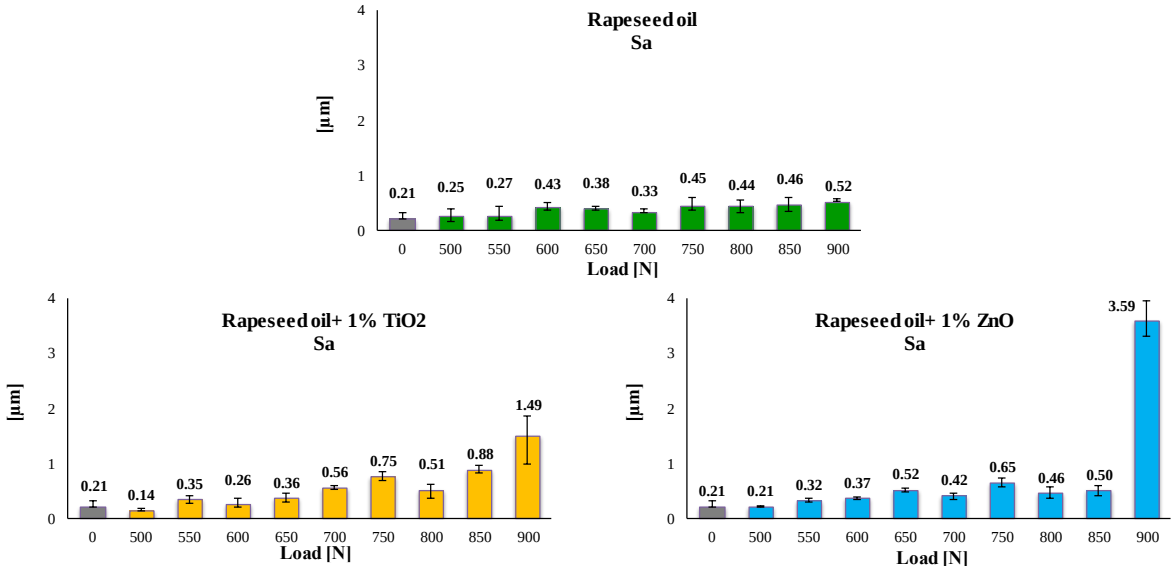

Fig. 6.11. The evolution of Sa parameter in severe regime

Figure 6.12 presents images of the wear scars, obtained with the help of the optical microscope, for the balls tested in severe regime. The applied forces were 850 N and 900 N, and the sliding speed was 0.53 m/s.

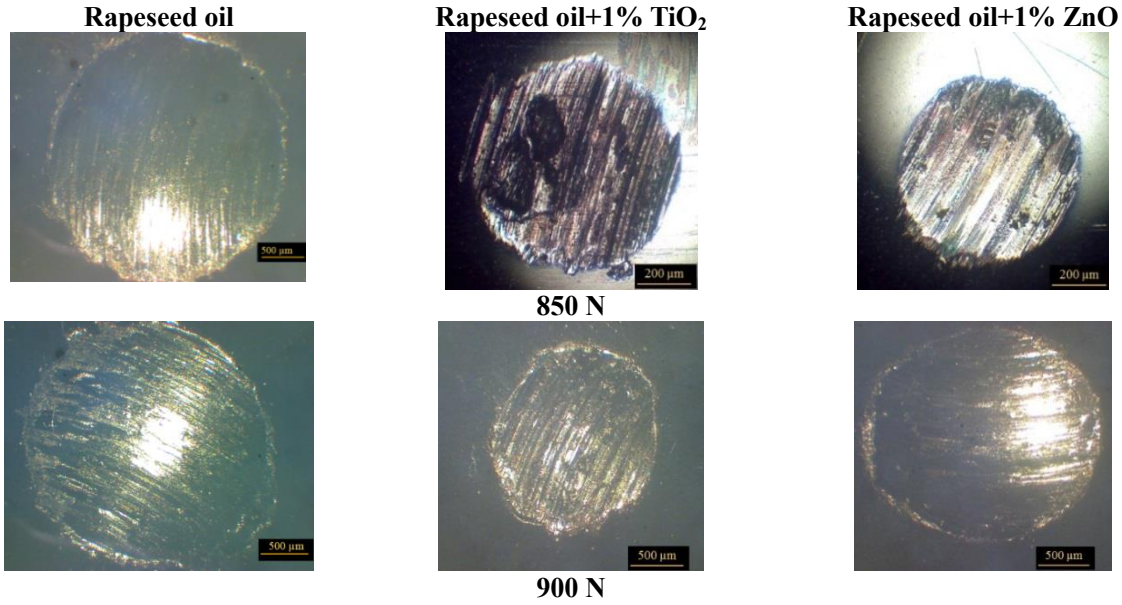

Fig. 6.12. Wear scars measured with an optical microscope, for the balls tested in severe regime

The maximum surface height, St [µm]

Regarding the evolution of the St parameter (Fig. 6.13), its increase can be observed with the increase of load, for all tested lubricants. For the rapeseed oil, the values of St are the lowest. The value starts to increase when testing the rapeseed oil additivated with 1% TiO_2, reaching the value of 41.21 µm, while testing the rapeseed oil additivated with 1% ZnO, there are obtained the highest values as comparing to the tested lubricants. In this case, the value of St reaches the value of 51.3 µm, for the load of 900 N.

The surface does not look like a scratched surface, but rather a grinded surface, visibly deformed.

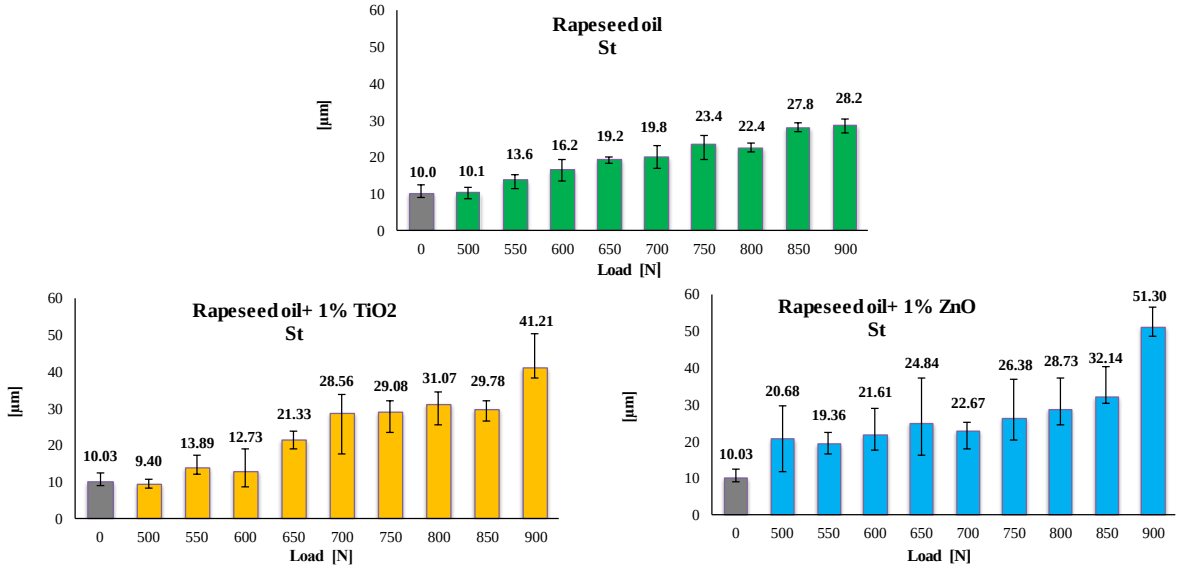

Fig. 6.13. The evolution of St parameter in severe regime

3D functional parameters in severe regime

As compared to the normal regime, the sum of the functional parameters in the severe regime (Fig. 6.14) is much higher for the additivated lubricants at high loads and a change in the weight of the parameters is seen in the sense that Spk is higher as compared to Sk.

The texture has a relatively small resistance core, that is the segment Sk in the sum is small, Svk changed substantially for 1% ZnO. The jump denotes the transition to another mode of wear, seizure possibly.

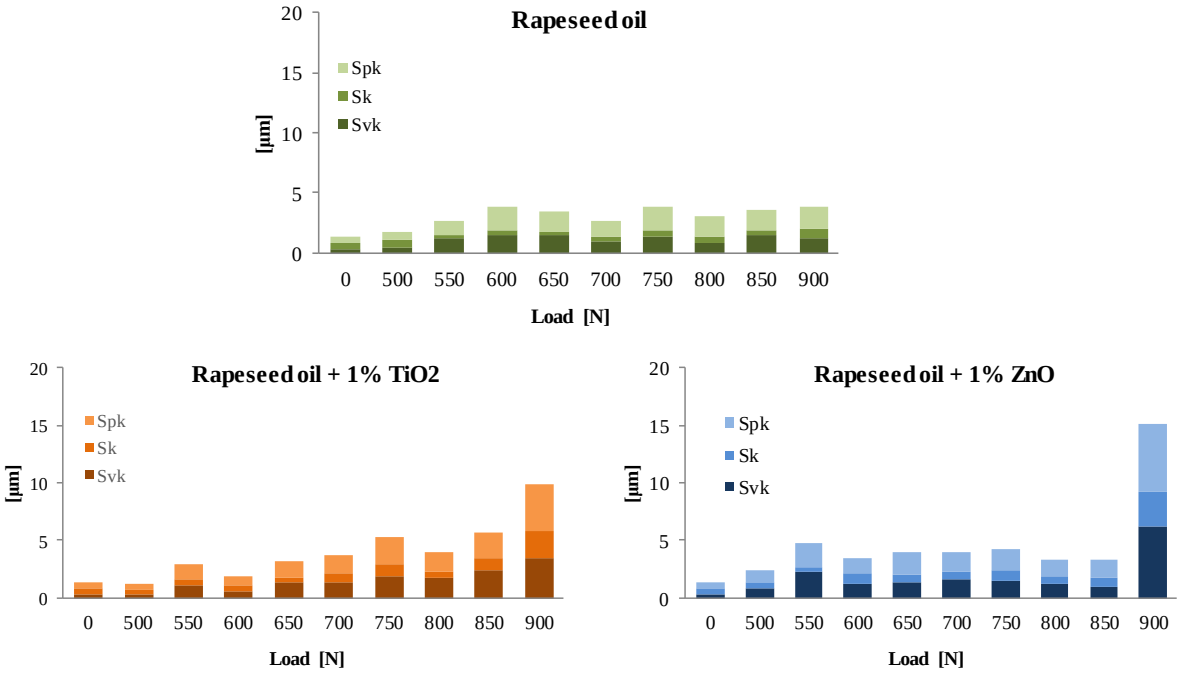

Fig. 6.14. Sum of 3D functional parameters (Spk+ Sk+ Svk) in severe regime

In support of this finding, Fig. 6.15 presents virtual images of wear scars, at the load of 500 N and 900 N, in the severe regime.

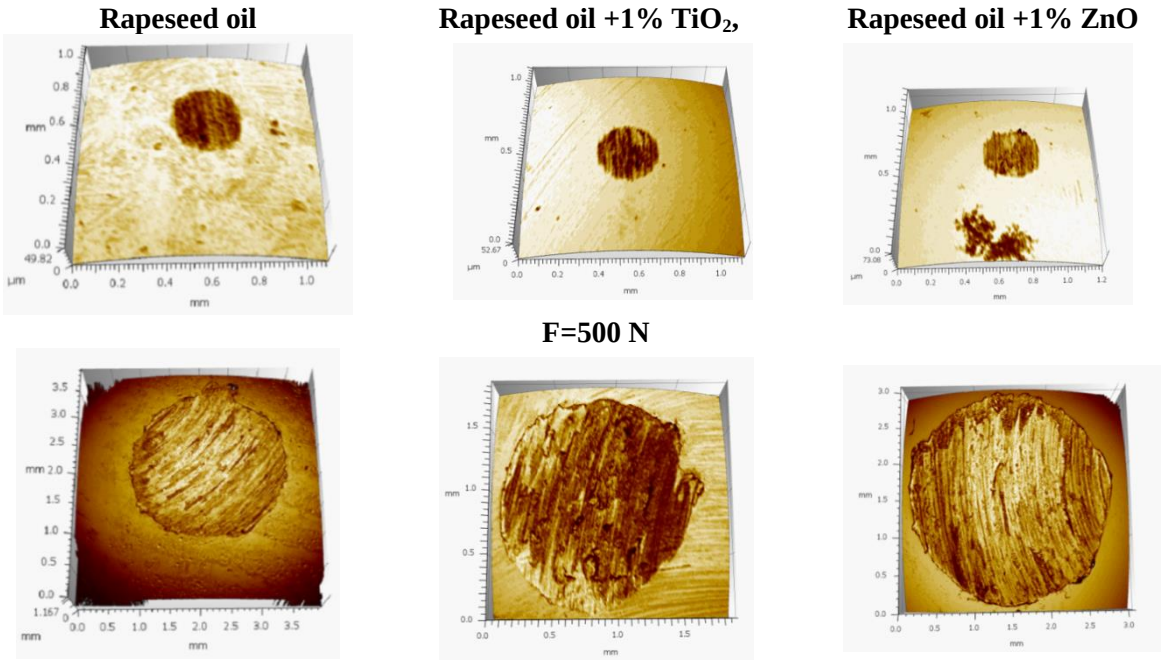

Fig. 6.15. Virtual images of wear scars

6.5. 2D parameters analysis for worn scars of the ball in normal regime

6.5.1. Normal operating regime

Amplitude parameters

Arithmetic average deviation of the profile, Ra [µm]

Figure 6.16 shows the evolution of the 2D parameter, the arithmetic average deviation of the profile (Ra), for rapeseed oil and rapeseed oil additivated with 1% TiO_2 and 1% ZnO, respectively.

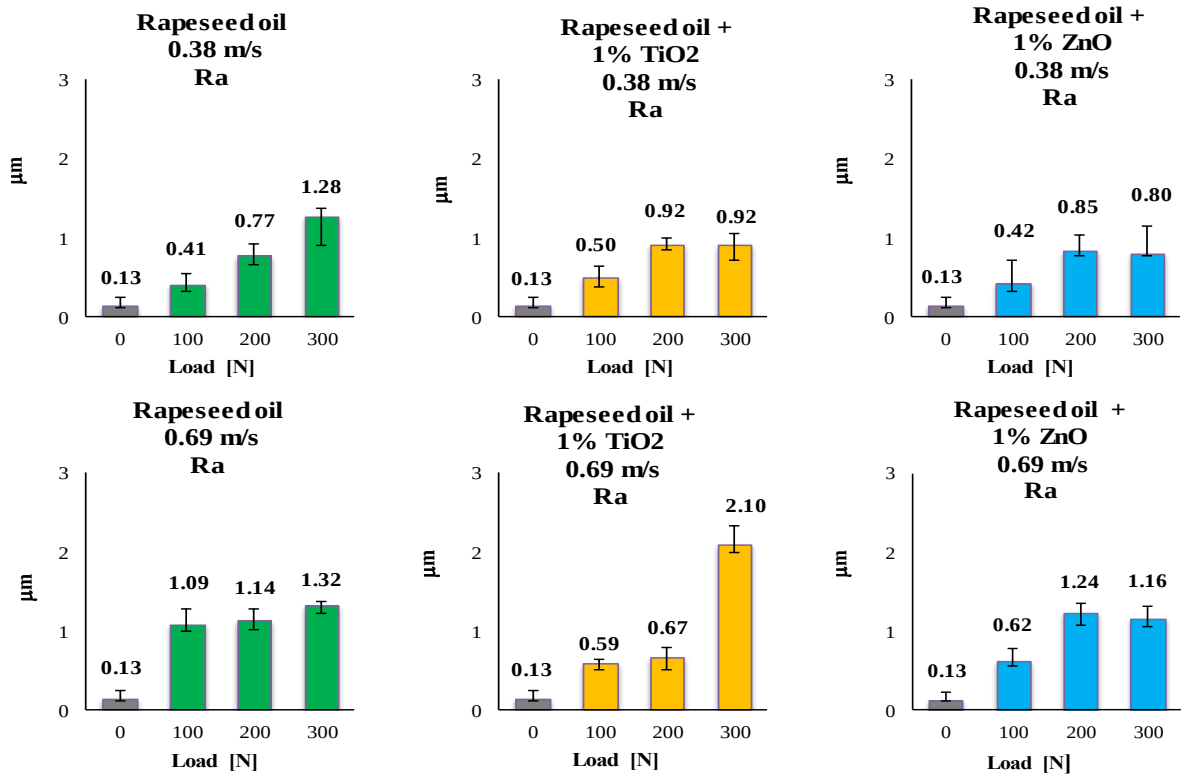

Fig. 6.16. Evolution of Ra in normal operating regime

For non-additivated rapeseed oil and for the lubricant additivated with 1% TiO_2, the increase of this parameter is observed with the increase of load. In the case of additivation with 1% ZnO, the

lowest average value of Ra is found at the lowest force of 100 N. A high value appears at F=300 N and v=0.69 m/s, for the lubricant with 1% TiO_2.

The maximum profile height, Rt [µm]

In Fig. 6.17, from the evolution of Rt parameter, it is observed the increase of the average values of the parameter with the load. The maximum value of this parameter is found in the case of rapeseed oil additivated with 1% TiO_2, tested under a load of 300 N and a speed of 0.69 m/s. Under normal regime, the parameter Rt increases sharply and substantially for rapeseed oil additivated with 1% TiO_2. The lowest values of Rt are recorded for non-additivated rapeseed oil, from where it can be seen how the surface quality is not improved by the additivation.

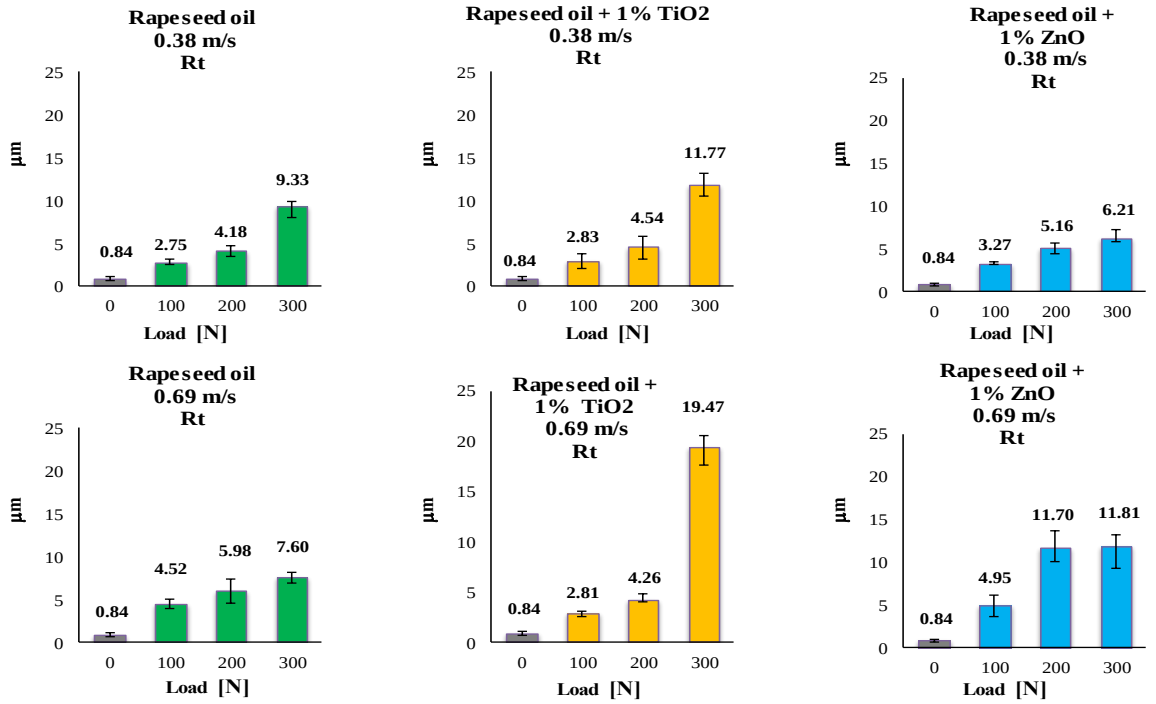

Fig. 6.17. The evolution of Rt parameter

2D functional parameters in normal regime

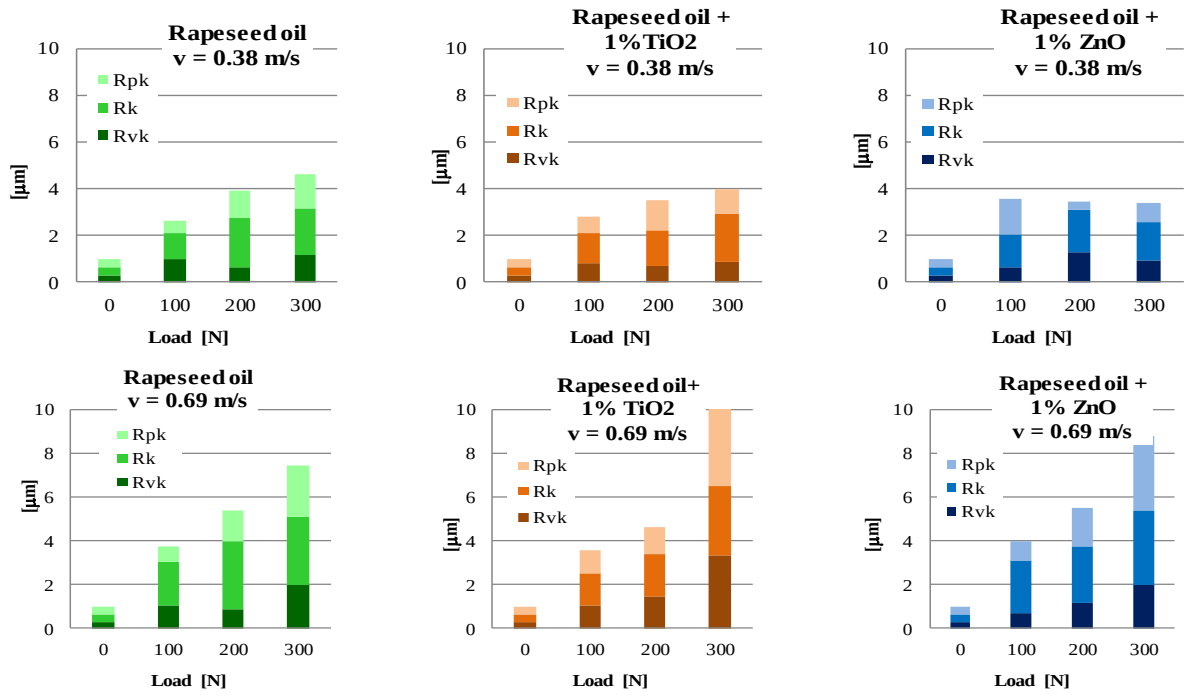

Fig. 6.18. Sum of 2D functional parameters (Rpk+ Rk+ Rvk) in normal regime, depending on the load and velocity

Figure 6.18 presents the functional parameters as a sum (Rpk+Rk+Rvk). It is observed that the sum of the functional parameters for the unused (non-worn) ball is much smaller than the sum of the parameters for the worn scars, for all the analyzed cases, which leads to the thought that the abrasive wear has performed a remodeling on the profile.

Maximum values of the sum of the functional parameters are observed in the case of rapeseed oil additivated with 1% TiO_2, at a load of 300 N and a speed of 0.69 m/s. Minimum values for (Rpk + Rk + Rvk) can be observed in the case of rapeseed oil additivated with 1% ZnO.

6.5.2. 2D parameters in severe regime

2D amplitude parameters

Arithmetic average deviation of the profile, Ra [µm]

In Fig. 6.19, the evolution of the arithmetic mean deviation of the profile texture in the severe operating regime is observed. For additivated lubricants, the maximum reached value of Ra (1.91 µm) is observed for the load of 900 N. At the load of 800 N, for both additivated lubricants, a decrease of the value of Ra is observed, as compared to the previous load, but at 850 N it begins to grow again. The lowest values of the Ra parameter were obtained for non-additivated rapeseed oil.

The evolution of Ra does not reflect the degree of severity with which the surface wear increases. Ra cannot be used to determine the transition from one regime to another.

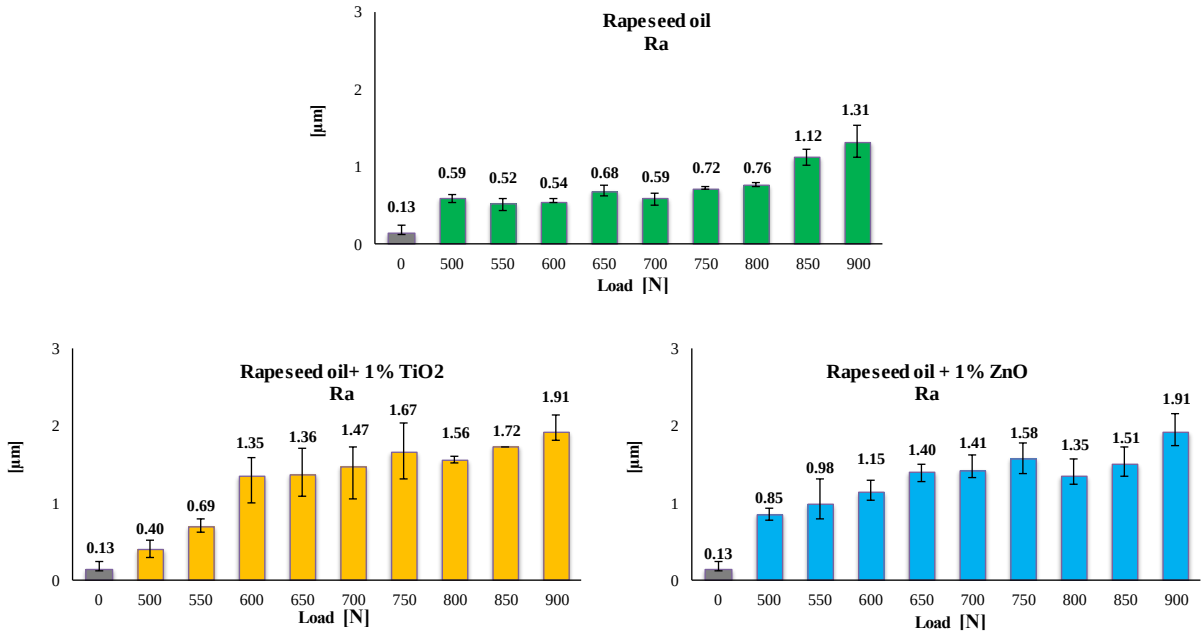

Fig. 6.19. The evolution of Ra parameter in severe regime

The maximum profile height, Rt [µm]

The evolution of the maximum profile height is given in Fig. 6.20. The Rt parameter must be used and carefully interpreted because it has sensitivity to isolated peaks and valleys. However, Rt may be relevant on surfaces that have been previously filtered with a λs filter that allows low frequencies to pass through.

The Rt parameter tends to increase at very high loads, as does the wear, too.

For non-additivated rapeseed oil, Rt increases to 850 N. For rapeseed oil additivated with 1% TiO_2, the big difference is between 600 N and 700 N. For rapeseed oil additivated with 1% ZnO, Rt increases between 850 N and 900 N, which means that ZnO would signal more clearly the entry into a very severe regime, towards seizure.

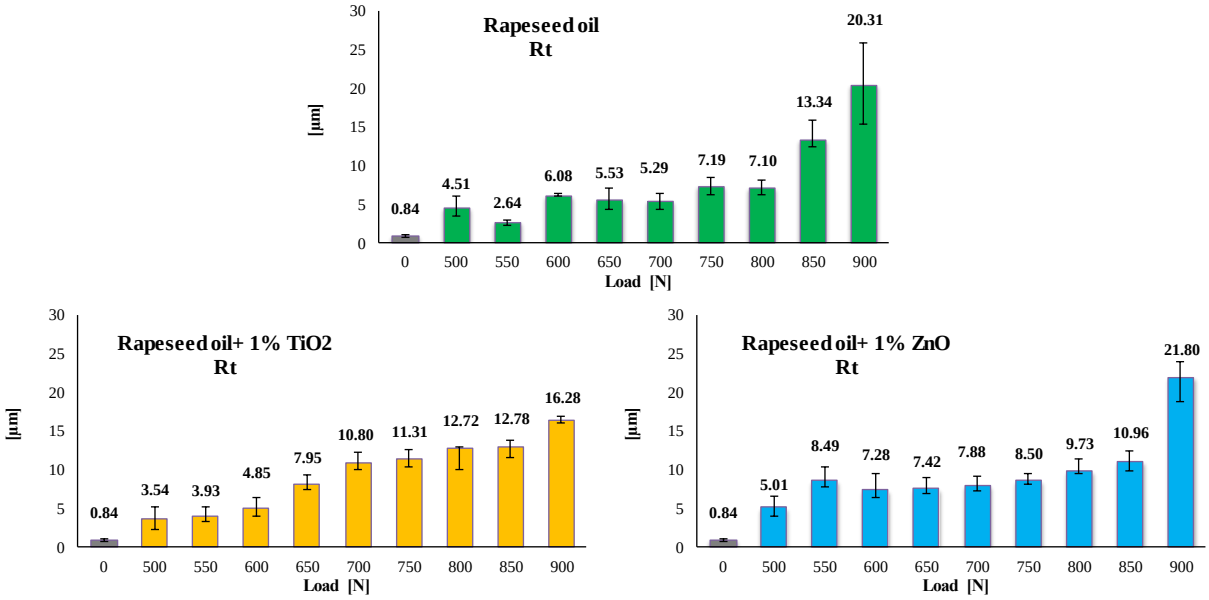

Fig. 6.20. The evolution of Rt parameter in severe regime

2D functional parameters in severe regime

Figure 6.21 shows the sum of the 2D functional parameters of the profile (Rpk+Rk+Rvk) for the severe regime. It is observed that the sum of the functional parameters for the non-worn ball gave the lowest value.

For rapeseed oil additivated with 1% TiO_2, the sum of the parameters remains constant, which may lead to the conclusion that the additive provides protection to the surface, except for the highest loads

Higher values of this sum of functional parameters were obtained for rapeseed oil additivated with 1% ZnO, at 850 N and 900 N.

In the case of non-additivated rapeseed oil, fluctuating values of the sum of the functional parameters were obtained throughout the load range.

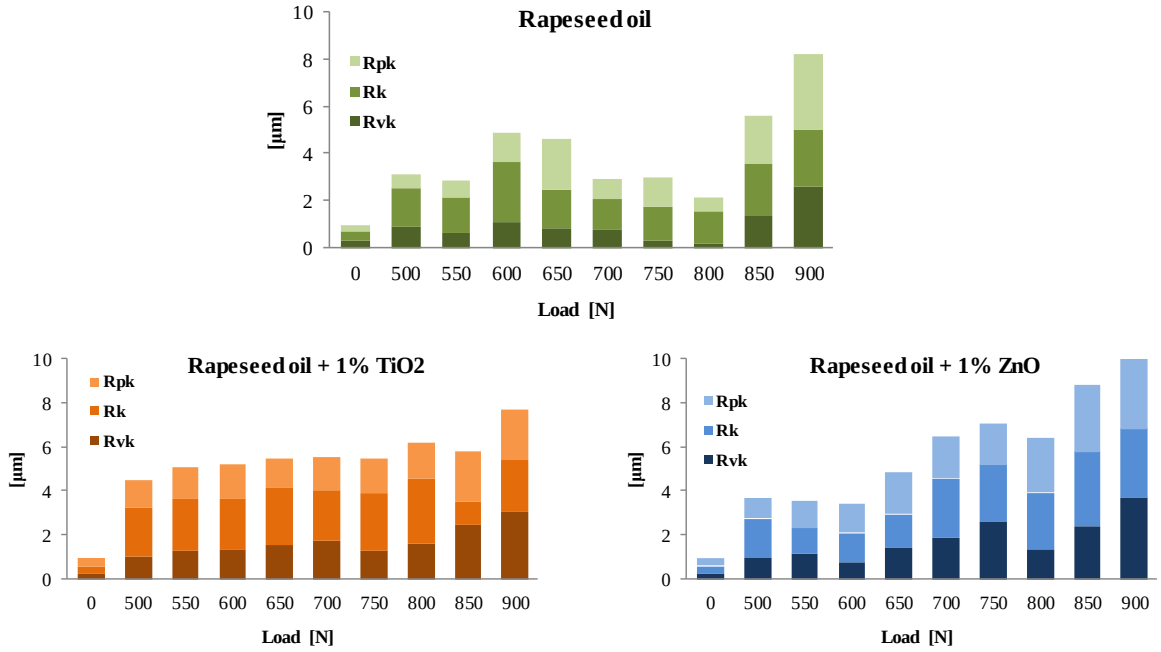

Fig. 6.21. Sum of 2D functional parameters (Rpk+ Rk+ Rvk) in severe regime

6.6. Abbott-Firestone curves

The use of Abbott-Firestone curve is an important method of characterizing the surface, especially when dealing with surfaces where it is necessary to introduce specific characteristics related

to surface integrity and functional requirements for certain applications, where specific tribological characteristics are investigated by the help of the distribution of peaks and valleys.

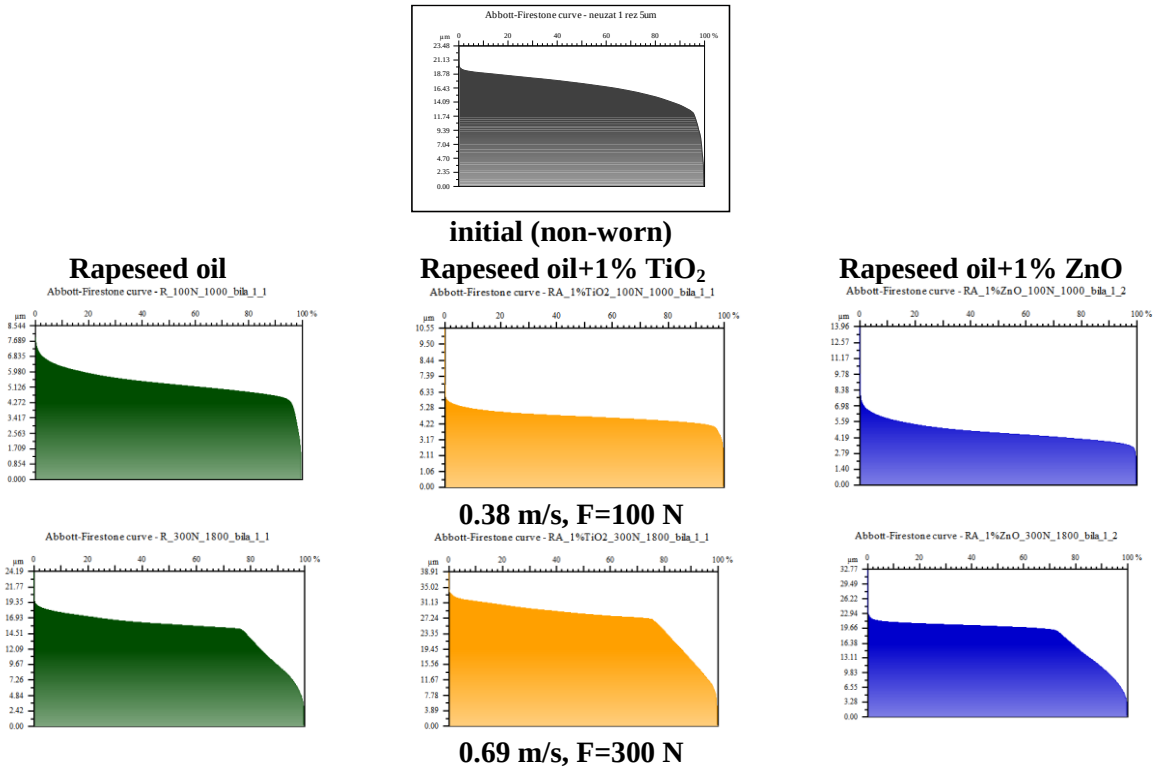

Fig. 6.22.Comparison Abbott-Firestone curves for two tests (F_1=100 N, v_1=0.38 m/s and F_2=300 N and v_2=0.69 m/s)

6.7. Correlation between wear parameters and texture parameters

Figure 6.23 shows the correlation between WSD and Sa, graphically represented .

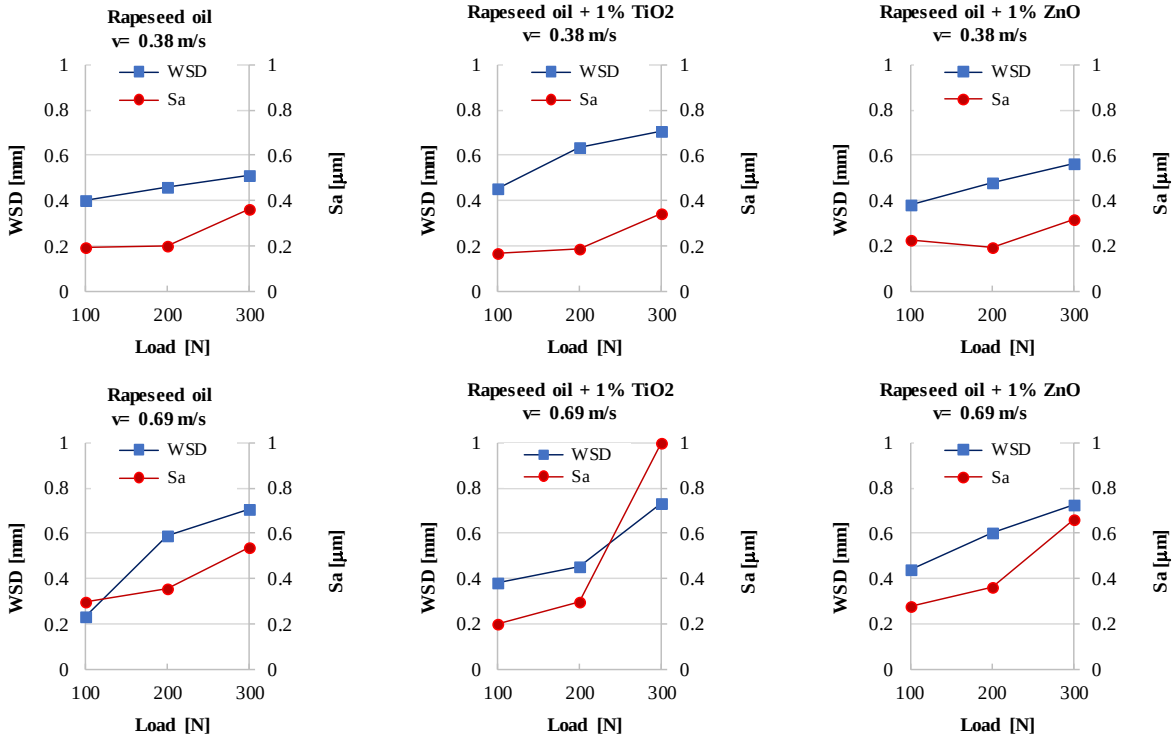

Fig. 6.23. Correlation between WSD and Sa, for different two sliding speed

These graphs are rarely used in technology, because they require a very large volume of information, but help to establish the influence of the parameter on the evolution of surface quality.

From the obtained data, it is observed that the roughness parameter Sa tends to follow the WSD, for additivated oils. High values of WSD and Sa were obtained for rapeseed oil additivated with 1% TiO_2 at the load F=300 N.

6.8. Conclusions regarding the study of the worn scars texture

The tribologists are interested in functions of the form f(v, F, t, WSD, texture parameter)=0 from which it is possible to evaluate an optimization or a delimitation of the operating regime based on wear and surface quality criteria.

In conclusion, when comparing worn surfaces and non-worn surfaces, it is recommended to consider similar surfaces in size (and geometry).

The conclusions that emerge from this study are:

- the ball load is not uniform, the difference between the measured values by profilometry being acceptable and highlighting the good quality of the 4-ball tribostester,
- the wear process is uniform on the balls, because the shape of the Abbott-Firestone curves is similar for all 3 balls,
- at low loads the wear is visible on 2D profilometry, more on the top of the profile; analyzing the 2D records for the severe regime of rapeseed oil and concentration of 1% for lubricants additivated with TiO_2 and ZnO, it was observed the overlap of damage by wear and plastic strain, the scar being visible, without major changes in texture,
- in order, for evaluate the quality of a surface as close to reality with the help of 3D parameters, the step of the profilometer must be as fine as possible, and the investigation area as large as possible.

Chapter 7
Conclusions and personal contributions

7.1. Final conclusions

The addition of nanoparticles (TiO_2, ZnO) as modifiers of friction and wear, can improve the tribological properties of vegetal oils. Friction is not always reduced, but increase of the friction coefficient is acceptable because it is accompanied by a substantial reduction in wear. The focus should be on the dispersion of the nanoadditive and the selection of the dispersant.

The reported results are satisfactory, but need to be extended to operational regimes closer to the applicable ones.

The main issues of additivated rapeseed oil with nanoadditives to reduce friction and wear are:

- keeping of a homogeneous dispersion of nanoparticles and the lubricants formulation,
- the lubricant response can be qualitative, very differentiated, depending on the test regime.

The results showed that the nanoadditivation of rapeseed oil with TiO_2 and ZnO reduced the wear rate of the wear scar diameter only at high loads and speeds, the influence in normal regime being reduced, but in severe regime the influence of these additives proved beneficial, in terms of increasing the length of the slope of the wear scar diameter (WSD) - load (F) and reducing its angle,

- the reporting of results favors the comparison of data with those in the literature and the formulation of relevant recommendations for lubricants formulated by the author,
- according this study, it can be concluded that the additivation of rapeseed oil with TiO_2 and ZnO would be efficient for operating systems with variable loads and possible large regime variations (towards the severe regime).

The FE model proposed by the author introduces the sliding on a simplified system of the four-ball machine, friction being calculated as shear stress between moving surfaces, according to Coulomb's law ($\tau_f = \mu \cdot Fn$). The displacement on z direction of the model was the same as that calculated from wear scar diameter and profile depth on both balls, associated to the actual loading.

In this model, the wear of the balls is not simulated and the surfaces are perfectly smooth, but in reality the abrasive wear dominates the normal regime. In the severe regime, plastic strain processes approach (visible also in simulation). The adhesive wear is not highlighted by simulation.

Based on the documentation done by on the additivation of vegetal oils with friction and wear modifiers, the author chose neat rapeseed oil as the base oil and as friction and wear modifiers, TiO_2 and ZnO. The author of this study took over the technology of mixing/dispersing nanoparticles from previous works [16], [30], carried out within the Research Center ”Mechanics and Tribology of Surface Layers” of „Dunărea de Jos” University of Galați.

The formulation of nanoadditivated lubricants was based on a sonication and alternative cooling regime, several times repeated (3-5 times), after which, the obtained lubricant with different concentrations of additive was subjected to a test campaign. Unlike many other scientific reports on lubricant testing, which focused on a single regime test, this thesis tested newly formulated lubricants in both regimes, normal and severe. This new approach made possible to highlight the role of nanoadditives in severe regime in which, although they did not form a continuous film, they still led to the protection of contact surfaces and the reduction of the WSD when testing on the four ball machine.

Four tribological parameters were analyzed, the friction coefficient, the wear scar diameter, the wear rate of the wear scar diameter and the temperature in the oil bath, to have a clear image of the tested lubricants behavior.

In the normal regime, it is observed that:

- for non-additivated rapeseed oil, the friction coefficient is less sensitive to load at high speeds,
- the additivation of rapeseed oil with TiO_2, makes the values of the friction coefficient to be lower than in the case of non-additivated rapeseed oil, at F =100 N; at high speed, an increase of the of friction coefficient values can be observed, which means that the film is formed,
- when rapeseed oil is additivated with ZnO nanoparticles, it is observed, at low concentrations the ZnO, nanoparticles increase the value of the friction coefficient,
- for the rapeseed oil, WSD increase with load and sliding speed, high values of WSD being obtained in the case of rapeseed oil additivated with TiO_2 at concentrations of 0.25% and 1%. The influence of the nanoadditive on wear is beneficial, especially at low sliding speeds, 0.38 m/s, which means that below this speed, the particles remain in contact and protect the surface. Wear scars increase with increasing load, at the highest loads, there were observed the largest wear scars, in the case of ZnO non-additivation. ZnO addition does not change the WSD values,
- when increasing load and sliding speed, a decrease of w(WSD) it is observed, in the case of rapeseed oil. For rapeseed oil additivated with TiO_2, a decrease in w(WSD) it is observed with the load, for all concentrations and sliding speeds,
- when rapeseed oil is additivated with ZnO, it can be seen that the wear rate of the wear scar diameter has a tendency to decrease with increasing load,
- for all tested lubricants, there is an increase of the temperature values, in the oil bath, throughout the test, as the load increases.

In the severe regime, it is observed that:

- for rapeseed oil, large variations of the friction coefficient are observed until the second 15 of the test, after which, the values have not large variations. This means that surface destruction or sudden processes that occur at high loads occur in the first period of the test, not towards the end. It is observed that the addition of the additive to the severe regime increased the friction coefficient, in the case of the addition with TiO_2 nanoparticles. The friction coefficient, for rapeseed oil additivated with ZnO nanoparticles, has very high values at the beginning of the test, after which it goes to the value of 0.1, which means a mixed friction regime,
- very high values of the wear scar diameter, (~2.7 mm), are observed for non-additivated rapeseed oil and for rapeseed oil additivated with 0.5% TiO_2. The last value for WSD is measured for 900 N, and between 850 N and 900 N the slope of each formulated lubricant is different. The best tribological behavior has the lubricant with 1% ZnO, for the severe regime,
- the lowest values of the temperature in the oil bath, obtained at the end of the 1 minute test, in the severe regime, have the non-additivated rapeseed oil (between 30 °C - 40 °C). The highest temperature in the oil bath at the end of the test was recorded for rapeseed oil additivated with 1% ZnO (exceeded 70 °C). It must be taken into account, that in the case of heavy loads, even accidentally, the temperature will rise, and the cooling system of the device must keep the temperature below the value of the oxidation temperature of vegetal oils (~140 °C).

The association of wear with surface quality can be qualitative, through images and appearance of the Abbott-Firestone curve, but also quantitative, through the values obtained for texture parameters (2D and 3D) and the dependence function between them.

The tribologists are interested in functions of the form f(v, F, t, WSD, texture parameter)=0, from which it is possible to evaluate an optimization or a delimitation of the operational regime based on wear and surface quality criteria.

In conclusion, when comparing used surfaces and unused surfaces, it is recommended to consider similar surfaces in size (and geometry). For evaluating the quality of a surface as close to reality, with the help of 3D parameters, the step of the profilometer must be as fine as possible, and the investigation area as large as possible.In this study, the step on a line was 5 μm, and between lines also 5 μm and the investigate darea was 1500 μm x 1500 μm.

7.2. Personal contributions

The purpose of this research was to evaluate, from a tribological point of view, the influence of TiO_2 and ZnO nanoadditives in rapeseed oil, the author made the following contributions:

- studying a documentation with reference to vegetal oils (rapeseed oil) and friction and wear modifiers (metal oxides),
- own methodology created for evaluating formulated lubricants with rapeseed oil and two nanoadditives, by designing a test campaign that included normal and severe regimes, aspect that is not found in the literature,
- lubricants formulation, at laboratory level, to ensure the additive dispersion,
- tribological behavior evaluation of formulated lubricants with rapeseed oil and nanoadditives by a set of parameters, including: friction coefficient, wear scar diameter, wear rate of wear scar diameter, temperature in the lubricant bath.
- formulated lubricants hierarchy, according to tribological parameters.

7.3. Future research directions

Based on the obtained results, the research can be continued in the following directions:

- increasing the test ranges for applied load and speed,
- using other investigative methods to explain the tribological behavior of these lubricants,
- complex additivation of rapeseed oil (introducing of a set of friction, wear modifiers and viscosity modifiers into the lubricants).

References

1. Abdullah, M. I. H. C., bin Abdollah, M. F., Tamaldin, N., Amiruddin, H., & Nuri, N. R. M. (2016). Effect of hexagonal boron nitride nanoparticles as an additive on the extreme pressure properties of engine oil. *Industrial Lubrication and Tribology*, *68*(4), 441-445

2. Adhvaryu, A., Erhan, S. Z., & Perez, J.M. (2004). Tribological studies of thermally and chemically modified vegetable oils for use as environmentally friendly lubricants. *Wear*, *257*, 359–367

3. Aldana, P.U., Dassenoy, F., Vacher, B., Le Mogne, T., & Thiebaut, B. (2016). WS2 nanoparticles anti-wear and friction reducing properties on rough surfaces in the presence of ZDDP additive. *Tribology International*, *102*, 213–221

4. Ali, M. K. A., Xianjun, H., Mai, L., Bicheng, C., Turkson, R. F., & Qingping, C. (2016). Reducing frictional power losses and improving the scuffing resistance in automotive engines using hybrid nano materials as nano-lubricant additives. *Wear*, *364-365*, 270–281

5. Ali, M. K. A., Xianjun, H., Mai, L., Qingping, C., Turkson, R. F., & Bicheng, C. (2016). Improving the tribological characteristics of piston ring assembly in automotive engines using Al_2O_3 and TiO_2 nanomaterials as nano-lubricant additives. *Tribology International*, *103*, 540–554

6. Alves, S. M., Barros, B. S., Trajano, M. F., Ribeiro, K. S. B., & Moura, E. (2013). Tribological behavior of vegetable oil-based lubricants with nanoparticles of oxides in boundary lubrication conditions. *Tribology International*, *65*, 28–36

7. Bakunin, V. N., Suslov, A. Y., Kuzmina, G. N., & Parenago, O. P. (2005). Recent achievements in the synthesis and application of inorganic nanoparticles as lubricant components. *Lubrication Science*, *17*, 127

8. Bakunin, V. N., Suslov, A. Y., Kuzmina, G. N., Parenago, O. P., & Topchiev, A. V. (2004). Synthesis and application of inorganic nanoparticles as lubricant components – a review. *Journal of Nanoparticle Research*, *6*, 273

9. Biresaw, G., Bantchev, G. B., & Cermak, S. C. (2011). Tribological properties of vegetable oils modified by reaction with butanethiol. *Tribology Letters*, *43*, 17–32

10. Blateyron, F. (2013). *Characterisation of Areal Surface Texture* (Richard Leach, Ed.) doi: 10.1007 / 978-3-642-36458-7_2

11. Blunt, L., & Jiang, X. (2003). *Advanced techniques for assessment surface topography*, Butterworth-Heinemann, London

12. Cermak, S.C., Biresaw, G., Isbell, T.A., Evangelista, R.L., Vaughn, S.F., & Murray, R. (2013). New crop oils—Properties as potential lubricants. *Industrial Crops and Products* ,*44*, 232–239

13. Charoo, M. S., Wani, M. F., Hanief, M., & Rather, M. A. (2017). Tribological properties of MoS2 particles as lubricant additive on EN31 alloy steel and AISI 52100 steel ball. *Materials Today: Proceedings*, *4*, 9967–9971

14. Creţu, S. S. (2009). *Contactul concentrat elastic-plastic*, Editura Politehnium, Iași, România

15. Cristea, G. C., Georgescu, C., Dima, D., & Deleanu, L. (2018, June 7-8). Influence of graphene as additive in soybean oil [Conference presentation] 8th International Conference on Advanced Concepts in Mechanical Engineering – ACME 2018, Iași, Romania

16. Cristea, G. C. (2017). *Tribological characterization of soybean oil additivated with nano materials based on carbon (black carbon, graphite and graphene*, [Doctoral dissertation, ,,Dunărea de Jos" University of Galați, Romania]

17. Czichos, H., Saito, T., & Smith, L. (2006). *Springer Handbook of Materials Measurement Methods*, Springer Science-Business Media, Berlin

18. Dai, W., Kheireddin, B., Gao, H., & Liang, H. (2016). Roles of nanoparticles in oil lubrication. *Tribology International*, *102*, 88–98

19. Deleanu, L., Cantaragiu, A., Bîrsan, I. G., Podaru, G., & Georgescu, C. (2011). Evaluation of the spread range of 3D parameters for coated surfaces. *Tribology in Industry*, *33*(2), 72-78

20. Deleanu, L., Georgescu, C., & Suciu, C. (2012). A comparison between 2D and 3D surface parameters for evaluating the quality of surfaces. *The Annals of "Dunarea de Jos" University of Galati*, *V*, Technologies in Machine Building, 10-17

21. Dong, W. P., Sullivan, P. J., & Stout, K. J. (1994). Comprehensive study of parameters for characterising three-dimensional surface topography. III: Parameters for characterising amplitude and some functional properties. *Wear*, *178*(1-2), 29-43

22. Dowson, D., & Higginson, G.R. (1977). *Elasto-hydrodynamic lubrication*, Pergamon Press, Oxford

23. Dowson, D., Priest, M., Taylor C., M., Ehret, P., Childs, T., Dalmaz, G., Berthier, Y., Flamand, L., Georges, J.-M., & Lubrecht, A. (1999). *Lubrication at the frontier. The role of the interface and surface layers in the thin film and boundary regime*. Elsevier Science

24. Erhan, S. Z. (2005). *Industrial Uses of Vegetable Oils*, AOCS Press, Peoria, Illinois.

25. Erhan, S. Z., Sharma, B. K., & Perez, J. M. (2006). Oxidation and low temperature stability of vegetable oil-based lubricants. *Industrial Crops and Products*, *24*, 292–299

26. Fiebig, H.J. (2011). *Fatty acid composition of important plant and animal fats and oils*, Münster. http://www.dgfett.de/material/fszus.php

27. Frunză, G., & Spînu, S. (2010). *Fundamentele teoriei plasticității. Aplicații în mecanica contactului elasto-plastic*, Editura Universității ,,Ștefan cel Mare" din Suceava, România. ISBN 978-973-666-336-9

28. Gangwani, P., Gupta, M. K., & Bijwe, J. (2017). Synergism between particles of PTFE and hBN to enhance the performance of oils. *Wear*, *384-385*, 169–177

29. Georgescu, C., Cristea, G .C., Solea, C. L., Deleanu, L., & Sandu, I. G. (2018). Flammability of Some Vegetal Oils on Hot Surface. *Revista de chimie*, *69*(3), 668-673

30. Georgescu, C., Șolea, L. C., Cristea, G. C., & Deleanu, L. (2015). On the lubrication capability of rapeseed oil. *Recent Advances in Mechanics and Materials in Design*, *5533*, Ponta Delgada, Azores, Portugal

31. Georgescu, C. (2012). *Stratul superficial în procesele de frecare şi uzură ale unor materiale compozite cu matrice de polibutilentereftalat* [Doctoral dissertation, ,,Dunărea de Jos" University of Galați, Romania

32. Gold, P.W. (2002). *Basics of Tribology (Lectures Notes)*, Institut für Maschinenelmente (IME) der RWTH-Aachen

33. Gow, G. (2009). *Lubricating Grease In: Chemistry and Technology of Lubricants*, 3rd edition, (Mortimer R, Fox M Orszulik S, Ed.), Springer, Dordrecht

34. Gu, K., Chen, B., Wang, X., Wang, J., Fang, J., Wu, J., & Huan, L. (2014). Preparation, friction and wear properties of hydrophobic lanthanum borate nanorods in rapeseed oil. *Transactions of Nonferrous Metals Society of China*, *24*, 3578−3584

35. Gulzar, M., Masjuk, H. H., Varman, M., Kalam, M. A., Mufti, R. A., Zulkifli, N. W. M., Yunus, R., & Zahid, R. (2015). Improving the AW/EP ability of chemically modified palm oil by adding CuO and MoS2 nanoparticles. *Tribology International*, *88*, 271–279

36. Guo, Y., B. (2002). Mechanical Properties of Hardened AISI 52100 Steel in Hard Machining Processes. *Journal of Manufacturing Science and Engineering*, *124*(1), 1-9. https://doi.org/10.1115/1.1413775

37. Habereder, T., Moore, D., & Lang, M. (2008). *Eco Requirements for Lubricant Additives in Lubricant Additive Chemistry and Applications*, 2nd edition, Chapter 26, (Rudnick, L R ,Ed.) CRC Press, Boca Raton

38. Hardy, C., Baronet, C. N., & Tordion, G. V. (1971). The elasto-plastic indentation of a half-space by a rigid sphere. *International Journal of Numerical Methods in Engineering*, *3*(4), 451-462

39. Ilie, F., & Covaliu, C. (2016). Tribological properties of the lubricant containing titanium dioxide nanoparticles as an additive. *Lubricants*, *4*, 12

40. Ingole, S., Charanpahari, A., Kakade, A., Umare, S., S., Bhatt, D., V., & Menghani, J. (2013). Tribological behavior of nano TiO2 as an additive in base oil. *Wear*, *301*, 776-785

41. Ionescu, T. F., Guglea, D., Georgescu, C., Dima, D., & Deleanu, L. (2020). Influence of ZnO concentration in rapeseed oil on tribological behavior. *IOP Conference Series: Materials Science and Engineering*, *724*(1). https://doi.org/10.1088/1757-899X/724/1/012045

42. Ionescu, T. F., Guglea, D., Georgescu, C., Dima, D., & Deleanu, L. (2020). Rapeseed oil with anti-wear additives on the four ball tester. *IOP Conference Series: Materials Science and Engineering*, *997*. https://iopscience.iop.org/article/10.1088/1757-899X/997/1/012013.

43. Ionescu, T.F., Guglea, D., Deleanu, L., Alexandru, P., & Georgescu, C. (2019). Tribological behavior of coarse rapeseed oil additivated with nanoparticles of Zinc oxide. *Proceedings on Engineering Sciences*, *1*(1). doi: 10.24874/PES01.01.002

44. Ionescu, T.F., Şorcaru, A.A., Guglea, D., Cristea, G.C., Georgescu, C., & Deleanu, L. (2020). Rapeseed oil additivated with hexagonal boron nitride. *INCAS BULLETIN*, *12*, 63-72. https://doi.org/10.13111/2066-8201.2020.12.2

45. Ionescu, T.F., Şolea, L.C., Guglea, D., Georgescu, C., & Deleanu, L. (2019). Evaluating seizure on four ball tester for rapeseed oil. *Mechanical Testing and Diagnosis*, *IX*(3), 18-23

46. Ionescu, T.F., Cristea, G.C., Guglea, D., Dima, D., Georgescu, C., & Deleanu, L. (2020, November 26-27). Wear-load curves in severe regime for rapeseed oil additivated with ZnO. 8th International Conference on Material Science and Technologies – ROMat 2020, Bucharest, Romania

47. Jatti, V., & Kumar, V. (2015). Titanium oxide nano-particles as anti-wear and friction-reduction additives in lubricating oil. *Journal of Chemical and Pharmaceutical Research*, *7*(4), 1049-1055

48. Johnson, K., L., Greenwood, J., A., & Higginson, J.,G. (1985). The contact of elastic regular wavysurfaces. *Int J Mech Sci*, *27*(6), 383–396

49. Karthik, V. S. N. (2012). Finite element analysis of spherical indentation to study pile-up/sink-in phenomena in steels and experimental validation. *International Journal of Mechanical Sciences*, *54*, 74-83

50. Kudish, I. I., & Covitch, M. J. (2010). *Modeling and Analytical Methods in Tribology*, CRC Press

51. Kurth, T. L., Byars, J. A., Cermak, S. C., Sharma, B. K., & Biresaw, G. (2007). Non-linear adsorption modeling of fatty esters and oleic estolide esters via boundary lubrication coefficient of friction measurements. *Wear*, *262*(5–6), 536–44

52. Laad, M., Kumar, V., & Jatti, S. (2018). Titanium oxide nanoparticles as additives in engine oil. *Journal of King Saud University- Engineering Sciences*, *30*, 116-122

53. Liu, Z., Sharma, B. K., Erhan, S. Z., Biswas, A., Wang, R., & Schuman, T. P. (2015). Oxidation and low temperature stability of polymerized soybean oil-based lubricants. *Thermochimica Acta, 601*, 9-16

54. Luna, F. M. T., Rocha, B. S., Rola Jr., E. M., Albuquerque, M. C.G., Azevedo, D. C. S., & Cavalcante Jr., C. L. (2011). Assessment of biodegradability and oxidation stability of mineral, vegetable and synthetic oil samples. *Industrial Crops and Products, 33*, 579–583

55. Malburg, M. C. (2002). Cylinder Bore Surface Texture Analysis, Digital Metrology Solutions Inc. http://www.digitalmetrology.com/Papers/CylinderBoreNoBkgd.pdf

56. Mariano, G. (2009). *Selection and application of solid lubricants as friction modifiers in Lubricant Additives*, (Rudnick, L. R., Ed.), 173

57. Meng, Y.; Su, F.; & Chen, Y. (2016). Supercritical Fluid Synthesis and Tribological Applications of Silver Nanoparticle-decorated Graphene in Engine Oil Nanofluid. *Sci. Rep*., *6*(31246)

58. Miller, M. (2008). *Additives for bioderived and biodegradable lubricants Lubricant Additive Chemistry and Applications*, 2nd edition, Chapter 18, (Rudnick L R, Erhan S. Z., Ed.), CRC Press, Taylor and Francis Group

59. Nazir, N. H., Zulfiqar, A. K., & Adil, S. (2018). Experimental analysis and modelling of c-crack propagation in silicon nitride ball bearing element under rolling contact fatigue. *Tribology International, 126*, 386-401

60. Norrby, T. (2003). Environmentally adapted lubricants – where are the opportunities? *Industrial Lubrication and Tribology, 55*(6), 268-274

61. Paredes, X., Comunasa, M. J. P., Pensado, A. S., Bazile, J.P., Boned, C., & Fernández, J. (2014). High pressure viscosity characterization of four vegetable and mineralhydraulic oils. *Industrial Crops and Products, 54*, (2014), 281–290

62. Pirvu, C., Georgescu, C., & Deleanu, L. (2013). Influence of grinding feed speed on 3D texture parameters. *Mechanical Testing and Diagnosis, 2*, 19-28

63. Quinchia, L. A., Delgado, M. A., Valencia, C., Franco, J .M., & Gallegos, C. (2010). Viscosity modification of different vegetable oils with EVA copolymer for lubricant applications. *Industrial Crops and Products, 32*, 607–612

64. Rakopoulos, D. C., Rakopoulos, C. D., Giakoumis, E. G., Dimaratos, A. M., & Founti, M. A. (2011). Comparative environmental behavior of bus engine operating on blends of diesel fuel with four straight vegetable oils of Greek origin: sunflower, cottonseed, corn and olive. *Fuel, 90*, 3439–3446

65. Rîpă, M., & Deleanu, L. (2006). Relevant parameters set for characterising engineered surface topography, Conferinţa Naţională de Fizică Aplicată, Galaţi, România

66. Rudnick, L. R. (2009). *Lubricant additives. Chemistry and applications*, Second Edition, CRC Press, Taylor & Frances Group

67. Rudnick, L. R., & Erhan, S. Z. (2006). *Natural oils as lubricants in Synthetics, mineral oils, and bio-based lubricants: chemistry and technology* (Rudnick L R, Erhan, S Z , Ed.) New York, CRC/Taylor & Francis Group

68. Sanukrishna, S. S., & Prakash, M., J. (2018). Experimental studies on thermal and rheological behaviour of TiO_2-PAG nanolubricant for refrigeration system. *International Journal of Refrigeration, 86*, 356-372

69. Shahnazar, S., Bagheri, S., & Hamid, S. B. A. (2016). Enhancing lubricant properties by nanoparticle additives. *International journal of hydrogen energy, 41*, 3153-3170

70. Spikes, H. A. (2002). Film-forming additives-direct and indirect ways to reduce friction. *Lubrication Science*, *14*, 147

71. Stachowiak, G. W., & Batchelor, A.W. (2005). *Engineering tribology*, Butterworth-Heinemann, Team Lrn.

72. Stachowiak, G. W., & Podsiadlo P. (2004). Classification of tribological surfaces. *Tribology International*, *37*, 211-217

73. Stachowiak, G. W., & Podsiadlo, P. (2006). Fast classification of engineering surfaces without surface parameters. *Tribology International*, *39*, 1624-1633

74. Stout, K. J., Sullivan, P. J., Dong, W. P., Mainsah, E., Luo, N., Mathia, T., & Zahouani, H. (1994). The development of methods for the characterisation of roughness in three dimensions, *Publication no. EUR 15178 EN of the Commission of the European Communities*: Brussels-Luxembourg

75. Sunqing, Q., Junxiu, D., & Guoxu, C. (1999). A review of ultrafine particles as antiwear additives and friction modifiers in lubricating oils. *Lubrication Science*, *11*, 217

76. Syahrullai, S., Ani, F. H., & Golshkouh, I. (2013). Wear resistance characteristic of vegetable oil. The 2nd International Conference on Sustainable Materials Engineering, Penang, Malaysia, 44-47

77. Șolea, L. C. (2013). *Contribuţii la studiul comportării reologice şi tribologice a unor lubrifianţi biodegradabili pe bază de uleiuri vegetale* [Doctoral dissertation, „Dunărea de Jos" University of Galați

78. Tang, Z., & Li, S. (2017). A review of recent developments of friction modifiers for liquid lubricants (2007–present). *Current Opinion in Solid State and Materials Science*, *18*, 119–139

79. Tarrago-Trani, M. T., Phillips, K. M., Lemar, L. E., & Holden, J. M. (2006). Review. New and existing oils and fats used in products with reduced trans-fatty acid content. Nutrient database. *Journal of the American Dietetic Association*, *24* (2006), 867-880

80. Thornton, C. (2015). *Granular Dynamics, Contact Mechanics and Particle System Simulations*, Springer International Publishing Switzerland, https://doi.org/10.1007/978-3-319-18711-2

81. Uflyand, I., E., Zhinzhilo, V., A., & Burlakova, V., E. (2019). Metal-containing nanomaterials as lubricant additives: State-of-the-art and future development. *Friction*, *7* (2), 93-116. https://doi.org/10.1007/s40544-019-0261-y

82. Wang, M. (2014). *Biolubricants and biolubrication*, [Doctoral dissertation KTH Royal Institute of Technology, Stockholm]

83. Wang, R., & Schuman, T. P. (2015). Oxidation and low temperature stability of polymerized soybean oil-based lubricants. *Thermochimica Acta*, *601*, 9–16

84. Wu, H., Zhao, J., Xia, W., Cheng, X., He, A., Yun, J. H., Wang, L., Huang, H., Jiao, S., Huang, L., Zhang, S., & Jiang, Z. (2017). A study of the tribological behaviour of TiO_2 nanoadditive water-based lubricants. *Tribology International*, *109*, 398–408

85. Wu, Y. Y., Tsui, W. C., & Liu, T. C. (2007). Experimental analysis of tribological properties of lubricating oils with nanoparticle additives. *Wear*, *262*(7-8), 819–825

86. Xiao, H., & Liu, S. (2017). 2D nanomaterials as lubricant additive: A review. *Materials and Design*, *135*, 319–332

87. Yan, S. L., & Li, L. Y. (2003). Finite element analysis of cyclic indentation of an elastic-perfectly plastic half-space by a rigid sphere. *Journal of Mechanical Engineering Science*, *217*, 505-514

88. You, J., Li, F., & Huang, Y. (2010). Tribological performance of two potential environmentally friendly ashless vegetable oil additives. *China Petroleum Processing and Petrochemical Technology*, *12*(1), 43-48

89. Zhao, J., Kan, Q., Fu, P., Kang, G., & Wang, P. (2020). An Elasto-plastic Contact Solving Method for Two Spheres. *Acta Mechanica Solida Sinica*, *33* (5), 612–634. https://doi.org/10.1007/s10338-020-00164-1

90. Zulkifli, N. W. M., Kalam, M. A., Masjuki, H. H., & Yunus, R. (2013). Experimental analysis of tribological properties of biolubricant with nanoparticle additive. *Procedia Engineering*, *68*, 152–157

91. *** Environmentally Acceptable Lubricants, United States Environmental Protection https://www3.epa.gov/npdes/pubs/vgp_environmentally_acceptable_lubricants.pdf

92. *** Mountains Lab Premium 8.1 Version (2020), disponibil on-line: http://www.imagemetrology.com.

93. *** International Organization of Standardization. (2012). (2012).Specificaţii geometrice pentru produse (GPS). Starea suprafeţei: Areal. Partea 3: Operatori de specificaţie. (ISO Standard No. 25178-3:2012)

94. *** International Organization of Standardization (2003). Specificaţii geometrice pentru produse (GPS). Starea suprafeţei: Metoda profilului. Termeni, definiţii şi parametri de stare ai profilului. (ISO Standard No. 4287:2003)

Author's scientific papers

eng. Traian Florian Ionescu

1. **Ionescu T. F**., Guglea D., Georgescu C., Dima D., & Deleanu L.(2020). Influence of ZnO concentration in rapeseed oil on tribological behavior. *IOP Conference Series: Materials Science and Engineering, Romania, 724*(1). https://doi.org/10.1088/1757-899X/724/1/012045.
2. Guglea D., **Ionescu T. F**., Dima D., Georgescu C., & Deleanu L. (2020). Tribological behavior of rapeseed oil additivated with boron nitride, *IOP Conference Series: Materials Science and Engineering, Romania, 724*(1). https://doi.org/10.1088/1757-899X/724/1/012046
3. **Ionescu T. F**., Guglea D., Georgescu C., Dima D., & Deleanu L.(2020). Rapeseed oil with anti-wear additives on the four ball tester. *IOP Conference Series: Materials Science and Engineering, Romania, 997*. https://iopscience.iop.org/article/10.1088/1757-899X/997/1/012013.
4. Deleanu L., Georgescu C., **Ionescu T. F**., Guglea D., & Isacescu D. (2020). SR EN ISO 20623 - A standard for tribological evaluation of lubricants that may bust innovation. *IOP Conference Series: Materials Science and Engineering, Romania, 997*. https://iopscience.iop.org/article/10.1088/1757-899X/997/1/012008
5. **Ionescu T.F**., Guglea D., Deleanu L., Alexandru P., & Georgescu C. (2019). Tribological behavior of coarse rapeseed oil additivated with nanoparticles of zinc oxide. *Proceedings on Engineering Sciences, Serbia, 1*(1). doi: 10.24874/PES01.01.002.
6. **Ionescu T.F**., Şorcaru A.A., Guglea D., Cristea G.C., Georgescu C., & Deleanu L. (2020). Rapeseed oil additivated with hexagonal boron nitride. INCAS BULLETIN, 12, 63-72. https://doi.org/10.13111/2066-8201.2020.12.2
7. **Ionescu T.F**., Şolea L.C., Guglea D., Georgescu C., & Deleanu L. (2019). Evaluating seizure on four ball tester for rapeseed oil. Mechanical Testing and Diagnosis, IX (3). https://doi.org/10.35219/mtd.2019.3.03
8. Guglea, D., **Ionescu, T. F**., Dima, D., Georgescu, C., & Deleanu, L. (2020). Nano additivation of rapeseed oil with ZnO and BN. *Academia Forţelor Terestre ,,Nicolae Bălcescu" din Sibiu, Buletin ştiinţific supliment, Catalogul oficial al salonului ,,Cadet INOVA"-Cercetări şi inovaţii în viziunea tinerilor cercetători, 5*, 281-285. http://37.251.175.30/documente/Supliment_Inova_20.pdf
9. Guglea D., **Ionescu T.F**., Deleanu L., Georgescu C., Dima D., & Ojoc G. G. (2019). Boron nitride as additive in rapeseed oil, tested on four ball tester. *Proceedings on Engineering Sciences, Serbia, 1*(1). doi: 10.24874/PES01.01.076

10. **Ionescu T.F**., Guglea D., Georgescu C., Dima D., & Deleanu L. (2019, October 16-18). *Influence of nano particles of ZnO as additive in rapeseed oil for evaluating the tribological behavior* [Conference presentation]. UGAL INVENT 2019, Galați, Romania. http://www.invent.ugal.ro
11. Guglea D., **Ionescu T.F**., Dima D., Georgescu C., & Deleanu L. (2019, October 16-18). *Influence of nano particles of hBN as additive in rapeseed oil for evaluating the tribological behavior* [Conference presentation]. UGAL INVENT 2019, Galați, Romania. http://www.invent.ugal.ro
12. Deleanu, L., Georgescu, C., Șolea, L.C., **Ionescu, T.F**., & Ojoc, G.G. (2019, October 16-18). *Manifold ignition test inter-lab study for ISO 20823* [Conference presentation]. UGAL INVENT 2019, Galați, Romania. http://www.invent.ugal.ro
13. Boţan, M., Mustață, A.E., **Ionescu, T.F**., Georgescu, C., & Deleanu, L. (2017). Adding aramid fibres to improve tribological characteristics of two polymers. *Tribology in Industry*, *39*(3), 283-293. doi: 10.24874/ti.2017.39.03.02
14. **Ionescu, T.F**., Pîrvu, C., Georgescu, C., & Deleanu L. (2017, May 17-19). *The influence of friction characteristics in simulating the impact bullet- stratified materials* [Conference presentation]. SerbiaTrib 2017, Kragujevak, Serbia.
15. Pîrvu, C., **Ionescu, T.F.,** Deleanu, L., & Badea S. (2017). Simplified simulation of impact bullet- stratified pack for restraining ballistic tests. *MATEC Web of Conferences, 112*. doi:10.1051/matecconf/201711206023
16. **Ionescu, T.F**., Pîrvu, C., Badea, S., Georgescu, C., & Deleanu L. (2017, October 19-20). *Simulation of the impact bullet- stratified materials* [Conference presentation]. UGAL INVENT 2017, Galați, Romania. http://www.invent.ugal.ro
17. **Ionescu T.F**., Cristea G.C., Guglea D., Dima D., Georgescu C., & Deleanu L. (2020, November 26-27). Wear-load curves in severe regime for rapeseed oil additivated with ZnO [Conference presentation]. 8th International Conference on Material Science and Technologies – ROMat 2020, Bucharest, Romania
18. **Ionescu, T.F**., Guglea, D., Deleanu, L.,Alexandru, P., & Georgescu, C. (2019, June 13-14). *Tribological behavior of coarse rapeseed tested on four ball tester* [Conference presentation] Scientific Conference of Doctoral Schools SCDS-UDJG, Galaţi, Romania. http://www.cssd-udjg.ugal.ro/index.php/2019/abstracts-2019
19. **Ionescu T.F**., Guglea D., Georgescu C., & Deleanu L. (2020, June 18-19). *Influence of nano-additive ZnO on wear load curve in severe regime* [Conference presentation] Scientific Conference Of Doctoral Schools – Perspectives and challenges in doctoral research. http://www.cssd-udjg.ugal.ro/index.php/2020/abstracts-20201